CHALMERS
UNIVERSITY OF TECHNOLOGY

Characterization of neutrophil chemoattractants in inflamed synovial fluid

Method development and evaluation for the study of inflamed synovial fluid from patients with inflammatory arthritis

Master's thesis in Physics

LINNÉA ÖGREN

DEPARTMENT OF PHYSICS

CHALMERS UNIVERSITY OF TECHNOLOGY
Gothenburg, Sweden 2023
www.chalmers.se

Master's thesis 2023

Characterization of neutrophil chemoattractants in inflamed synovial fluid

Method development and evaluation for the study of inflamed synovial fluid from patients with inflammatory arthritis

LINNÉA ÖGREN

CHALMERS
UNIVERSITY OF TECHNOLOGY

Department of Physics
Division of Chemical Physics
Chalmers University of Technology
Gothenburg, Sweden 2023

Characterization of neutrophil chemoattractants in inflamed synovial fluid
Method development and evaluation for the study of inflamed synovial fluid from patients with inflammatory arthritis
LINNÉA ÖGREN

Supervisor: Martina Sundqvist, Department of Rheumatology and Inflammation Research, Institute of Medicine, Sahlgrenska Academy, University of Gothenburg
Examiner: Christoph Langhammer, Division of Chemical Physics, Department of Physics, Chalmers University of Technology

Master's Thesis 2023
Department of Physics
Division of Chemical Physics
Chalmers University of Technology
SE-412 96 Gothenburg
Telephone +46 31 772 1000

Typeset in LaTeX
Printed by Chalmers Reproservice
Gothenburg, Sweden 2023

Characterization of neutrophil chemoattractants in inflamed synovial fluid
Method development and evaluation for the study of inflamed synovial fluid from patients with inflammatory arthritis
LINNÉA ÖGREN
Department of Some Subject or Technology
Chalmers University of Technology

Abstract

Inflammatory arthritis is a group of inflammatory diseases mainly characterized by inflammation in synovial cavities, eventually leading to the destruction of cartilage and bone in joints. The complete mechanisms behind this inflammatory process are not fully understood today, but some signs indicate that it might differ from the normal inflammatory response associated with acute inflammation. This project focuses on signaling molecules, called chemoattractants, that are responsible for recruiting neutrophils to the inflamed synovial fluid in patients with inflammatory arthritis. More specifically, the aim is to develop and evaluate a possible methodology as a first step toward identifying and characterizing the neutrophil chemoattractants. In order to do this, the complexity of the problem can be reduced by dividing the components of synovial fluid into fractions based on different molecular properties. Two possible approaches were investigated here; one where the components were divided through gel electrophoresis, and one where the components were separated using liquid chromatography methods, after which their chemotactic abilities were measured with a chemotaxis assay. The separated fractions yielded from both approaches were then measured with liquid chromatography-mass spectrometry to obtain more information and clues about the contents and success of separations. Based on the results, the course of action based on liquid chromatography and chemotaxis assay was concluded as most promising for successful separation of components and narrowing of the problem, as is proposed as a first step of methodology in further search for the neutrophil chemoattractants.

Keywords: neutrophils, chemoattractants, inflammation, synovial fluid, inflammatory arthritis, chromatography, chemotaxis, mass spectrometry.

Acknowledgements

My thesis was a collaborative effort involving two research groups at the University of Gothenburg; Huamei Forsmans's research group at the department of rheumatology and inflammation and Alesia Tietze's research group at the department of chemistry and molecular biology. First, I want to express my deep gratitude to my supervisor Martina Sundqvist and co-supervisors Lena Björkman, Alesia Tietze and Daniel Tietze for their continuous support and guidance throughout the project. I also want to thank Irena Burmann for giving me access to the ÄKTA system as well as helping out with the measurements and sharing valuable thoughts and ideas.

Furthermore, I would like to thank everyone that in some shape or form has been involved in this project, whether through helping out with practical issues or discussing problems and results. It has been invaluable to have all these people around me to share ideas with. I especially want to thank Huamei Forsman and Claes Dahlgren. I would also like to thank Hanna Olvhammar for kindly proofreading my report and providing new perspectives.

Finally, I would like to thank Johan and my family for their constant love and support.

Linnéa Ögren, Gothenburg, June 2023

List of Acronyms

ACN acetonitrile. 31
AS ankylosing spondylitis. 1, 9

BSA bovine serum albumin. 27, 29

C5a complement component 5a. 9

DTT dithiothreitol. 22, 23, 25, 26, 40, 51, 53

EDTA ethylenediaminetetraacetic acid. 24, 30

fMLF N-Formylmethionine-leucyl-phenylalanine. 9, 28, 42, 43

G-CSF granulocyte colony-stimulating factor. 7
GDP guanosine diphosphate. 9
GPCR G protein-coupled receptor. 9
GTP guanosine triphosphate. 9

HPLC high performance liquid chromatography. 18

IA inflammatory arthritis. 1–3, 5, 9, 10, 13, 33, 43, 50, 53
IEC ion-exchange chromatography. 2, 13, 15, 16, 22, 24–26, 36, 38, 40–44, 47, 51, 53
IL interleukin. 9, 10

KRG Krebs-Ringer Glucose phosphate buffer. 27, 29

LC-MS liquid chromatography-mass spectrometry. 2, 13, 15, 16, 18, 22–24, 31, 33–36, 44, 45, 47, 51–53
LDS lithium dodecyl sulfate. 23

MCP monocyte chemotactic protein. 10
MIP macrophage inflammatory protein. 10

NET neutrophil extracellular trap. 8

PBS phosphate-buffered saline. 22, 24, 25, 35, 45, 47
PFA paraformaldehyde. 30
psA psoriatic arthropathy. 1, 9

RA rheumatoid arthritis. 1, 9–11, 21

RP-HPLC reversed-phase high-performance liquid chromatography. 13, 15, 16, 22, 23, 44, 46

SDS sodium dodecyl sulfate. 14, 22, 23

SEC size-exclusion chromatography. 2, 13, 15, 16, 22, 24–27, 36–38, 40–45, 47, 48, 51, 53

UV ultraviolet. 13, 15, 17, 18

Contents

List of Figures

List of Tables

1
Introduction

1.1 Background

The inflammatory response plays a major role in the human body's defense system against infection and injury. There are two types of inflammatory processes; acute inflammation, which only lasts for a few hours or days, and chronic inflammation, which can last for months or even years. Proper regulation of the inflammatory response is important in order to avoid host tissue damage [1], and persistent acute inflammation may develop into chronic inflammatory conditions [2, 3]. Inflammation-related diseases include stroke, cancer, chronic kidney disease, and autoimmune and neurodegenerative conditions [4, 3].

In this project, the specific inflammatory process associated with inflamed synovial cavities in patients with inflammatory arthritis (IA) is studied, a process that is not completely understood today. IA covers a group of inflammatory diseases including rheumatoid arthritis (RA), psoriatic arthropathy (psA) and ankylosing spondylitis (AS) [5], which are mainly characterized by inflammation in the joints caused by a dysregulated immune system [6, 7]. This eventually leads to the destruction of cartilage and bone in joints. In addition, inflammatory arthritis can increase the risk for other complications and diseases affecting organs such as the heart, kidneys, lungs, eyes, skin digestive system, and nervous system if more widespread inflammation occurs [8, 6, 9]. For example, the risk for RA patients to develop coronary artery disease is 1.5 to 2 times greater than for the general population [10]. About 0.5 to 1 % of the Swedish population has RA and around 0.25 % has psA [11]. Disease onset usually occurs between 35 and 60 years, differing somewhat between the individual diseases [8, 12]. There also exists juvenile versions of the conditions [8, 13, 14].

During the usual acute inflammatory response, neutrophils – the most abundant white blood cell in human circulation – are recruited from the blood to the site of inflammation in the tissue as a result of chemoattractants that are released at the inflamed site [15, 16, 17]. Concentration variations of chemoattractants create a chemotactic gradient which directs the motion of the neutrophils towards the inflamed site [18], while simultaneously inducing phenotypic changes, denoted priming, of the neutrophils [19]. However, in inflamed synovial cavities of IA patients, the chemoattractants are thought to differ from those that regulate the acute inflammatory response, based on the fact that the recruitment of unprimed neutrophils to inflamed synovial cavities has been observed [20]. Further knowledge and under-

standing of the specific inflammatory process associated with IA is important for the ultimate development of better treatment, which could greatly improve upon the lives of those affected.

1.2 Aim

To gain more insight into the inflammatory process in inflamed cavities of patients with IA – and more specifically the cause behind neutrophil migration to the synovial fluid – this project aims to develop and evaluate methods for further characterization of the content of synovial fluid collected from patients with IA. Furthermore, the possibility of detected components being neutrophil chemoattractants that might be responsible for neutrophil migration to synovial cavities of IA patients, is evaluated.

1.3 Limitations

Since the aim of this thesis is to present a methodology that has the potential of identifying neutrophil chemoattractants in inflamed synovial fluid of IA patients, the focus of this project is quite narrow regarding the number of different samples investigated. Synovial fluid from two patients is used in the examination and evaluation of the experimental methodology. Due to the methodological nature of this thesis, the limited number of studied samples should not affect the results significantly.

Furthermore, the focus of this project is on one type of condition/disease, to study the specific process of inflamed synovial cavities in patients with inflammatory arthritis.

1.4 Methods

To characterize the contents of synovial fluids in IA patients, samples of collected fluids are first separated into components based on different molecular properties to simplify the problem, since synovial fluid contains a great number of proteins. The separation was done by implementing gel electrophoresis, size-exclusion chromatography (SEC), ion-exchange chromatography (IEC) and liquid chromatography-mass spectrometry (LC-MS). These methods were chosen as they allow for separation, quantification and characterization of components based on various properties such as size, hydrophilic and hydrophobic properties and mass-to-charge ratio. Furthermore, obtained fractions from SEC and IEC are investigated for their chemotactic ability using a chemotaxis assay, to identify which separated fractions might contribute most to neutrophil recruitment and therefore potentially contain neutrophil chemoattractants.

1.5 Social, ethical and ecological aspects

Today, several pieces are missing in the puzzle to a full understanding of the underlying pathogenesis of this group of inflammatory chronic diseases. Current treatments aim at reducing inflammation and subsequently reducing permanent joint destruction and pain. However, not all patients respond to treatment, and there might also be unwanted side effects [8, 12]. To improve future treatments, more research is needed to understand the mechanism underlying the disease and will be of great value for those affected by IA.

This project consists of basic research on the inflammatory process itself; treatment is not tested or proposed, and no animal testing is conducted. However, the project consists of handling of biological samples from human patients, why ethical permission was received for the project and all patient data was anonymized.

In addition, as there is a possibility of samples containing viruses, bacteria or other pathogens, all samples are continuously regarded as biohazardous, and appropriate measures are taken during the handling of waste products. Standard safety routines for laboratory work are followed carefully.

2

The inflammatory process and inflammatory arthritis

To provide the fundamental theory underlying the motivation for this thesis, this chapter starts by introducing the necessary parts of basic cell biology in the context of this project. This is followed by a brief overview of the immune system and the general procedure of the inflammatory response. Furthermore, the spotlight is directed towards the neutrophil, with descriptions of both its structure, function and role in inflammation – specifically its recruitment to inflamed sites. This recruitment is guided by signaling molecules denoted chemoattractants, which are reviewed next. Finally, an overview of inflammatory arthritis is described, with a special focus on neutrophils.

2.1 Brief introduction to cell biology relevant for this report

To understand the most important concepts of inflammation, and the specific inflammatory process occurring in IA patients, the basic concepts and terminology of cell biology are briefly introduced in this section. This includes the structure and function of cells and proteins, with an emphasis on cell signaling.

The cell is the fundamental unit of life and can be either prokaryotic or eukaryotic. Prokaryotic cells are single-celled organisms, such as bacteria, while eukaryotic cells can be both single-celled organisms as well as the building blocks for multicellular organisms. Examples of eukaryotic organisms include fungi, plants and animals. In contrast to prokaryotic cells, eukaryotic cells contain intracellular membrane-bound organelles such as a nucleus [21].

One important function of cells is signaling, which allows for cells to respond to the surrounding environment, which is essential for cell development, cell growth and division, migration and apoptosis (programmed cell death), to name a few [22]. Additionally, it provides the basis for the functionality of multicellular organisms through communication with other cells. There are different types of signals, for example autocrine, of which the same cell is both messenger and recipient, paracrine, of which cells in the vicinity of the messenger cell are recipients, and endocrine signaling, where signals travel to target cells further away. To receive signals from the environment, cells have receptors integrated into the cell membrane, to which

signaling molecules – ligands – bind and activate [23].

Multiple signaling molecules, as well as receptors, are proteins. In addition to being involved in cell signaling processes, proteins are essential for living organisms and are involved in and perform a vast number of different tasks, such as replicating and transcribing DNA, acting as hormones, antibodies or enzymes, transporting molecules, repairing tissue, providing energy. Proteins are composed of amino acid chains of different lengths and orders, and are constructed based on information contained in DNA.

2.2 The immune system

The immune system is the defense system of the human body against pathogens, cancer cells and foreign substances. It is composed of organs, cells and proteins. The immune system can be divided into two subsystems that cooperate closely; the innate immune system (to which neutrophils belong) and the adaptive immune system [24]. Where the innate immune system is more general, the adaptive immune system has specific defense responses against antigens[1].

Leukocytes, or white blood cells, play a vital part in the immune system. All leukocytes are produced in the bone marrow, and there are multiple different types of leukocytes that all have different physical properties and functions. The five main types are neutrophils, eosinophils, basophils, lymphocytes and monocytes.

The adaptive immune system is slower than the innate immune system, since the pathogens first have to be identified, but is more effective due to its specialized response. After an antigen has been encountered once, the adaptive immune system will respond much faster upon the next encounter [24]. Immune cells that belong to the adaptive immune system include T lymphocytes and B lymphocytes [26]. In addition, the proteins called antibodies, or immunoglobulins, are produced during the adaptive immune response.

As mentioned above, the innate immune system has a fast and general immune response, and is the body's first line of defense [27]. It responds equally to all threats, and is sometimes also referred to as the nonspecific immune system. It consists of different parts including the skin, mucous membranes, mediators of for example high temperature and low pH, and immune system cells such as macrophages, neutrophils, basophils, eosinophils and natural killer cells [27]. Neutrophils, which is the focus of this project, will be covered extensively in section 2.4.

[1] A substance capable of activating the immune system [25]

2.3 The inflammatory process

The inflammatory response is a vital defense system of the human body, which is activated after some kind of tissue damage such as blunt trauma, ischemia or infectious organisms. As explained in section 1.1, inflammation can be either acute or chronic. The acute inflammatory process consists of a complex sequence of events including activation of endothelial cells[2], adhesion of leukocytes to endothelium and further recruitment of leukocytes to the inflamed site, activation of tissue macrophages[3] and platelets (resulting in clotting), and the release of proteases and oxidants. A more detailed description of the neutrophil recruitment during inflammation is covered in section 2.4. Despite the importance of the inflammatory response, it is carefully regulated by several pro- and anti-inflammatory mediators, to avoid host tissue damage while still retaining an effective response. A prolonged acute inflammatory response may develop into chronic inflammatory conditions [2, 3].

The first type of leukocyte to arrive at the site of inflammation are neutrophils, which are involved in the killing of pathogens through several mechanisms. The structure and function of neutrophils are discussed in more detail in Section 2.4. During the inflammatory process, chemoattractants are released at the inflamed site and recruit leukocytes.

2.4 Neutrophils and their recruitment in inflammation

The neutrophil is the most abundant leukocyte in human blood, and is an important component of the innate immune system [28]. They are produced in the bone marrow and released into blood circulation when they are mature [29]. The process of neutrophil production and release from the bone marrow is regulated by e.g. granulocyte colony-stimulating factor (G-CSF) [30]. Both the retention of neutrophils in the bone marrow, and their release into the bloodstream, are dependent on the presence of different chemokines of which abundances in turn are regulated by G-CSF. The further influence of chemokines on neutrophils during inflammation is described below.
Neutrophils are so-called granulocytes, meaning they contain granules – a type of intracellular vesicles[4] – from which antimicrobial proteases can be released during immune response [31]. These granules are represented with small circles in Figure 2.1, which is a general illustration of the intracellular structure of a neutrophil. In addition to the granules, the multi-lobular nucleus of neutrophils is depicted in the figure as a dark red, large structure. This multi-lobular structure is thought to simplify nuclear deformation and thus ease the cell in passing through small gaps in endothelium and extracellular matrix [32]. In addition to degranulation, neutrophils

[2]A single layer of cells that line the interior of blood vessels
[3]A type of white blood cell that engulfs and digests pathogens
[4]Membrane bound sphere of fluid

employ other mechanisms for killing pathogens; phagocytosis (engulfing and digestion as well as killing by the production of NADPH[5]-oxidase derived reactive oxygen species[6]) and the formation of neutrophil extracellular traps (NETs) [33]. NETs are composed of contents from granules and nuclei of neutrophils, such as DNA and proteins [34].

Under normal homeostatic conditions, neutrophils circulate in a resting state in the bloodstream, but when an inflammatory response is initialized they are recruited to the site of inflammation [15, 16]. This recruitment occurs as a result of the release of so-called chemoattractants (of which chemokines are a subgroup) at the inflamed site [17], whose concentration variation creates a chemotactic gradient that directs the motion of the neutrophils towards the inflamed site [18]. The recruitment is initiated by a change in the surface of endothelial tissue, which occurs as a consequence of stimulation by inflammatory mediators released at the infected site [17, 35].

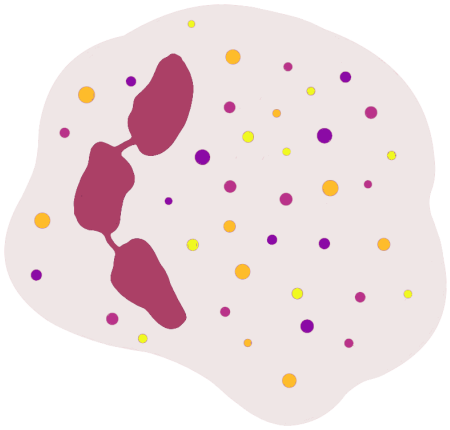

Figure 2.1: An outline of the neutrophil intracellular structure. The dark, large structure is the multi-lobular nucleus, while the small circles represent different types of granules.

Weak, selectin-mediated interactions between neutrophils and the endothelial cells initiate a rolling motion of the neutrophils along the endothelium [36]. Conformational changes are then induced to transmembrane integrin proteins, which interact strongly with adhesion molecules on the endothelial cells and result in strong adherence of neutrophils to the endothelium [37]. The neutrophils then transmigrate between or through the endothelial cells towards the inflamed site, guided by a chemotactic gradient induced by chemoattractants, that direct the motion of the neutrophils [38]. In addition to the recruitment of neutrophils, chemoattractants of acute inflammation induce changes in the neutrophil phenotype - a process that is termed priming - from an inactive state to one more prone to activation by stimuli [19]. The primed state is associated to multiple alterations such as exocytosis[7] NET formation, adhesion, reorganization of the cytoskeleton and translocation and expression of receptors [39].

[5]Nicotinamide adenine dinucleotide phosphate
[6]An electron transfer system
[7]Merging of secretory vesicles with the membrane

2.5 Chemoattractants

Chemoattractants are molecules that induce directional movement of susceptible cells. In humans, chemoattractants can be divided into four classes; chemotactic lipids, chemokines, complement anaphylatoxins and formyl peptides [38]. Chemoattractants function by binding to G protein-coupled receptors (GPCRs), which are transmembrane proteins that interact with G-proteins[8]. Each individual chemoattractant binds to specific cell receptors. Chemoattractants may be released at sites of inflammation either through liberation from protein, production by inflammatory cells, or bacteria. Some notable chemoattractants for neutrophil recruitment include interleukin (IL)-8, complement component 5a (C5a), N-Formylmethionine-leucyl-phenylalanine (fMLF) and leukotriene B4.

Neutrophils, just like many other leukocytes and cells, sense chemotactic gradients caused by variations in concentrations of chemoattractants. This gradient is detected by receptors scattered throughout the neutrophil cell membrane. This sensing mechanism is sensitive enough such that only a small difference in the number of bound chemoattractants on one side of the neutrophil compared to the other can yield directional neutrophil movement. In addition to this, the attachment of chemoattractants to neutrophil membrane receptors may for example induce neutrophil priming.

2.6 Pathology of inflammatory arthritis

As explained in section 1.1, IA is a group of systemic, inflammatory diseases – including RA, AS and psA [5] – mainly characterized by inflammation in the joints caused by a dysregulated immune system. Eventually, this leads to the destruction of cartilage and bone in joints but could also affect other organs [8, 6, 9]. In this section, more details behind the pathology and inflammatory process of IA is described. It is known that B cells, T cells, macrophages and neutrophils all contribute to inflammation of synovial fluid in RA [40], however, the complete mechanism behind the inflammatory process in patients with IA is not fully understood today. Existing treatments for IA aim at reducing pain, inflammation and other symptoms, but not all patients respond sufficiently well to the available treatments, which might also introduce unwanted side effects [8, 12].

[8]Proteins that mediate their effect by binding the nucleotides guanosine triphosphate (GTP) and guanosine diphosphate (GDP) in the cell membrane

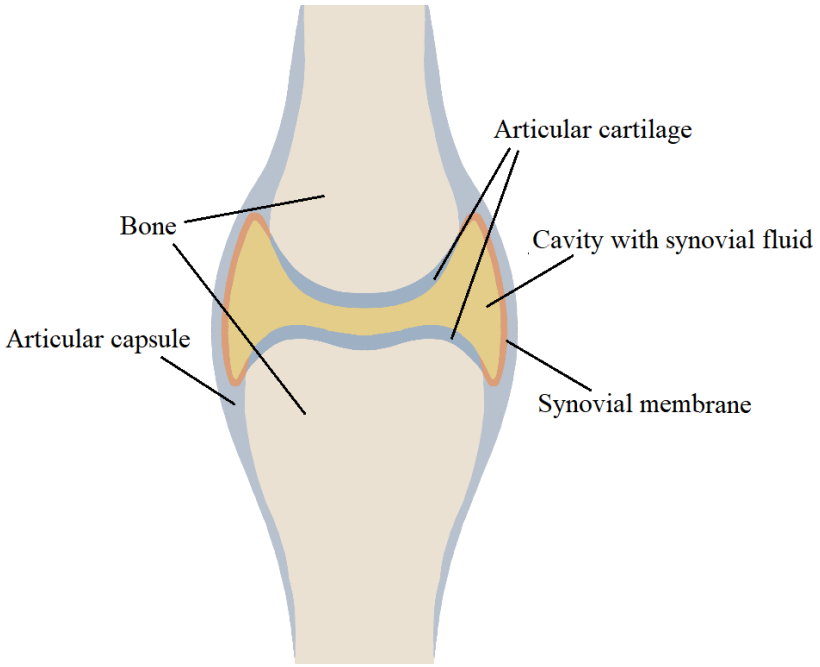

Figure 2.2: An illustration of the anatomy of a synovial joint, showing the synovial fluid inside the joint cavity, the articular cartilages, synovial membrane, articular capsule and bones.

Synovial fluid is located in the cavities of so-called synovial joints. It is a viscous fluid whose main function is to reduce friction between bones during movement. In patients with IA, an excess amount of synovial fluid is produced by the synovial membrane due to swelling and thickening of the synovial membrane, resulting in joint pain and stiffness. Synovial fluid normally has a similar protein content as blood plasma, but also contains proteins secreted from for example the articular cartilage and synovial membrane [41]. Figure 2.2 illustrates the anatomy of a synovial joint.

Previous studies have identified several hundred proteins in synovial fluid, with a somewhat varying proteome for different diagnoses [42], and as always with biology, there are individual fluctuations of types and amounts of components. Additionally, the chemoattractants IL-15, IL-8, monocyte chemotactic protein (MCP)-1 and macrophage inflammatory protein (MIP)-1α alpha have been found in synovial fluid of RA patients [43], where IL-8 and MIP-1α are involved in neutrophil recruitment.

The recruitment of neutrophils to the synovial fluid in IA patients is thought to differ from the normal process prescribed to the acute inflammatory process. One indication of this is the fact that neutrophils that have migrated to synovial fluid have been found to display a phenotype resembling that of resting peripheral blood neutrophils [20], in contrast to neutrophils recruited in an acute inflammatory reaction which display a primed phenotype. Since all known chemoattractants (such as IL-8) induce priming, this may indicate a relatively low concentration of known chemoattractants and that other, possibly unknown, chemoattractants are present in the synovial fluid of patients with IA that recruits neutrophils to the synovial

fluid without inducing priming.

In contrast to acute inflammation, which is an innate immune response, chronic inflammation includes activation of both the innate and adaptive immune systems. However, the role of neutrophils has been found to be deleterious, and increased evidence points to neutrophils playing a role [44], and have been found as activated phenotypes in for instance inflamed synovial cavities of patients with RA [45].

3

Theory and principles of the experimental methods

Now that all necessary background information has been provided, it is time to move on to the implemented methods. As a reminder, this thesis aims to develop and evaluate methods for future characterization of neutrophil chemoattractants in inflamed synovial fluid from IA patients. As explained in section 2.6, the synovial fluid contains at least several hundred different proteins, meaning the search for chemoattractants in the fluid is like looking for a needle in a haystack. In addition to the difficulty of simultaneously detecting and identifying several hundred proteins in a sample, the possibility of unknown neutrophil chemoattractants being present makes full understanding impossible that way. To simplify the problem and thoroughly dissect the inflammatory process, the components can be separated into different parts based on different molecular properties, thus reducing the number of different molecules in each fraction.

This chapter describes the working principles and set-ups for the implemented methods. In the two initial sections, the methods used to separate the synovial fluid components – gel electrophoresis and liquid chromatography – are introduced. The liquid chromatography section encompasses multiple different chromatographic techniques employed in this project; SEC, IEC and reversed-phase high-performance liquid chromatography (RP-HPLC). They are all based on the same principle and setup, but differ in some aspects of specifications and applications and will therefore be described in separate subsections. RP-HPLC is not implemented independently in this project, but is part of subsequent LC-MS measurements. In addition to the different chromatographic techniques, detection through ultraviolet (UV)-spectroscopy is reviewed in the liquid chromatography section.

The principles underlying LC-MS, Boyden chamber assay and flow cytometry, which were used to further analyze the properties of the sample contents, are presented next. LC-MS can analyze sample components in a more detailed manner by measuring the mass-to-charge ratios of detected molecules. Furthermore, Boyden chamber assay together with flow cytometry can be used to assess the chemotactic potential of a sample, in other words its ability to attract neutrophils. The materials and method specifications applied in this project, including settings and conditions used for the different measurements, are described in Chapter 4.

3.1 Gel electrophoresis

Gel electrophoresis is a widely employed method used to separate protein mixtures with high resolution [46]. To separate the proteins by size, a negatively charged detergent is added to the sample, which denatures and binds to the proteins in such a way that each protein obtains a similar mass-to-charge ratio. This means that proteins of resulting high charge have a high mass, and vice versa. The sample proteins then move through a porous gel matrix by applying an electric field, where smaller molecules move faster than larger ones. Size separation is thus obtained. Reducing agents can also be added to the sample prior to the electrophoresis, in order to ease separation by disrupting potential disulfide bonds between proteins [47].

There are different types of gels that can be used, where polyacrylamide gels have the most suitable pore sizes for protein separation. As detergents, sodium dodecyl sulfate (SDS) is usually applied. The proteins are denatured (altered in native structure) and stretched out in the process [47], which might result in an alteration of the biological functions of the proteins.

After running the electrophoresis, the protein distribution on the gel can be visualized by staining the proteins. There are multiple methods for this, such as coomassie blue, silver and fluorescent staining [48]. In this project, coomassie blue is employed, which displays a blue color when binding to proteins [49]. When applied to a gel, bands will appear at the locations of proteins.

3.2 Liquid chromatography

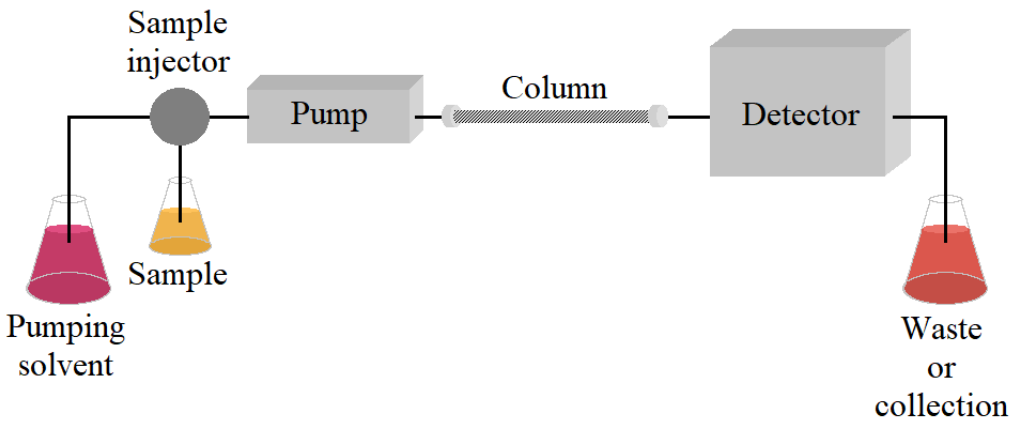

Figure 3.1: The set-up for liquid chromatography. The mobile phase (pumping solvent) is pumped through a column together with the sample to be studied. In the column, the components are separated into fractions that exit at different times. The different fractions are detected through absorption spectroscopy, and are then either collected or disposed of as waste.

There are several types of liquid chromatography, of which SEC, IEC and RP-HPLC (in the context of LC-MS) are employed in this project. In all types of liquid chromatography methods, the sample to be analyzed is pumped through a column packed with particles, also referred to as the stationary phase. In addition to the stationary phase, there is a so-called mobile phase; a solvent that is pumped through the column together with the sample. The components of the sample separate into fractions due to their different retention times (the time it takes for a certain compound to exit the column), depending on interactions with the stationary phase, mobile phase and other sample molecules.

The fractions that exit the column are then detected by a detector before either being collected for further analysis or disposed of as waste. Figure 3.1 illustrates a general scheme of the setup for liquid chromatography. A common choice for detecting the fractions is UV absorption spectroscopy, which is employed in this project.

3.2.1 Size-exclusion chromatography

SEC is a chromatographic technique that, just as gel electrophoresis, separates proteins and other molecules based on size. The sample is transported through a column filled with porous beads, typically made of dextran, agarose, or polyacrylamide polymers, of which pore sizes determine how long a molecule remains within a pore. Smaller molecules will remain longer than larger ones due to having access to a bigger column volume, compared to the larger molecules which cannot enter into the beads. This is illustrated in Figure 3.2. Larger molecules will therefore elute first followed by molecules of decreasing size. One advantage of SEC over size separation with gel electrophoresis is the possibility to preserve the proteins' biological properties.

It should be noted that the size separation by SEC is not necessarily based on molecular size, the hydrodynamic volume – the volume of a molecule when in a solution – also affects their flow behavior [50]. The hydrodynamic volume is dependent on molecular weight, but also on the interaction between the molecule and the solvent. The method assumes all molecules to have the same, symmetrical shape, which often is an adequate assumption. In the case of protein separation, they are usually assumed to be globular proteins. However, an asymmetrical molecule will elute faster than symmetrical molecules of similar mass. For the application of SEC in this project, this is

Figure 3.2: An illustration of the motion of sample and mobile phase molecules in relation to the stationary phase beads (with differently sized pores) used in SEC.

not a problem since it is not important how separation is obtained, only that it is.

3.2.2 Ion-exchange chromatography

IEC is another chromatographic technique that separates molecules based on net surface charges. There are two types of IEC; anion-exchange chromatography to separate negatively charged molecules, and cation-exchange chromatography to separate positively charged molecules [51]. To achieve these separations, the column in anion-exchange chromatography employs positively charged resins inside the column, while cation-exchange chromatography instead has negatively charged resins. The molecules in the sample form ionic or electrostatic interactions with oppositely charged stationary resins and are captured in the column, and both electrostatic charge, charge density and surface charge distribution influence the interactions.

After having captured the sample molecules in the columns based on either negative or positive net surface charge, the molecules can be eluted by applying a mobile phase with a gradually increasing ionic strength [51], in other words from lower to higher salt concentration. The ions formed in the salt solution can then replace the bonds between the sample molecules and the stationary phase resins, consequently releasing the captured molecules from the column. When the salt concentration increases, more strongly bounded molecules can be eluted.

3.2.3 Reversed-phase high-performance liquid chromatography

RP-HPLC is the final liquid chromatography method implemented in this project. It operates on the same principle as SEC and IEC, but separates molecules based on hydrophobicity and operates under higher pressure. Hydrophobicity is a physical property of molecules that implies being repelled from polar molecules due to their non-polarity. If a molecule is attracted to water (or any other polar substance), it is instead called a hydrophilic molecule. A well-known example of hydrophobic molecules are oils, which do not mix with water and instead create a phase separation. Hydrophobic interactions are important for many biological functions such as protein folding and the formation of cell membranes [52].

In this context, “reversed-phase” refers to a mode of action where a hydrophobic stationary phase and polar or moderately polar mobile phase is used, instead of the normal-phase HPLC setting which instead applies a hydrophilic column and non-polar mobile phase solvent [53, 54]. This means that for RP-HPLC, the most hydrophilic molecules will elute first, while the least polar molecules will be retarded by interactions with the stationary phase and exit the column at later times. Columns used for RP-HPLC usually have a stationary phase composed of silica with attached hydrophobic alkyl chains [55, 56]. In this project, a C4 column (composed of butyl groups) was used for the LC-MS measurements, which is recommended for

separation of proteins.

The mobile phase solvent and sample are continuously pumped through the column using high pressure. This is where HPLC differs from traditional liquid chromatography, which instead relies on the force of gravity to move the mobile phase and sample through the column. The use of high pressure is beneficial in order to speed up measurement times. The column pressure decreases with increased column temperature, which in turn reduces tear on the column. In addition, higher temperatures yield shorter retention time for analytes.

Different modes of action for mobile phase elution can be applied, such as isocratic or gradient elution. Gradient elution, in which the mobile phase is continuously altered during the measurement, is most often applied when the sample molecules have a wide range of retention times [57, 58]. The gradient shape can be either linear, segmented linear or non-linear, where linear is most common due to simpler optimization and operation, and can involve mixtures of two or three different solvents [59]. In contrast, isocratic elution implies the use of a mobile phase mixture that does not change composition over time [58]. In this project, linear gradient elution is implemented.

For gradient elution in RP-HPLC, the initial mobile phase solvent is composed of mainly the more polar solvent (usually water), with a gradually increasing proportion of the less polar solvent (usually an organic compound) throughout the analysis. The reason for this is to continuously increase the elution strength (the capacity of the mobile phase to remove analytes from the stationary phase) during the run.

3.2.4 Detection by ultraviolet absorption spectroscopy

The components that exit the columns in the chromatographic techniques described above are usually detected through UV absorption spectroscopy, which measures light absorbance for electromagnetic radiation in the ultraviolet range. The absorbance, A, of a compound can be related to its inherent absorption properties and concentration through Beer Lambert's law,

$$A = \log_{10}\frac{I_0}{I} = l\sum_i \varepsilon_i(\lambda)c_i \tag{3.1}$$

where I_0 and I are the intensities of the light beam before and after traveling through the sample, respectively, l is the optical path length, $\varepsilon_i(\lambda)$ is the molar attenuation coefficient of compound i for wavelength λ, and c_i the concentration of compound i [60]. The intensities I_0 and I are the properties measured during UV absorption spectroscopy. The value of $\varepsilon_i(\lambda)$ determines how strongly a material absorbs light at a specific wavelength. Equation 3.1 implies that a compound can be detected by measuring absorbance for a wavelength where its value of ε is high.
When used with chromatographic techniques, detection by UV-spectroscopy yield a graph of absorption over time for the liquid that exits the column for specified

wavelengths, in order to detect different fractions of components that pass through. The positions of distinct peaks indicate the retention time of an identified fraction of compounds. Proteins usually display high absorption for UV-light at around 280 nm, a property which originates from the aromatic amino acids tryptophan and tyrosine [61, 62]. Proteins can also be detected by measuring 214 nm absorption, due to absorbance by peptide bonds [63].

One drawback of Equation 3.1 is that deviations from the described relationship are expected if a non-monochromatic light source is used, due to the molecules absorbing light of multiple wavelengths at different proportions. In this project, polychromatic light sources were used, but since almost all proteins contain segments and parts (namely tryptophan, tyrosine and the peptide bonds) that absorb in a similar pattern regardless of the protein itself, it does not interfere with the aim of detecting proteins.

3.3 Liquid chromatography-mass spectrometry

LC-MS consists of an high performance liquid chromatography (HPLC) instrument coupled to a mass spectrometer, which allows for mass-to-charge ratio (and subsequently absolute mass) analysis of the different fractions separated in HPLC. LC-MS has numerous applications in biotechnical, pharmaceutical, food and environmental areas, to name a few. Additionally, mass spectrometry in itself is a central tool in biology, chemistry and physics.

In LC-MS, the HPLC instrument and mass spectrometer are coupled through an interface, which is necessary to transfer sample components from the HPLC column to the ionizer of the mass spectrometer. This is necessary due to the incompatibility of the two instruments, since the mobile phase of HPLC is a pressurized liquid while the mass spectrometer requires high vacuum.

As previously mentioned, mass spectrometry measures the mass-to-charge ratio of detected molecules. The principle of mass spectrometry is based on ionizing analyte molecules, from which resulting ions and charged molecules move through an electric field and hits a detector. The mass-to-charge ratio can be determined in different ways depending on the type of mass spectrometer. In this project, a quadrupole time-of-flight mass spectrometer is used, which combines quadrupole and time-of-flight mass analyzers. The setup of the quadrupole consists of four parallel metallic, conducting rods between which an alternating voltage is applied.

The mass and charge of each molecule determine the trajectory through the center of the rods, and only ions with a stable trajectory will hit the detector. The mass spectra are produced based on the time-of-flight for the molecules hitting the detector. Prior to sample molecules entering the mass spectrometer, they are ionized by an ion source. In this case, electrospray ionization was implemented as ion source; a technique that only causes very little fragmentation, meaning the whole molecules are most often ionized and detected.

3.4 Boyden chamber Assay

Boyden chamber Assay is a technique used for measuring leukocyte chemotaxis, first proposed in 1962 by Stephen Boyden [64]. In other words, it measures the extent of directional migration of leukocytes to a sample due to a chemotactic gradient. In principle, the method measures cell migration through a porous membrane from one chamber compartment to another that contains the sample with possible chemoattractants; see Figure 3.3 for an illustration of the set-up. The upper chamber consists of a serum-free medium, which is designed for cell culture.

For measuring neutrophil migration, a pore size of 3 µm is suitable since it is small enough for neutrophils to be able to pass through only by means of active migration (they can pass through gaps as small as 2 µm [65]) and not through diffusion since the neutrophil diameter is around 9-15 µm [66]. After some incubation time, the cells on the lower side of the membrane are collected and counted [64] using flow cytometry.

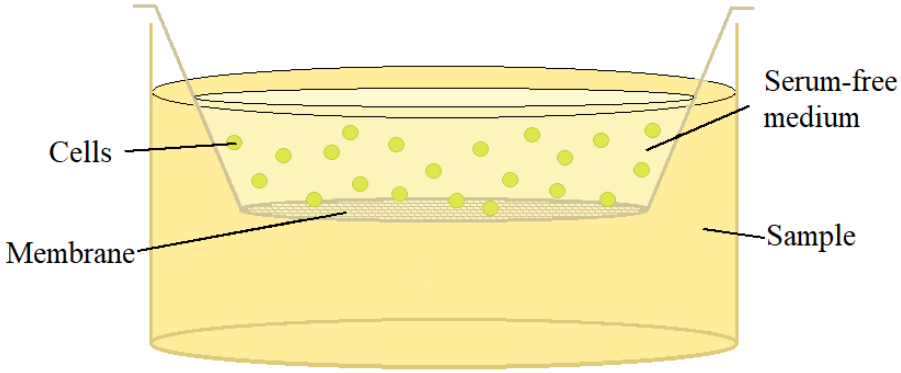

Figure 3.3: A sketch of the Boyden chamber assay used for chemotaxis measurements. The chamber is divided into two compartments by the porous membrane that allows for active, directional cell migration.

3.5 Flow cytometry

Flow cytometry is a technique with many applications for studying cells and other particles. For instance, it can be used to count particles, sort particles, measure size, granularity, fluorescence and more [67]. It is a widely used technique with applications in science as well as in medicine as a diagnostic tool. When used in combination with Boyden chamber assay, both cell size and granularity are of interest in order to identify the quantity of a specific cell type, in this case neutrophils.

The sample with cells is pumped to a flow cell where the so-called sheath fluid directs the cells by forming an outer liquid shell around the cell sample fluid. The sample is directed through the flow cell such that the cells pass by the light beam one by one, due to the sample having a higher pressure than the sheath fluid [68]. Figure 3.4 displays the set-up of a flow cytometer.

A light source illuminates the sample traveling through the flow cell, and the outgoing light is detected by detectors and converted to electronic signals that are amplified and processed [68]. Different cellular properties can be deduced by analyzing different outgoing light; forward scattered light to measure cell size, side scattered light to measure granularity (amount of intracellular granules) or intracellular complexity, and fluorescent light to determine other properties.

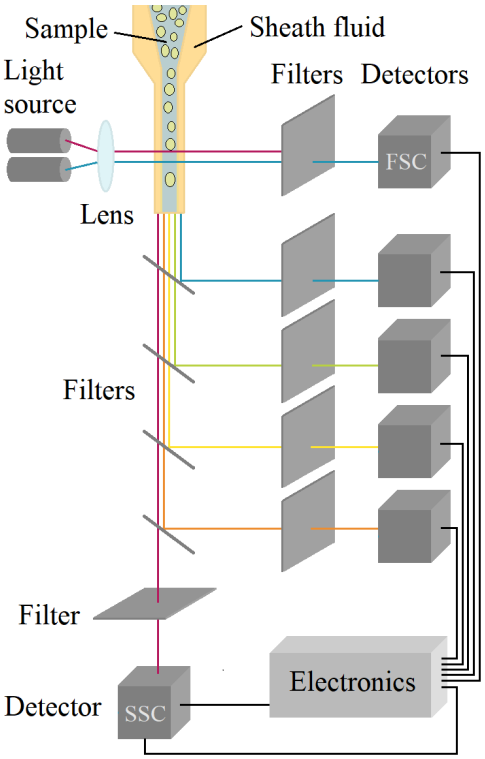

Figure 3.4: The set-up of a flow cytometer. The cell sample is guided through the flow cell with the help of sheath fluid such that only one cell at a time passes the light illuminated from the light source. Outgoing light from the sample hits the detectors and is converted to electronic signals which are then amplified.

To count the number of cells of a specific cell type, forward scattered light and side scattered light can be combined in a 2-dimensional scatterplot which in principle shows the size versus granularity of the detected cells. The number of counts for a specific cell type can then be approximated by excluding all detected cells which have a different granularity, size, or granularity-size-ratio than expected for the cell of interest.

4

Materials and methods

The theory and principles of the methods used in this project were covered in chapter 3. In this chapter, the materials and specific conditions used for these methods are described, starting with the sample preparation that was performed before all experiments. Furthermore, the step-by-step methodology is reviewed.

As stated previously, the complexity of the problem of searching for chemoattractants among several hundred, or more, other molecules was reduced by separation of synovial fluid components. A general overview of the methods applied to achieve this was provided in chapter 3, but in practice these methods were divided into two different approaches; one which uses gel electrophoresis as a basis for component separation (denoted approach one) and one which relies on liquid chromatography methods (denoted approach two). An overview of the step-by-step structure for methods used is presented in Figure 4.1. The description of the methodology is thus divided into two sections, one for each approach.

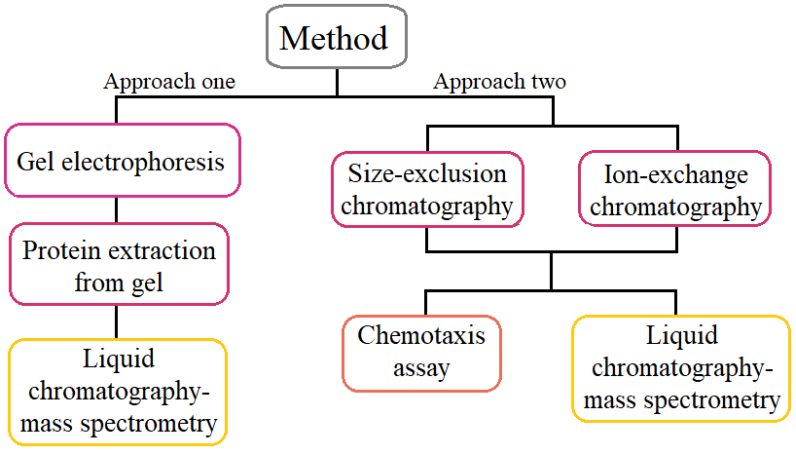

Figure 4.1: An overview of the methodology implemented in this project.

4.1 Sample preparation

The cells in the synovial fluid samples were spun down and removed prior to the start of the project, and cell-free synovial fluids were provided by the supervisors. Synovial fluid from two different patients was used; one with ≈90 % (with RA diagnosis) neutrophils and one with ≈5 % neutrophils (with monoarthritis diagnosis), of the

total leukocyte population in the fluid before filtering out the cells (as determined based on flow cytometry plots, which can be found in Appendix A). This allowed for a more detailed investigation of which components might attract neutrophils to a larger degree, since a higher concentration of neutrophils could indicate a higher presence of chemoattractants, or a different chemoattractant composition.

Before conducting measurements, the synovial fluids were treated with hyaluronidase from bovine testes (Sigma-Aldrich, #H3506) to digest the highly viscous hyaluronic acid, which is present in high concentration in synovial fluid [69]. The reason for this is to increase the solubility of the synovial fluid, which is a necessity for the chromatographic measurements (SEC, IEC and RP-HPLC). The hyaluronidase treatment was executed in accordance with protocols [70, 71], by preparing a fresh solution of 1 mg/mL hyaluronidase in phosphate-buffered saline (PBS) which was added to the synovial fluid in a 1:11 ratio. The samples were incubated in an Eppendorf Thermomixer at 37 °C, with 550 revolutions per minute (rpm), for 30-60 minutes, before being centrifuged for 20-30 minutes in Grant Combi-spin Centrifuge PCV-2400 or for 10 minutes in an Eppendorf Centrifuge 5418 R with 16000 relative centrifugal force (rcf). The supernatants were transferred to new tubes and used for further experiments.

4.2 Approach one: Separation by gel electrophoresis

This approach is based on the separation of components in the synovial fluid samples on the basis of size using gel electrophoresis. This method may alter the biological functions of the proteins, including the chemoattractants of interest, why further measurements on the chemotactic activity of the samples are not considered. Instead, the contents are directly examined using LC-MS. This approach may be one potentially reliable choice in the aspiration for identifying neutrophil chemoattractants, since molecules identified by LC-MS can be tested for chemotactic activity in a later stage by directly running chemotaxis experiment on recombinant varieties of those molecules.

4.2.1 Gel electrophoresis

The hyaluronidase-treated synovial fluid samples were diluted in distilled water (that was pre-heated to 37 °C to match the temperature of the synovial fluid) to the desired dilution. The sample was then centrifuged for another 20-30 minutes in Grant Combi-spin Centrifuge PCV-2400, and its supernatant was used for the gel electrophoresis.

The gel electrophoresis was performed with SDS sample buffer with 0.1 M dithiothreitol (DTT) (to make it reducing). 5 µl of sample was mixed with 2.5 µl of sample buffer and 2.5 µl of 0.2 M DTT-solution (to make sample buffer reducing), and 10 µl of the mixture was loaded in each well. In addition to the sample mixtures, 10 µl

of Precision Plus Protein Dual Color Standards protein ladder (Bio-Rad, #1610374) was loaded to one of the wells. The experiment was run with an applied voltage of 90 V and a current of 400 mA on the gel for approximately 55 minutes.

The gel was then put in a fixing solution overnight, in order to fix the proteins in the gel to prevent smearing, after which it was stained in a staining solution for around 2.5-3 hours. Finally, the gel was destained in 10 % acetic acid (and 90 % distilled water) until the protein bands were distinct.

The fixing solution used was prepared according to:

- 7.708 g ammonium acetate
- 100 ml acetic acid
- 500 ml methanol
- 400 ml distilled water

The staining solution was made with:

- 50 ml acetic acid
- 0.126 g Coomassie Brilliant blue R
- 449.875 ml distilled water

4.2.1.1 Preparative gel electrophoresis for LC-MS

To divide the sample into different size fractions, as well as remove proteins of sizes too large for the RP-HPLC column used in LC-MS (proteins $\geq$ 100 kDa), preparative gel electrophoresis was conducted. The methodology of the preparative gel electrophoresis is identical to the analytical gel electrophoresis, but fractions of the resulting gels are cut out and collected and the staining procedure differs somewhat. To maximize the amount of sample that can be recovered from the gel, a gel on which a higher volume of sample can be loaded was used. As a sample buffer lithium dodecyl sulfate (LDS) with 0.1 M DTT was used. LDS has the same functional group – dodecyl sulfate – as SDS.

The gel electrophoresis was performed with identical procedure and conditions as the analytical gel electrophoresis, with the exception of loading $\approx$ 48µl of 50 % sample, 25 % LDS sample buffer and 25 % 0.2 M DTT. After having incubated the gel in fixing solution overnight, the ladders were cut out and removed from the rest of the gel, and put in staining solution. The ladders were then re-aligned with the unstained portion of the gel, and each well with sample in the unstained gel was cut into 4 different mass intervals; <15 kDa, 15-25 kDa, 25-37 kDa, 37-50 kDa approximately, using a razor blade.

4.2.1.2 Protein extraction from gel

Proteins were extracted from each small cut-out gel piece by first crushing the gel pieces using a pestle, after which 500 µl extraction buffer was added. The extraction buffer was made according to:

- 0.0790 g Tris-HCl
- 0.0881 g NaCl
- 0.0028 g ethylenediaminetetraacetic acid (EDTA)
- 10 ml distilled water

The final solution had a pH value of ≈ 4.6. The tubes with crushed gel and extraction buffer were then incubated in an Eppendorf Thermomixer overnight, with 30 °C and 550 rpm.

To achieve a higher protein concentration in the samples for the LC-MS measurements, the sample fractions of recovered synovial fluid proteins from gel electrophoresis were lyophilized (freeze-dried) in a Martin Christ Alpha 1-2 LDplus freeze-dryer, with -60 °C and $\approx$ 0.02 mbar. For this, the samples were taken directly from a -80 °C freezer, since the samples have to be frozen before the lyophilization. After lyophilization, the freeze-dried protein samples were re-diluted in 50 µl PBS (resulting in the samples being concentrated 10 times from the initial volumes of 500 µl).

4.3 Approach two: Separation by liquid chromatography

The second approach consists of separation based on several chromatographic methods, which can be managed with conditions that preserve the biological function of proteins. This allows for measuring the chemotactic activity of fractions to illuminate which fractions are of the highest interest for the purpose of this study. To separate the contents of the synovial fluid samples into fractions with different components, SEC and IEC were employed, after which a chemotaxis assay was used to measure the chemotactic activity of obtained fractions from SEC and IEC. Just as for approach one, the fractions are also examined using LC-MS.

4.3.1 Size-exclusion chromatography

The sample preparation for SEC follows the same procedure as for the gel electrophoresis experiment.

For the measurement, an ÄKTA chromatography system was used, with the column Superdex 75 10/300 GL, with 13 µm average particle size, column volume 23.562 ml. The column can separate molecules in size range 3 kDa to 70 kDa. As a running

buffer, PBS (pH 7.4) was used, with a flow rate of 0.500 ml per minute. Approximately 0.3 ml of sample was injected. Detection of the eluted solution was set at 280 nm and 214 nm, and collection of the eluted solution was done in a well-plate, with 0.5 ml collected in each well.

This measurement was done for both the synovial fluids (the one with initially 90 % neutrophils, as well as the one with initially 5 % neutrophils).

4.3.1.1 Gel electrophoresis of fractions from size-exclusion chromatography

To examine if the size separation was successful, gel electrophoresis was run for all fractions with peaks in the UV-spectra.

In preparation for the gel electrophoresis, 15 µl of each sample was mixed with 5 µl of 4x Laemmli sample buffer (Bio-Rad, #1610747) which has DTT added from before to make it reducing, and the mixture was boiled in 98 °C for about 1.5 minutes. Each well was loaded with 8 µl of the boiled mixtures or protein ladder Precision Plus Protein Unstained Standards (Bio-Rad, #1610363), according to the set-up.

A Mini-PROTEAN TGX Stain-Free Precast Gel (Bio-Rad, #456-8096) with polyacrylamide gradient of 4-20 % was used, with running buffer 10x Tris/Glycine/SDS buffer (Bio-Rad, #1610772) diluted 10 times. The electrophoresis was run for 30 minutes with 200 V and 400 mA. The gels were then stained using SimplyBlue SafeStain (Thermo Fischer Scientific, #LC6065), which is a coomassie blue stain.

4.3.2 Ion-exchange chromatography

Due to small proteins sticking to the larger one and eluting together with them during the SEC (see Results section 5.2.1), IEC was performed in order to try separating the proteins from each other.

To achieve this, the sample was initially run through two succeeding columns, one column (HiTrap Q XL column) to capture anions and one (HiTrap SP XL column) to capture cations, of 1 ml column volume each. As a running buffer, 25 mM Tris-HCl (pH 7.2) with 1 mM DTT was used. The reason for the inclusion of DTT is to reduce disulfide bonds that are often formed between proteins. A flow rate of 1.000 ml per minute was applied. Even though in principle all proteins should get stuck in the columns, the eluting solvent was collected and saved.

The sample that was injected for this initial run was a solvent of total 50 ml composed of eluting solvent collected from a previous SEC run where approximately 0.3 ml treated synovial fluid (IEC was only performed for the 90 % neutrophils synovial fluid due to time restrictions) sample was injected, with a running buffer of PBS with 1 m KCl that were later dialysed in a SnakeSkin Dialysis Tubing (Thermo Fisher Scientific, #88244) placed in 2 l of 25 mM Tris-HCl with magnetic stirring

for 70 minutes, in room temperature.

To collect the proteins captured in the two columns, two additional runs were performed, one for each column, where linear gradient running buffer was used, starting with low salt concentration and successively increasing to elute proteins with higher affinity for the column (in principle more charged proteins). To achieve this, two different buffers were used, one with 25 mM Tris-HCl and 1 mM DTT (denoted A) for low salt concentration, and one with 25 mM Tris-HCl, 1 M NaCl and 1 mM DTT (denoted B) for high salt concentration. The linear gradient was implemented as follows:

1. Five column volumes of 100 % A, 0 % B.
2. Five column volumes of 95 % A, 5 % B.
3. Ten column volumes of linear gradient from 95 % A, 5 % B to 0 % A, 100 % B.
4. Five column volumes 0 % A, 100 % B.
5. Three column volumes of 100 % A, 0 % B.

A flow rate of 1.000 ml per minute was applied. The eluted solvent was collected in well-plates with 0.5 ml collected in each well, with detection at 280 nm, 214 nm and 254 nm.

4.3.2.1 Gel electrophoresis of fractions from ion-exchange chromatography

To verify separation of smaller proteins from larger proteins, gel electrophoresis was run with identical conditions and procedure as for the gel electrophoresis after SEC (see Section 4.3.1.1). This was done for each well in the IEC with a distinct peak, and for every other well for places in the spectra with constantly high absorption.

4.3.3 Chemotaxis assay

The chemotaxis assay experiment is dependent on the usage of fresh, isolated cells. Therefore, this section first covers how neutrophils were isolated from blood prior to the chemotaxis assay, after which the set-up and running conditions of the Boyden chamber assay and subsequent counting by flow cytometry are described. The whole chemotaxis assay experiment was performed two different times, with two different sample set-ups, to include all fractions of interest in the experiment.

4.3.3.1 Isolation of neutrophils

Initially, the erythrocytes (red blood cells) had to be separated and removed from the blood. This was done by mixing fresh blood with physiological saline (0.9 % NaCl) with 2% dextran T500 (Pharmacosmos, #6962) which induces erythrocyte aggregation [72]. Physiological saline has the same osmotic pressure as blood, which also contains 0.9 % NaCl, a necessity to maintain viable conditions for the cells [73]. The mixture rested at 1 g for $\approx 25 - 30$ minutes to let the erythrocytes sediment

to the bottom, yielding a clear separation from the supernatant (which contains the leukocytes).

The supernatant is then centrifuged in an Beckman Coulter Allegra X-12R (Rotor SX4750) with 900 rpm, 4 °C, for 10 minutes. After this, the pellet is kept while the supernatant is removed. Any remaining erythrocytes are lysed (broken down).

To separate the mononuclear leukocytes (monocytes and lymphocytes) from the polymorphonuclear leukocytes of interest, 15 ml Ficoll-paque (GE-Healthcare Bio-Sciences), was gently added to the bottom of the tube. The solution was then centrifuged once more in Beckman Coulter Allegra X-12R (Rotor SX4750) with 1200 rpm, 4 °C, for 30 minutes. Ficoll-paque has a density between that of the mononuclear cells and the polymorhponuclear cells, and can thus be used to separate the two cell types by adding it to the sample of interest and centrifuging. This places the granulocytes (and potential remaining erythrocytes) in the pellet, with a Ficoll-paque layer between that and a layer of mononuclear cells. There will also be an uppermost phase of supernatant. Everything but the pellet was removed.

The solution was then washed with 35 ml Krebs-Ringer Glucose phosphate buffer (KRG) and centrifuged in Beckman Coulter Allegra X-12R (Rotor SX4750) with 900 rpm, 4 °C, for 10 minutes. KRG was made with 120 mM NaCl, 4.9 mM KCl, 1.7 mM KH_2PO_4, 8.3 mM NaH_2PO_4, 1.2 mM $MgSO_4$ and 10 mM glucose in distilled water (pH 7.3). The cells in the resulting pellet were then resuspended in KRG with 1 mM $CaCl_2$, and neutrophil purity and yield were analyzed with Sysmex KX-21N Hematology Analyzer. The obtained neutrophil purity was 94.9 % for the first experiment, and 91.5 % for the second. The solution with cells was finally diluted with KRG with 0.3% bovine serum albumin (BSA) (Sigma-Aldrich, #A9647-50G) to a concentration of $\approx 2 \cdot 10^6$ cells per ml.

4.3.3.2 Boyden chamber assay

A Boyden Chamber Assay was employed to measure the chemotactic capacity of different synovial fluid fractions divided based on protein sizes. For this, only the fractions obtained from the SEC was used and not the ones obtained from the preparative gel electrophoresis, since intact biological properties is a necessity to accurately measure the chemotactic potential of the proteins.

	1	2	3	4	5	6	7	8	9	10	11	12
A	Spont	→	→	100% control	→	→	fMLF (10 nM)	→	→	SF 90%	→	→
B	SF 90% H	→	→	SF 90% SEC B6-B7	→	→	SF 90% SEC B8	→	→	SF 90% SEC B9-B10	→	→
C	SF 90% SEC B11	→	→	SF 90% SEC B12	→	→	SF 90% SEC C1	→	→	SF 90% SEC C2	→	→
D	SF 90% SEC C3-C6	→	→	SF 90% SEC C7-C12	→	→	SF 90% SEC D1	→	→	SF 90% SEC D2-D4	→	→
E	SF 90% SEC D5	→	→	SF 90% SEC D6-D7	→	→	SF 90% SEC D8-D10	→	→	SF 90% SEC D11	→	→
F	SF 90% SEC D12	→	→	SF 90% SEC E1-E2	→	→	SF 90% SEC E3-E4	→	→	SF 90% SEC E5-E8	→	→
G	SF 90% IEC SP A6-A7	→	→	SF 90% IEC SP A10-A11	→	→	SF 90% IEC SP B2-B3	→	→	SF 90% IEC SP B6-B7	→	→
H	SF 90% IEC SP B10-B11	→	→	SF 90% IEC SP C2-C3	→	→	SF 90% IEC SP C6-C7	→	→	SF 90% IEC SP C10-C11	→	→

Table 4.1: The set-up on the chemotaxis plate for an assay of size-exclusion chromatography fractions (wells B4 to F10) and ion-exchange chromatography anion fractions (wells G1-H10) of the synovial fluid with initially 90 % neutrophils. Samples of naive synovial fluid (well A10) and hyaluronidase-treated synovial fluid indicated by an H (well B1), both diluted 1:4 in KRG + 0.3 % BSA, were also measured. All size-exclusion chromatography and ion-exchange chromatography anion fractions were collected from 90 % synovial fluid treated with hyaluronidase.

The samples were run in triplicates in order to obtain higher certainty and guard against potential errors in one or more of the wells due to the vulnerability of the method. This can be seen in the set-up in Table 4.1, where the measured samples are noted. The first three triplicates correspond to positive and negative controls as references for chemotaxis. For the first triplicate, a buffer without chemoattractants is loaded in the bottom well, to act as a negative control for spontaneous migration. This is followed by a positive control, where cells are loaded directly in the bottom well instead of the top of the membrane, where a buffer without cells is added on top of the membrane. Finally, a triplicate with 10 nM of the neutrophil chemoattractant fMLF is used.

Pure synovial fluid samples, untreated and treated with hyaluronidase, respectively, were also measured for chemotactic ability as references. They were diluted 1:4 in

KRG with 0.3% BSA prior to transfer to the 96-well plate. Unlike previous sample preparation for hyaluronidase treatment, the hyaluronidase-treated sample was incubated in a 35 °C room on a rotary shaker for 80 minutes before centrifugation, due to the lack of access to an Eppendorf Thermomixer.

	1	**2**	**3**	**4**	**5**	**6**	**7**	**8**	**9**	**10**	**11**	**12**
A	Spont	→	→	100% control	→	→	fMLF (10 nM)	→	→	SF 90%	→	→
B	SF 90% H	→	→	SF 4%	→	→	SF 4% H	→	→	SF 4% SEC B4-B5	→	→
C	SF 4% SEC B6	→	→	SF 4% SEC B7	→	→	SF 4% SEC B8-B9	→	→	SF 4% SEC B10-C2	→	→
D	SF 5 % SEC C3-C7	→	→	SF 5 % SEC C8-C11	→	→	SF 5 % SEC C12-D1	→	→	SF 5 % SEC D2	→	→
E	SF 5 % SEC D3	→	→	SF 5 % SEC D4-D5	→	→	SF 5 % SEC D6-D7	→	→	SF 5 % SEC D8-D10	→	→
F	SF 5 % SEC D11-E1	→	→	SF 5 % SEC E2	→	→	SF 5 % SEC E3-E6	→	→	SF 5 % SEC E7-E8	→	→
G	SF 90% IEC elution	→	→	SF 90% IEC Q B6-B7	→	→	SF 90% IEC Q B8-B9	→	→	SF 90% IEC Q B10-B11	→	→
H	SF 90% IEC Q B12-C1	→	→	SF 90% IEC Q C2-C3	→	→	SF 90% IEC Q C4-C5	→	→	SF 90% IEC Q C6-C7	→	→

Table 4.2: The set-up on the chemotaxis plate for an assay of size-exclusion chromatography fractions (wells B10 to F10) and ion-exchange chromatography elution (well G1) as well as ion-exchange chromatography cation fractions (wells G2-H10) of the synovial fluid with initially 90 % neutrophils. Samples of naive synovial fluids (well A10 and B4) and hyaluronidase-treated synovial fluids, indicated by an H (wells B1 and B7), both diluted 1:4 in KRG + 0.3 % BSA, were also measured. All size-exclusion chromatography fractions are collected from 5 % synovial fluid treated with hyaluronidase, while the ion-exchange chromatography elution as well as ion-exchange chromatography cation fractions are collected from 90 % synovial fluid treated with hyaluronidase.

30 µl of each sample was added into the wells of the chemotaxis plate, using a multichannel pipette. The 3 µm filter membrane was then applied, making sure that the membrane makes contact with all sample droplets. Finally, 30 µl of cell suspension with in total $\approx 6 \cdot 10^4$ neutrophils was added on top of the membrane for each well except for the positive control wells A4-A6, onto which KRG with BSA was added.

The cover lid was applied and the plate was incubated with 37 °C and 5 % CO_2 in a Forma Steri-Cycle CO2 Incubator (Model 371, Thermo Scientific) for 90 minutes. After incubation, the cover lid and membrane were carefully removed, and the cells that had migrated to the bottom of the wells were collected through repeated washing with 0.48 mM EDTA to detach adherent cells.

To preserve the collected neutrophils in a life-like state for the next day's counting, the cells were fixated with paraformaldehyde (PFA) to a final concentration of 2 %. In short, fixation by PFA hardens the cell surface [74]. The fixated cells were counted in a CytoFLEX S flow cytometer (Beckman Coulter). A total volume of 30 µl was recorded for each sample, with a flow rate of 30 µl per minute. The software FlowJo v10.9.0 was used to analyze the data.

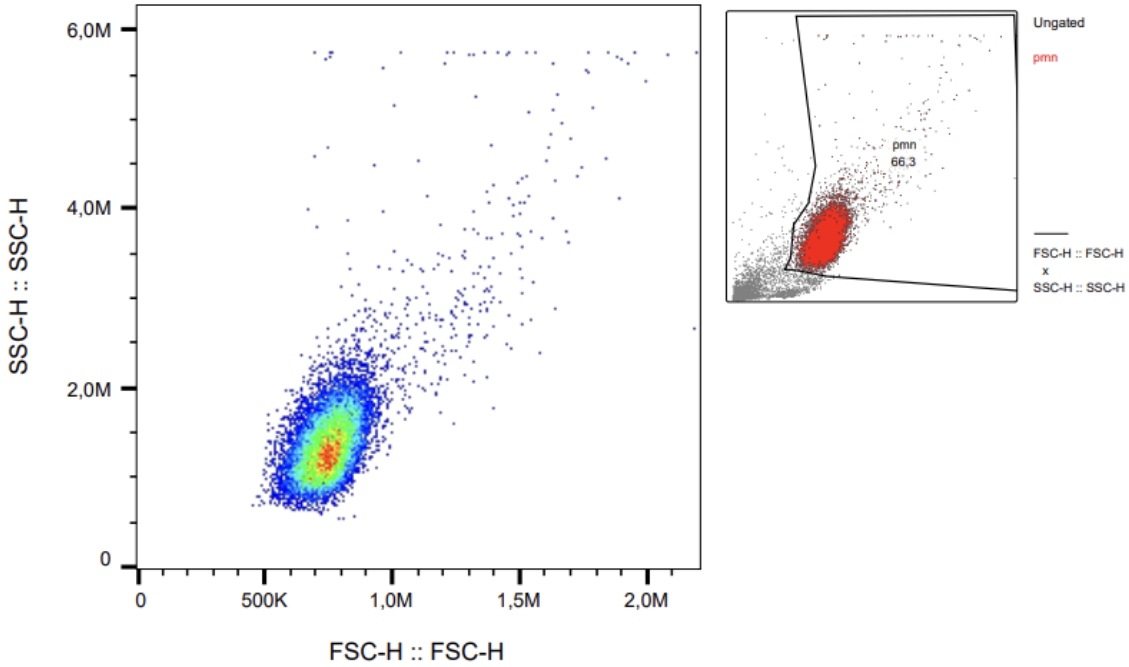

Figure 4.2: The gate used for all samples to include only granulocytes is shown in the upper right figure. All particle counts (for the positive control sample from the first chemotaxis set-up, in this case) are also shown as an example of which cells the gate include and exclude. The red dots represent counts included in the gate while the grey detections are excluded. The left figure is the resulting SSC-FSC plot when only the counts inside the gate are displayed.

A scatter plot was produced for all detections by the flow cytometer, with the value of side-scattered light (SSC) versus the value of forward-scattered light (FSC) for each particle. The total number of counts is not of interest here, since that includes all types of cells (since 100 % neutrophil purity was not obtained during the isolation of neutrophils from blood) and other particles such as dirt, in addition to neutrophils. Therefore, a gate was applied to mark an area in the SSC-FSC plot corresponding to the properties of neutrophils, to exclude all other particles which are not of interest here.

Neutrophils are quite large in comparison to other leukocytes – generating quite a high FSC value – and have a high granularity – yielding a high SSC value. The gate was therefore applied to include only the larger and high granularity cells detected. The same gate was used for all samples, and is presented in the upper right picture in Figure 4.2, which also displays the cells that are excluded and included for that particular sample (the positive control of the first chemotaxis run).

4.4 Liquid chromatography-mass spectrometry

The LC-MS measurements were run on a Waters Acquity UPLC system (Waters, Milford, MA, USA) with a Waters 2998 photodiode array (PDA), coupled with a Waters SYNAPT G2-Si HD-MS spectrometer. The measurements were run with 60° C column temperature, with an ACQUITY UPLC Protein BEH C4 1.7 µm (2.1 mm x 50 mm) column.

For the mobile phase composition, a mixture of distilled water with 0.1 % formic acid, denoted A, and acetonitrile (ACN) with 0.1 % formic acid, denoted B, was implemented with a step-wise linear gradient, for seven minutes in total, according to:

1. Two minutes with 100 % A, 0 % B.
2. 2.3 minutes of linear gradient from 100 % A, 0 % B to 40 % A, 60 % B.
3. 0.3 minutes with 40 % A, 60 % B.
4. 0.6 minutes of linear gradient from 40 % A, 60 % B to 10 % A, 90 % B.
5. One minute of 10 % A, 90 % B.
6. 0.2 minutes of linear gradient from 10 % A, 90 % B to 90 % A, 10 % B.
7. 0.6 minutes with 90 % A, 10 % B.

The formic acid is included to provide protons for the LC-MS analysis [75]. A flow rate of 0.400 ml per minute was used. Steps 6 and 7 were executed in order to prepare the instrument for the next measurement.

For the mass spectrometer part of the set-up, it was configured for the detection of compounds with mass-to-size ratios of 100 - 4000 Da, however with lower sensitivity approximately for mass-to-charge ratios of 100 - 500 Da.

5
Results and discussion

In this chapter, the results from the implemented methods introduced in chapters 3 and 4 are first presented and discussed individually, one approach at a time and one implemented method at a time. As the aim of this project is to develop and evaluate methods for identification and characterization of chemoattractants in inflamed synovial fluid from patients with IA, the results are mainly discussed in regards to the success of the method rather than the results themselves. However, in some cases the results themselves are also quite interesting and will in those cases be discussed. This chapter concludes with a section analyzing all results in combination, in order to fully evaluate the two approaches (separation by gel electrophoresis and separation by liquid chromatography).

5.1 Approach one: Separation by gel electrophoresis

The results from the experiments conducted as part of the approach involving separation by gel electrophoresis are presented in this section, accompanied by associated discussions. First, the results from the initial gel electrophoresis measurements are presented, where the sample composition in terms of protein sizes was loosely examined in preparation for the preparative gel electrophoresis procedure. The results from the LC-MS measurements of extracted proteins from different bands cut out from the gel are then presented and discussed.

5.1.1 Gel electrophoresis

To examine the size distribution of synovial fluid components and investigate appropriate dilutions, initial gel electrophoresis measurements were performed before proceeding with running gel electrophoresis in preparation for protein extraction.

Figure 5.1 displays the gel from gel electrophoresis of both synovial fluids, with the protein ladder in the center. Both synovial samples were run with dilutions 1:3 and 1:7 in distilled water, in order to investigate concentration dependencies on the result. A too low concentration yields too few proteins for bands to appear, while too high a concentration might clog the pores in the gel, blocking smaller proteins from traveling further. The values of the protein ladder are indicated to the right of the sample wells.

The majority of proteins present in the synovial fluid samples seem to be of large sizes between 37 kDa and 250 kDa. The 1:3 sample dilutions show more small protein bands, and are therefore considered more optimal for further investigation of smaller proteins (of which most known chemoattractants are). Comparing the two synovial fluids, the overall contents seem quite similar, although the 90 % synovial fluid seems to have some bands under 20 kDa that are not as visible for the 5 % synovial fluid.

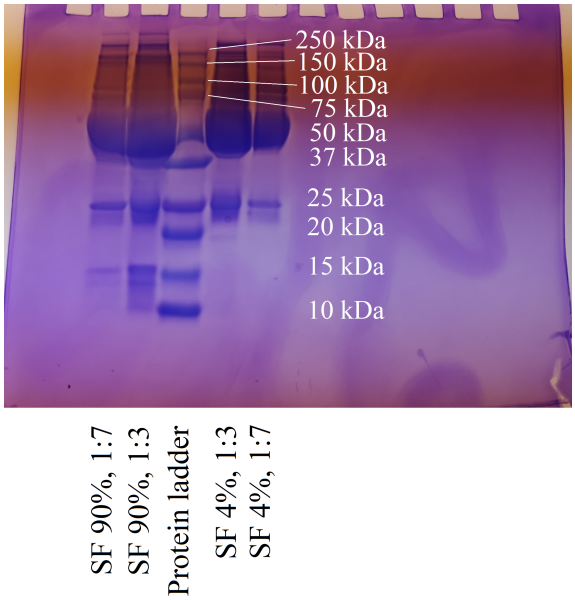

Figure 5.1: The gel from electrophoresis of the synovial fluid with 90 % neutrophils and 5 % neutrophils, respectively (prior to cell removal). Of each sample two different dilutions are shown; a 1:3 ratio of sample versus distilled water and a 1:7 ratio of sample versus distilled water.

Based on the results, a dilution of 1:3 in distilled water was chosen for the preparative gel electrophoresis. No direct results were obtained from the preparative gel electrophoresis since the gel was not stained in that case, but indications of those results can be found in the LC-MS measurements, which are presented next in section 5.1.2.

5.1.2 Liquid chromatography-mass spectrometry of fractions from gel electrophoresis

After running the preparative gel electrophoresis, where different pieces of non-stained gel were cut out, proteins were extracted and freeze-dried for further analysis using LC-MS. Due to time restrictions, freeze-drying and subsequent LC-MS measurements were only performed for the 90 % synovial fluid. The results from the LC-MS are presented in the forms of total ion chromatograms and UV-absorption at 280 nm, over time. The total ion chromatogram is composed of the summed intensities of all detected masses by the mass detector for each time.

Figure 5.2 displays detection for the extracted proteins with sizes <15 kDa and 15-25 kDa, respectively, from the gel with the 90 % synovial fluid, with the total ion chromatogram in (a) and UV-absorption at 280 nm in (b). A blank measurement (of pure PBS), conducted just before the measurement of the samples with <15 kDa proteins, is also included as a background reference. No measurements were performed on proteins extracted from the 5 % synovial fluid, due to space restrictions (for the freeze-dryer) and limited time for this project.

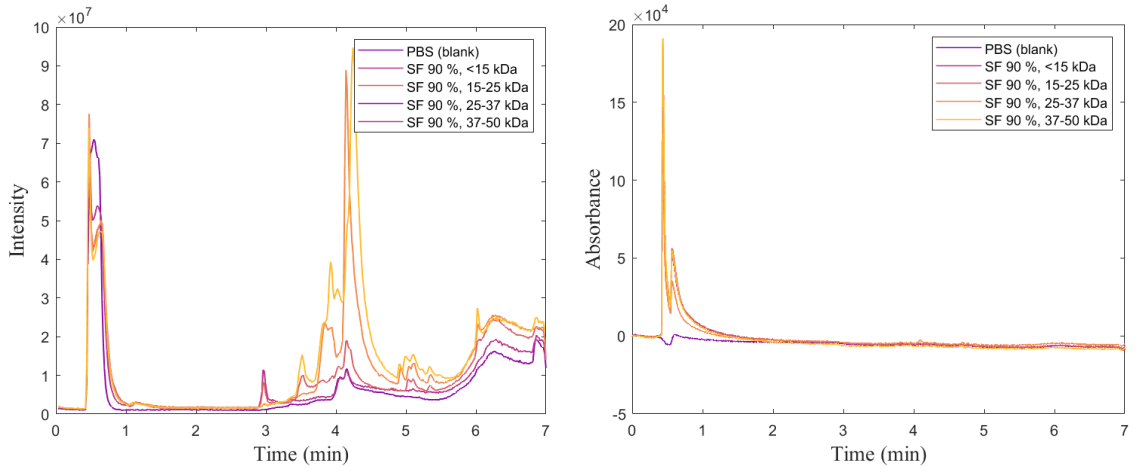

(a) (b)

Figure 5.2: The total ion chromatogram in (a) and UV-absorption at 280 nm in (b) for proteins extracted from gel electrophoresis of the 90 % synovial fluid, with size ranges <15 kDa, 15-25 kDa, 25-37 kDa and 37-50 kDa, as well as the PBS (blank) measurement run before the <15 kDa sample.

For both the total ion chromatogram and the UV-absorption at 280 nm, almost all visible peaks are common between the different protein samples, but in different intensities. All the peaks that are not visible in the blank measurement could indicate proteins extracted from the gels, however, since the peaks are visible for all samples, this is probably not the case. Since gel pieces corresponding to different size ranges were cut from the gels, the different pieces should contain different proteins. This could indicate the presence of some contamination from for example the extraction solution (and reagents used to prepare it), which was used for all the samples. The peaks that are also visible for the PBS sample could be attributed to column contaminations.

Overall, the LC-MS results do not show promise for the separation with gel electrophoresis. There is a possibility for the method to work if there were no contaminations in the samples. However, the whole protein extraction procedure might also have to be revised.

5.2 Approach two: Separation by liquid chromatography

Moving on from the separation using gel electrophoresis, this section comprises the results and discussion of each experimental method belonging to the approach based on separation with chromatography. First, the results for the fractions obtained from SEC are presented and discussed, whereupon the gels from gel electrophoresis of different collected fractions are presented. Following this, the same is repeated for the results from the IEC. The chemotaxis assay experiments, where the chemotactic ability of fractions collected from both SEC and IEC was investigated, are then discussed. Finally, results from the LC-MS measurements are presented, first for the SEC fractions, then for the IEC fractions. Both LC-MS sections present total ion chromatograms and UV-absorption at 280 nm, followed by a more detailed analysis of compounds through dissection of the obtained mass spectra for peaks of interest.

5.2.1 Size-exclusion chromatography

Initially, size separation of synovial fluid components was attempted using SEC. The UV-absorption at 280 and 214 nm are presented in Figures 5.3 and 5.4 for the synovial fluids initially containing 90 % neutrophils and 5 % neutrophils, respectively. These wavelengths were chosen due to the high protein absorption (as explained in section 3.2.4). The UV absorption is plotted as a function of eluted volume from the column. The grey vertical lines separate the wells where the eluting solvent is collected (of which well labels are indicated at the bottom).

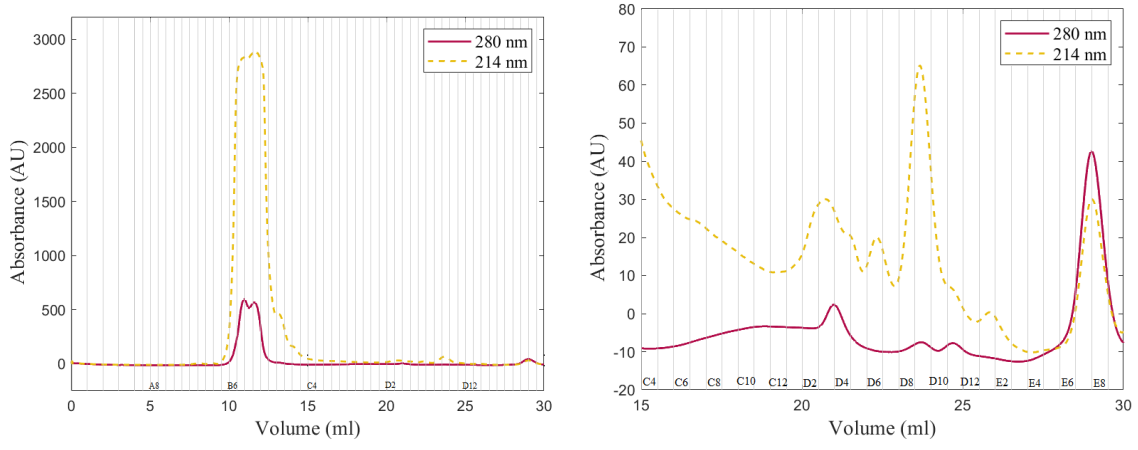

(a) (b)

Figure 5.3: UV-absorption as a function of eluting volume from the column for SEC of ≈ 0.3 ml hyaluronidase treated 90 % synovial fluid. The absorbance is measured at wavelengths 280 nm and 214 nm. Figure (a) shows the entire spectrum, while (b) is magnified for the segment between 15 and 30 column volumes.

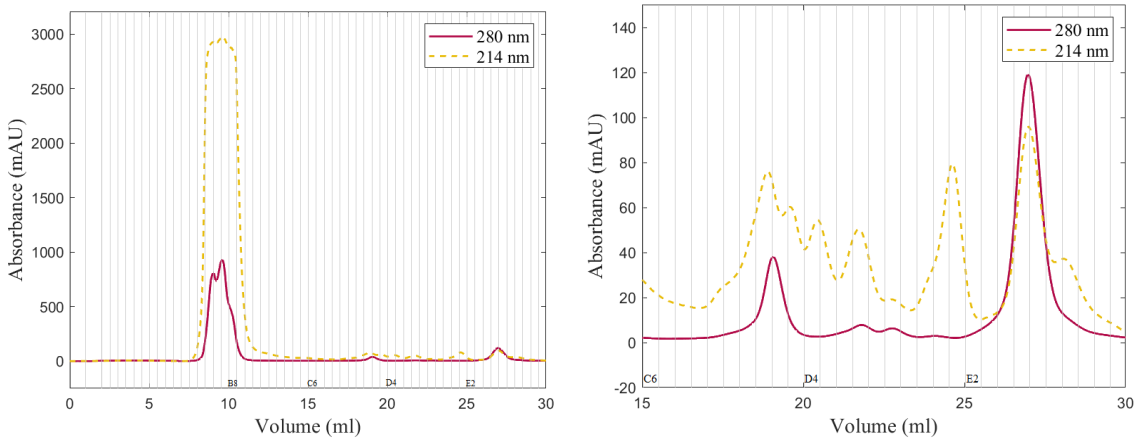

(a) (b)

Figure 5.4: UV-absorption as a function of eluting volume from the column for SEC of ≈ 0.35 ml hyaluronidase treated 5 % synovial fluid. The absorbance is measured at wavelengths 280 nm and 214 nm. Figure (a) shows the entire spectrum, while (b) is magnified for the segment between 15 and 30 column volumes.

The proteins elute with decreasing sizes as a function of volume. In Figures 5.3 (a) and 5.4 (a), it is clear that the majority of sample contents elute between 10 and 15 ml and indicate relatively large sizes, while smaller proteins only give rise to very small peaks.

For both synovial fluids, there is some separation occurring, based on the different peaks. However, the first peaks are very large and could imply either that the samples are composed of a lot of similarly sized, relatively large proteins, or that proteins of other sizes aggregate with the larger proteins and elute together with those.

The UV-absorption over time for the two synovial fluids is very similar but exhibits a few differences. This occurs mainly in the zoomed-in area, but is also somewhat visible at the end of the initial large peak, where the spectrum for the 90 % synovial fluid exhibits a small bump that is not visible on the spectrum for the 5 % synovial fluid. The spectrum for the 5 % synovial fluid is somewhat shifted to the left, which might be a result of a higher sample volume being injected (around 0.35 ml compared to 0.3 ml), but could also be attributed to differences in sample composition.

In addition to this shift, it is possible to note some more differences in elution for the zoomed-in part of the plot, where the 5 % synovial fluid exhibits more individual peaks and seems somewhat more separated. Due to the shift on the x-axis, it is difficult to determine directly which fractions differ between the two synovial fluids.

One limitation of the SEC method is not being able to derive the sizes of the molecules eluted and collected in the different fractions, but instead only approximate estimations and comparisons between different fractions can be made.

5.2.1.1 Gel electrophoresis of fractions from size-exclusion chromatography

To investigate the protein contents, and consequently the degree of successful size separation, of the collected fractions from SEC, gel electrophoresis of some selected fractions was performed. The result is presented in Figure 5.5, with the synovial fluid with initial 90 % neutrophils in (a) and the synovial fluid with initial 5 % neutrophils in (b). The values to the left of each picture represent the size indications of the protein ladder, while the labels at the bottom indicate the samples loaded in the well.

It is obvious for both synovial fluid samples that size separation was not optimally obtained; the first few fractions contain a lot of proteins, essentially from the whole interval of less than 10 kDa up to over 250 kDa, while the rightmost fractions seem to contain very few proteins, if not any. This confirms the hypothesis introduced in section 5.2.1; the majority of smaller proteins stick to the larger ones and dilute along with them.

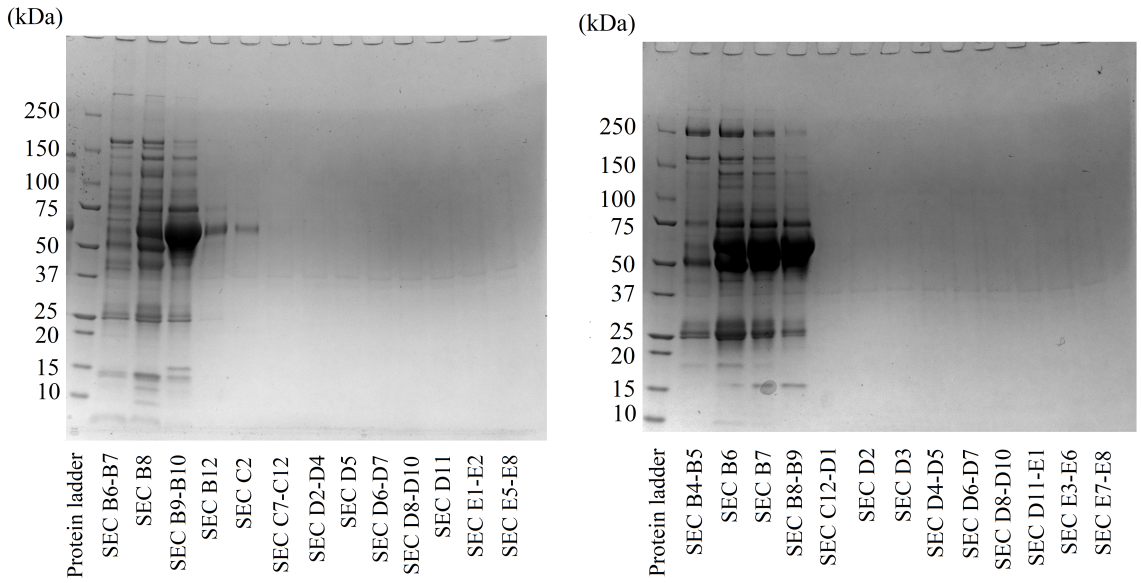

Figure 5.5: Gel electrophoresis of (a) synovial fluid with 90 % neutrophils initially and (b) synovial fluid with 5 % neutrophils initially. The values to the left indicates the size values of the protein ladder marks, and the labels at the bottom denotes the samples loaded in the wells.

5.2.2 Ion-exchange chromatography

Due to the poorly achieved separation from SEC, IEC was performed to try to separate the proteins that might have stuck together. The resulting UV-absorption at 280 nm as a function of eluting volume are plotted in Figure 5.6, with elution of the anion column in (a) and elution from the cation column in (b), for the synovial fluid

initially containing 90 % neutrophils. UV-absorption at 214 nm was also measured and displayed a similar shape as that for 280 nm, but with much higher intensity. As mentioned in the methods section 4.3.2, this measurement was not performed for the 5 % synovial fluid due to time restrictions. The grey vertical lines once again indicate the separation of wells where the eluting solvent is collected, with well labels indicated at the bottom.

There are two distinct peaks of absorption for the anion-exchange chromatography graph, while the cation-exchange chromatography displays one broad and one more distinct peak. The broad peak may indicate a relatively constant elution of molecules that were not separated optimally.

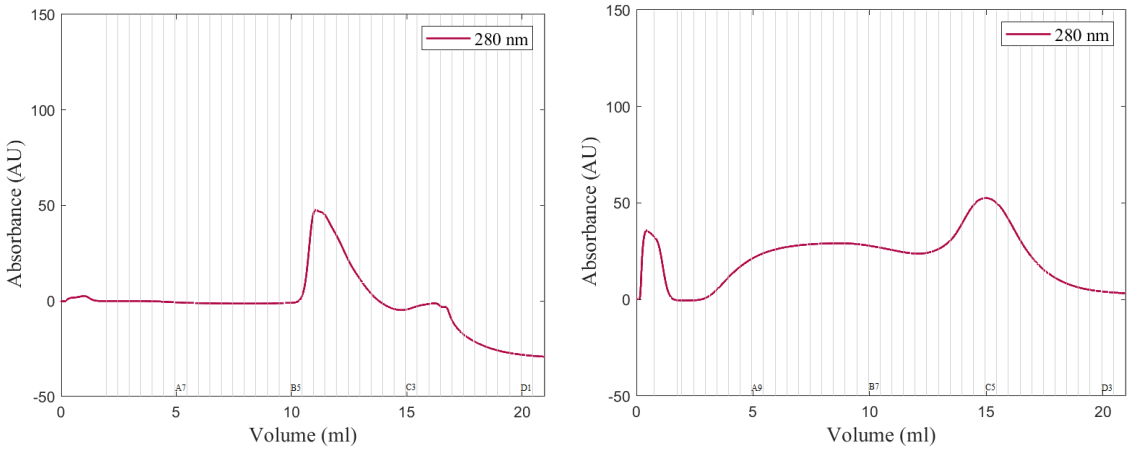

(a) (b)

Figure 5.6: UV-absorption at 280 nm as a function of eluting volume from the column for IEC of ≈0.3 ml of the synovial fluid with 90 % neutrophils, where (a) shows elution from the anion column and (b) from the cation column.

5.2.2.1 Gel electrophoresis of fractions from ion-exchange chromatography

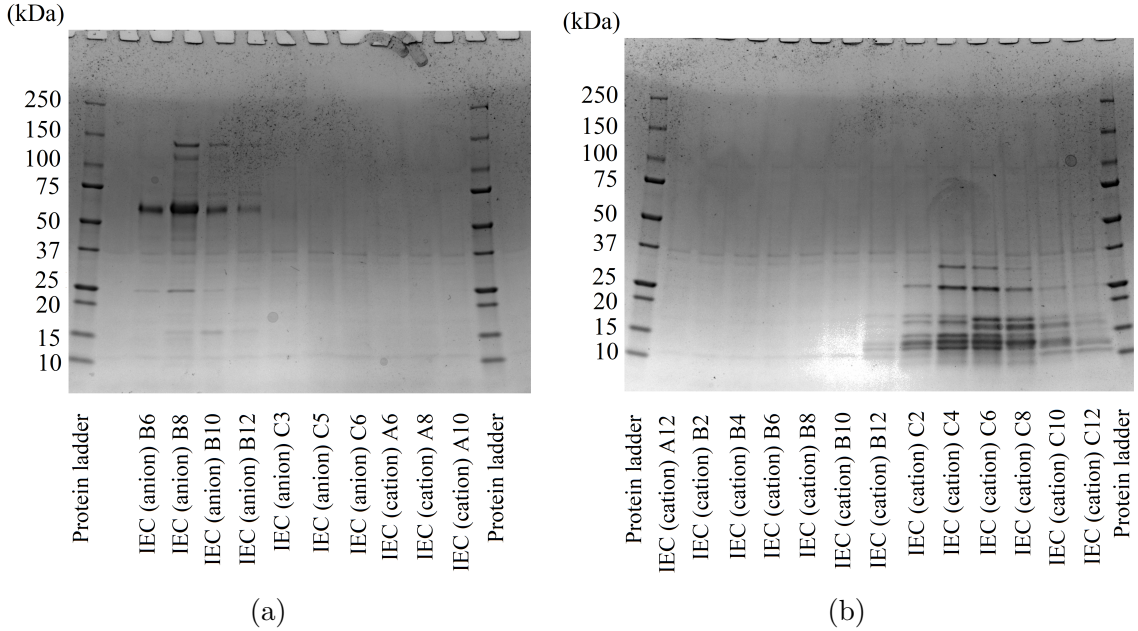

Figure 5.7: Gel electrophoresis of fractions collected from IEC (both anion and cation), with anion fractions B6 to C6 and cation fractions A8 and A10 in (a), and cation fractions A12-C12 in (b). The values to the left indicate the size values of the protein ladder marks, and the labels at the bottom denote the samples loaded in the wells.

To verify the success of separation from IEC, just as was done after SEC, gel electrophoresis was conducted. The resulting gels are shown in Figure 5.7, with the fractions from the anion and cation columns divided among the two gels. The values to the left of each picture represent the size indications of the protein ladder, while the labels at the bottom denote the sample loaded in the well.

On the contrary to the gels with fractions from SEC, successful separation of smaller proteins from larger proteins accomplished with IEC is verified, with the majority of larger proteins recovered in the anion column while most smaller proteins were captured in the cation column. There are two possibilities for how this separation was achieved; the first is of course that the IEC itself yielded this separation, while a second possibility is that the addition of DTT to the sample and buffer broke disulfide bonds between proteins and yielded the separation. All parts of the gel display a similar baseline of pale bands, with only a few fractions (B6, B8, B10 and B12 for anion IEC and C2, C4, C6, C8, C10 and C12 for cation-exchange chromatography) having more distinct bands.

Those fractions seem to have very similar band patterns visible on the gels, and thus similar protein contents. Some of the very pale bands may still contain proteins in one fraction that the other fractions do not, just in very low concentration, but this

could indicate that not much gradual size separation was achieved, instead larger and smaller proteins were separated from each other.

5.2.3 Chemotaxis assay

To evaluate the chemotactic potentials of the fractions obtained from SEC and IEC, chemotaxis assay measurements were conducted. The results are presented as bar graphs with the number of migrated neutrophils, as counted through flow cytometry, displayed for each measured sample. Here, a high neutrophil count indicates a high chemotactic activity of the sample.

Two different measurements, with set-ups according to Tables 4.1 and 4.2 in section 4.3.3.2, were performed in order to accommodate all fractions that might be of interest; from both SEC and IEC fractions of the 90 % synovial fluid as well as SEC fractions of the 5 % synovial fluid. Figure 5.8 shows the number of migrated neutrophils in the chemotaxis assay for each sample of the first chemotaxis set-up (Table 4.1), while the corresponding bar graph for the second chemotaxis set-up (Table 4.2) is presented in Figure 5.9. The labels at the bottom of the figures denote the sample contents.

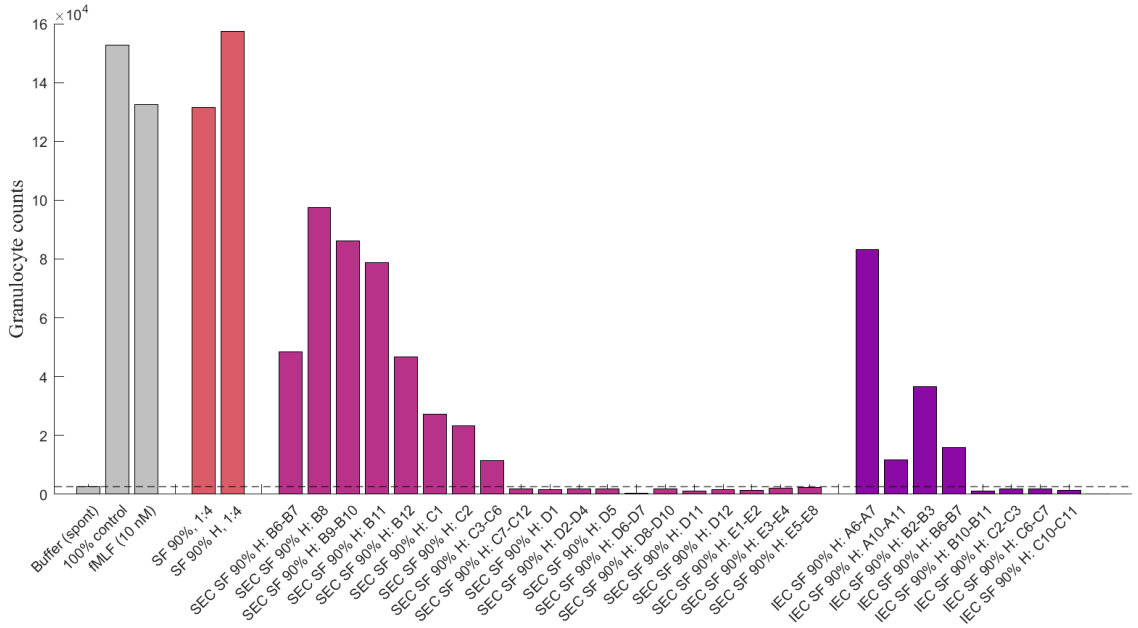

Figure 5.8: The neutrophil count from cells migrated through the filter membrane in the chemotaxis assay is shown as a bar for each sample. The horizontal dashed line indicates the value for the spontaneous migration (i.e., granulates that were allowed to migrate towards buffer, negative control). The grey bars indicate reference samples, with a buffer sample (spontaneous migration), a positive control and a fMLF control measurement. The labels indicate the sample content.

The horizontal dashed line indicates the value of the spontaneous migration, based

on the negative control count (the leftmost bar), and indicates the value of which cell migration does not belong to active migration. Following the negative control is a positive control and the fMLF control measurement. After that follows the pure synovial fluid samples, both untreated and treated with hyaluronidase, of which very high chemotactic activity is exhibited, as expected. The rest of the samples represent different fractions collected from SEC and IEC.

Let's start by considering Figure 5.8. The first approximately eight samples of fractions taken from SEC display quite high chemotactic activity, while the rest have very low or no chemotactic activity. Based on the gel electrophoresis of the SEC fractions, which showed that the majority of proteins (of both smaller and larger sizes) eluted in the first few fractions of interest, the chemoattractants in the synovial fluid seem to be divided among these first fractions.

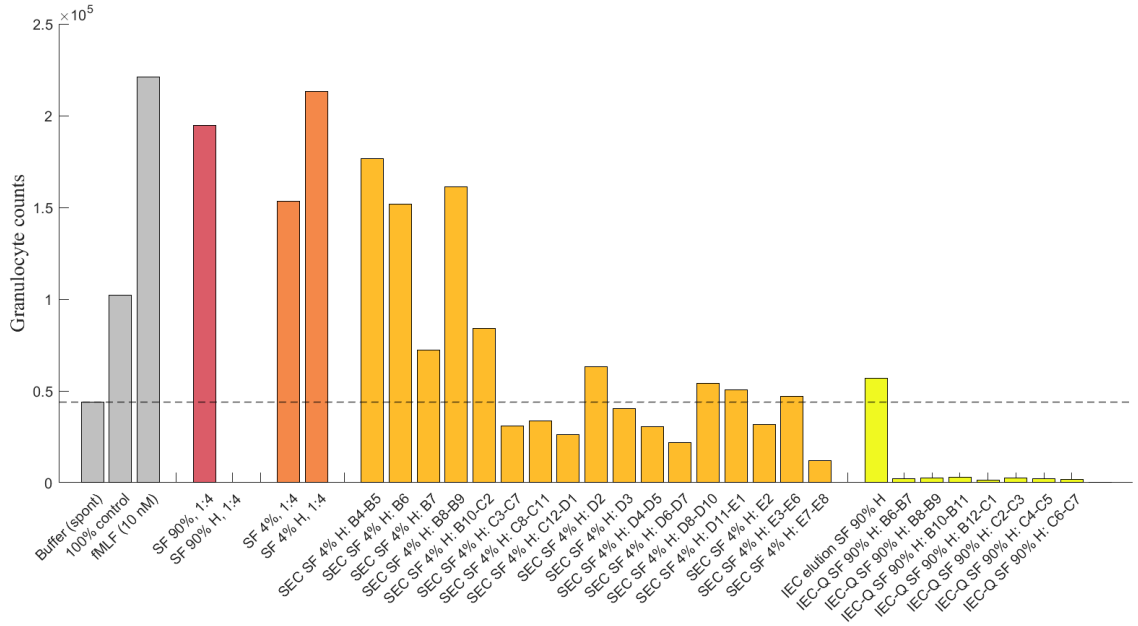

Figure 5.9: The neutrophil count from cells migrated through the filter membrane in the chemotaxis assay is shown as a bar for each sample. The horizontal dashed line indicates the value for the spontaneous migration (i.e., granulates that were allowed to migrate towards buffer, negative control). The grey bars indicate reference samples, with a buffer sample (spontaneous migration), a positive control and a fMLF control measurement. The labels indicate the sample content.

As for the IEC fractions, the sample containing fractions A6-A7 stands out with relatively high chemotactic activity, while the following three samples also display some degree of activity. The last samples do not exhibit any chemotactic activity.

Due to the difference in dilutions between all samples, it is difficult to make a direct comparison of chemotactic activity between all samples. However, some rough conclusions about which fractions in SEC and IEC, respectively, seem to contain the

highest concentration of chemoattractants are possible to draw, as well as approximate comparison to the pure synovial fluid samples (both untreated and treated) which have known dilutions of 1:4.

The chemotaxis assay is an especially vulnerable method for fluctuations in the result. To produce reliable results and obtain an overall pattern, the measurement has to be re-produced several times. In this project, only one run was conducted for each fraction. This means that no comparisons can be made regarding the level of chemotactic activity. However, the exhibition of chemotactic activity at all can not be attributed to fluctuations to the same extent, meaning the chemotactic activity of some of the fractions is a good indication of the method working, and which fractions that may contain chemoattractants. Another factor that might influence the result is the choice of neutrophil gating for the final cell count, however, this should only alter the result very slightly.

Regarding the result presented in Figure 5.9, the negative control showing spontaneous migration (the first bar) has a somewhat higher value than that in Figure 5.8, and the difference between the positive control and fMLF sample, as well as between the samples of untreated and treated synovial fluid with initially 90 % neutrophils, are quite large. It can also be noted that the value for the positive control is expected to be higher than the value for the fMLF sample, which is not the case here. This indicates the relatively high fluctuations present in this type of experiment.

The SEC fractions for the 4% synovial fluid display a similar pattern as that of the 90 % neutrophil synovial fluid seen in Figure 5.8, with the first few fractions having a high chemotactic activity and the others almost no activity at all. None of the IEC fractions show any considerable chemotactic activity, especially the cation IEC fractions.

The high chemotactic ability of the 5 % synovial fluid is quite strange, considering the fact that the 5 % synovial fluid exhibited a much lower total amount of neutrophils in comparison to the 90 % synovial fluid (see Figures in Appendix A). This would indicate a much lower concentration of chemoattractants present in the fluid. One explanation for this behavior could be the different times in the patients' courses of disease when the synovial fluid was extracted. Since the joint inflammation in IA patients come and go in so-called flares, it is possible that synovial fluid was extracted from the patient with the 5 % neutrophils synovial fluid when the neutrophils had not yet migrated in any large number to the synovial cavity, while the opposite might be true for the patient with the 90 % synovial fluid. This would enable a high presence of chemoattractants in the 5 % synovial fluid as well.

In the context of being a method study, this fact does not affect the results, but in the long run of identifying chemoattractants it could be helpful to have samples with different known chemotactic capacities to compare contents with. These results highlight the importance to keep in mind during what period of the course of disease synovial fluid is extracted from patients.

The IEC fractions of both chemotaxis experiments display very low active neutrophil migration. This is especially clear in Figure 5.9, where almost no cells were detected for the last IEC samples even though the spontaneous migration was relatively high. Since the salt concentration is higher for the IEC fractions than the SEC fractions, with increasing salt concentration for each fraction, this could be an indication that the ionic environment in those samples is toxic to the cells, resulting in alteration of cell shape, cell death or no cell migration to begin with. Both cell shape change and cell death alter the size and granularity of the cell such that they are most likely not included in the gate.

The fluctuations in the chemotaxis experiment may emerge from some sample fractions not having enough contact with the membrane during incubation, the fragility of the filter membrane, difficulties to remove all cells from the chemotaxis plate after incubation and insufficient fixation by PFA. It can also be noted that even though each well should contain maximum $6 \cdot 10^4$ cells, many samples exceeds this number and exhibit the difficulty of achieving the desired cell concentration in the cell suspension. This provides another reason for comparisons between different measurements not being suitable.

The IEC method for separation still seems viable for achieving separation while preserving biological function, based on the fact that a few low-salt fractions still display chemotaxis. By desalting the IEC fractions, a conclusive result regarding which fractions have the highest chemotactic activity could probably be obtained and indicate where the focus should be directed for further continuation of identifying chemoattractants. This could not be executed during this project due to a lack of access to necessary materials.

5.2.4 Liquid chromatography-mass spectrometry

Further analysis of the contents of each fraction obtained from SEC and IEC, as a complement to the chemotaxis assay results, can be provided through LC-MS. The LC-MS measurements were performed for fractions collected from SEC and cation-exchange chromatography of the 90 % synovial fluid. Previous methods within this approach have included measurements of the 5 % synovial fluid, but this was excluded here due to time restrictions for the project. Additionally, the fractions B6-B7 to B12 from SEC of the 90 % synovial fluid were not measured since the gel electrophoresis confirmed the presence of some proteins too large for the implemented RP-HPLC column (see Figure 5.5). This is true for the anion-exchange chromatography fractions of the 90 % synovial fluid as well, which all contained very large proteins.

5.2.4.1 Liquid chromatography-mass spectrometry of fractions from size-exclusion chromatography

In Figure 5.10, the total ion chromatogram (in (a)) and UV-absorption at 280 nm (in (b)) are presented for some selected fractions collected from SEC of the 90 %

synovial fluid; C1, C2, D8-D10 and D11. These fractions were chosen since C1 and C2 are the only fractions displaying chemotactic ability and at the same time not containing proteins too large for the column, while the chemotactically inert fractions D8-D10 and D11 were chosen as comparisons. It is interesting to compare the chemotactic fractions to the non-chemotactic ones, since differences in detections from LC-MS might be possible explanations behind their different properties. These fractions were selected as good representatives for all fractions and their individual properties.

Blank (PBS) measurements were conducted before, between and after all fraction measurements. All blank measurements be found in Appendix D, together with the individual results for all measured SEC fractions (fractions C1, C2, D1, D2-D4, D5, D6-D7, D8-D10, D11). In principle, all blank measurements look identical, why only one blank measurement (the one conducted before measuring the C1 fraction) is included in Figure 5.10.

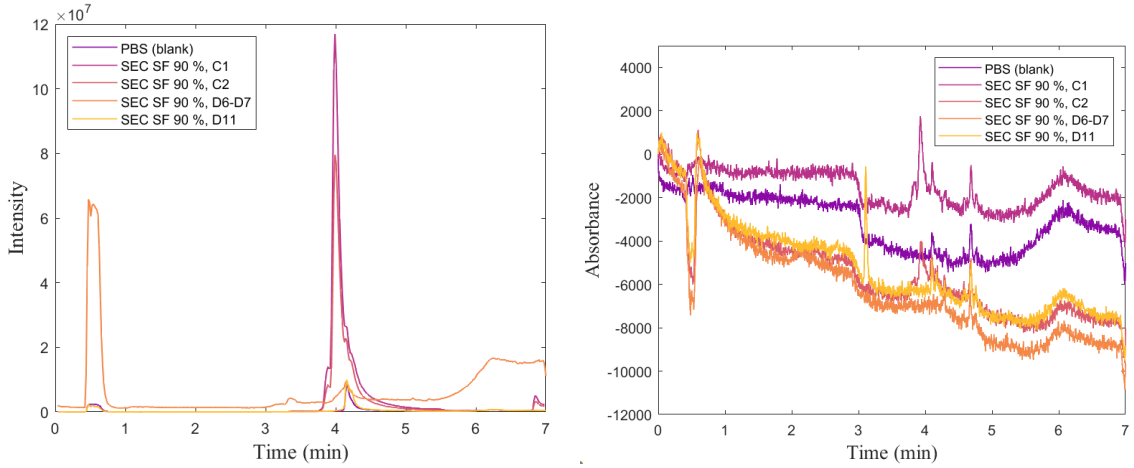

(a) (b)

Figure 5.10: The total ion chromatogram in (a) and UV-absorption at 280 nm in (b) for SEC fractions C1, C2 and D6-D7 of the 90 % synovial fluid, as well as the PBS (blank) measurement run before the C1 sample.

The UV-absorption at 280 nm is generally quite noisy with low intensities. The total ion chromatogram shows more distinct peaks, with an overall shape that is similar for all samples. However, fractions D6-D7 do stand out between 0.5 and 1 minute, while C1 and C2 display especially high intensity for the peak at around 4 minutes.

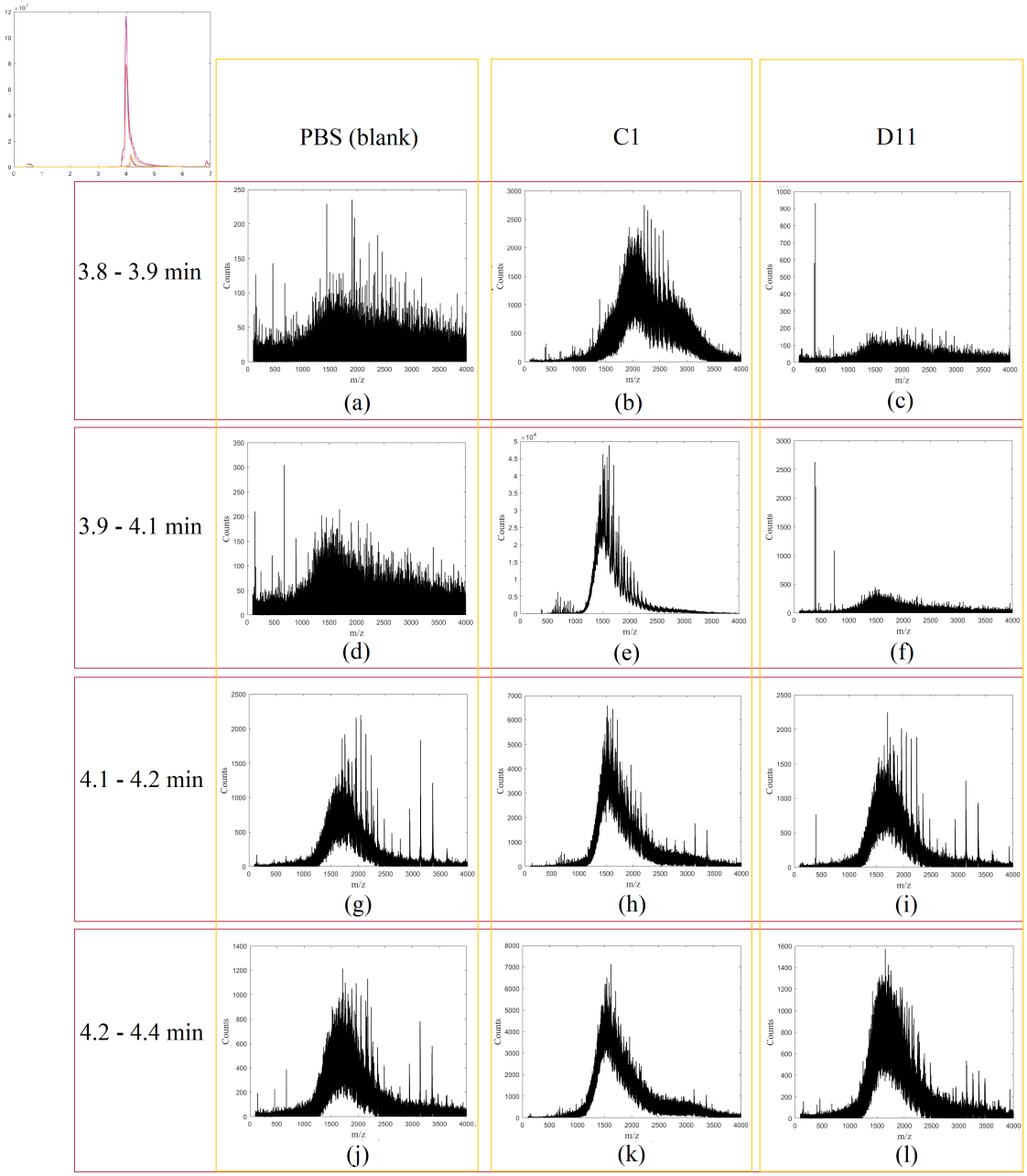

Figure 5.11: Mass spectra are plotted for SEC fractions C1 and D11 (from the 90 % synovial fluid), as well as a PBS (blank) measurement conducted before the C1 measurement, for multiple time intervals. Those time intervals are 0.4 to 0.5 minutes, 0.5 to 0.65 minutes, 0.65 to 0.9 minutes, 3.3 to 3.5 minutes and 3.8 to 4 minutes.

To gain more clues and insights, the mass spectra can be considered. In Figure 5.11, the mass spectra are plotted for the blank measurement, and fractions C1 and D11, for the time intervals 3.8 to 3.9 minutes, 3.9 to 4.1 minutes, 4.1 to 4.2 minutes and 4.2 to 4.4 minutes, as defined by the RP-HPLC detection. Due to the low chemotactic ability of fraction D6-D7, it is not necessary to include both it and fraction D11 for further analysis, in regards to the aim of this project.

Starting by considering time intervals 3.8 to 3.9 minutes and 3.9 to 4.1 minutes, it is clear that one or more compounds are detected for C1, while there is mostly noise in the PBS and D11 samples. The spectra for C1 at these two time points look quite different and indicate detection of different compounds. Looking at time intervals 4.1 to 4.2 and 4.2 to 4.4 minutes for C1, both spectra look very similar to that at 3.9 to 4.1 minutes but with a much lower number of counts, and thus signals detection of the same compound but in a lower concentration. By also comparing these spectra with those for PBS and D11 at the same time intervals of 4.1 to 4.2 and 4.2 to 4.4 minutes, those spectra seem to detect the same compound as well – also in a lower concentration.

Overall, this indicates that the compound present in the C1 sample might be the same that seem to stick and contaminate the column, leading to detection in blank measurement and other sample measurements as well. The reason for the compound contaminating the column could be its high concentration which might overcrowd the sample injection loop and/or column. At this point, it is impossible to know if one of the compounds detected for C1 at 3.8 to 3.9 and 3.9 to 4.1 minutes are a chemoattractant, but since C1 exhibited chemotactic capacity while D11 did not – and these components are present in C1 but not in D11 – there is a possibility of this being the case.

5.2.4.2 Liquid chromatography-mass spectrometry of fractions from ion-exchange chromatography

Regarding the IEC measurements, only fractions from cation-exchange chromatography were measured with LC-MS. As verified by the gel electrophoresis performed in section 5.2.2.1, the fractions collected from anion-exchange chromatography contain proteins too large to be measured by LC-MS with the implemented column.

All total ion chromatograms as well as UV-absorption at 280 nm, for the fractions collected from cation-exchange chromatography of the 90 % synovial fluid, as well as all blank measurements on pure PBS, can be found in Appendix E. Just as for the SEC fractions, the blank measurements were run before, between and after all fraction measurements. Regarding the cation-exchange chromatography fractions, the initial fractions A6-A7 to B10-B11 are very similar, and their total ion chromatograms look very similar to the blank measurements. Their absorption at 280 nm do however show two peaks between 0.5 and 1 minute that are not present in the blank measurements.

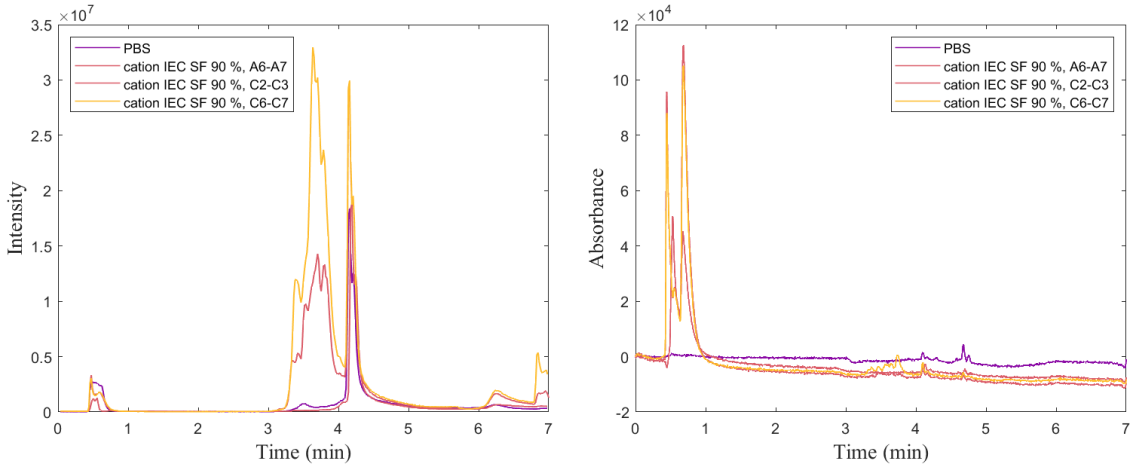

(a) (b)

Figure 5.12: The total ion chromatogram in (a) and UV-absorption at 280 nm in (b) for cation-exchange chromatography fractions A6-A7, C2-C3 and C6-C7 of the 90 % synovial fluid, as well as the PBS (blank) measurement run before the A6-A7 sample.

Fractions C2-C3 to C10-C11 display more additional peaks, both in the total ion chromatogram and the detection at 280 nm. To analyze the results, fractions A6-A7, C2-C3 and C6-C7 were chosen as good representations of all fractions as a whole, and are plotted in Figure 5.12, with (a) displaying the total ion chromatogram and (b) detection at 280 nm. In addition, the blank measurement conducted before the A6-A7 cation-exchange chromatography measurement is plotted in the Figure as a representation of the blank measurements.

The peaks in the blank measurement, especially the large peak at around 4.20, can be attributed to proteins and contamination that are stuck in the column or sample injection loop. The peak at 4.20 is the same as was noted for the SEC fractions in the previous section. The higher intensity of the peak for fractions C6-C7 than the other fractions and blank measurement, could indicate a higher presence of that compound in that fraction.

Focusing on the total ion chromatogram, some additional peaks arise between around 3 and 4 minutes for the C2-C3 and C6-C7 fractions. Regarding instead the detection at 280 nm, both C6-C7 and C10-C11 exhibit lower intensity of the injection peak at around 0.5 minutes, and higher intensity of the one at around 0.6 minutes, compared to A6-A7. Additionally, they display a peak at around 0.4 minutes that A6-A7 lacks. Fractions C6-C7 also displays some small peaks at around 3 and 4 minutes which are not visible for neither A6-A7 nor C10-C11. These peaks are most likely induced by the same compounds responsible for the peaks between 3 and 4 minutes in the total ion chromatogram, which have the highest intensity for fractions C6-C7.

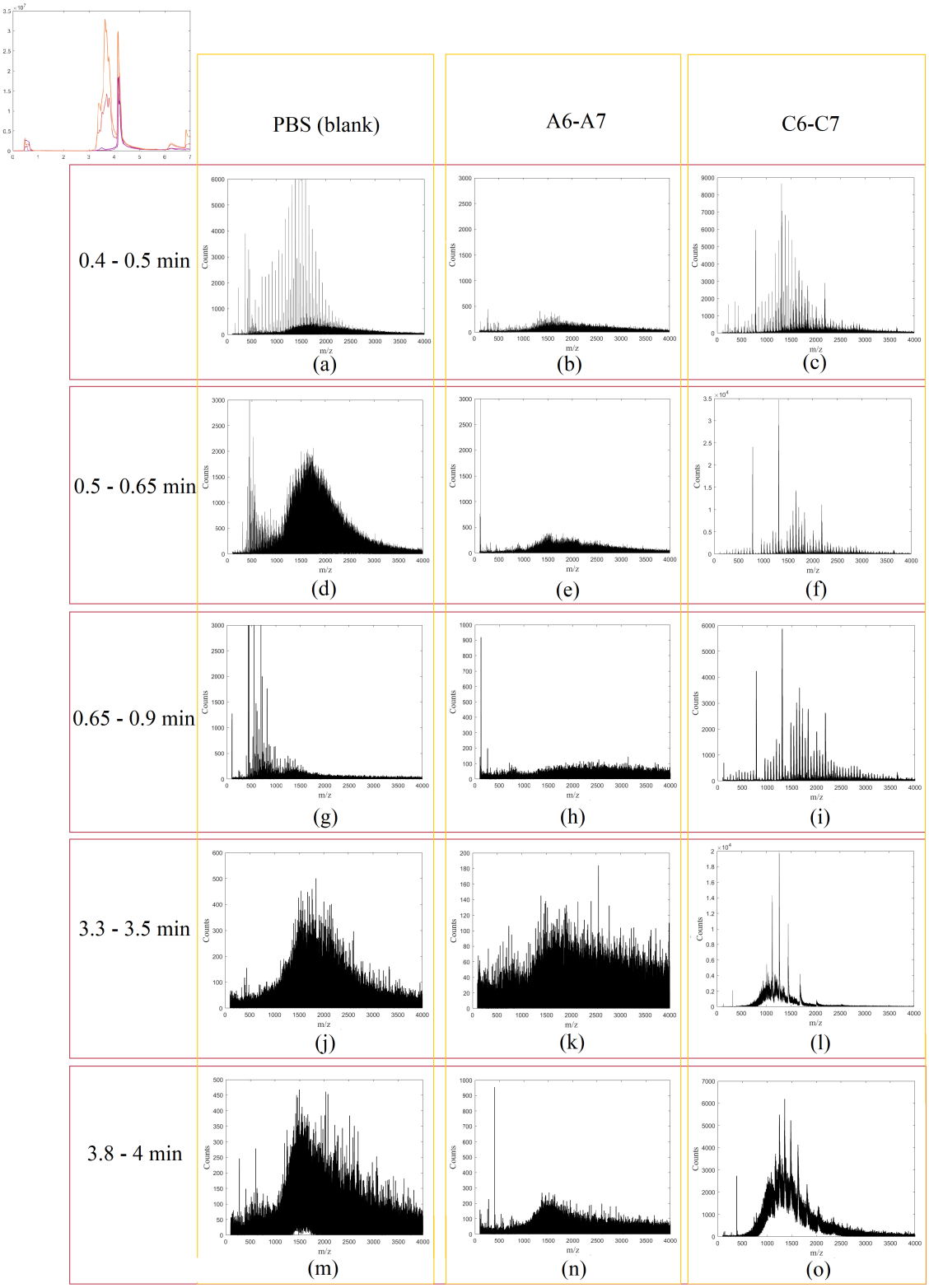

Figure 5.13: Mass spectra are plotted for cation-exchange fractions A6-A7 and C6-C7 (from the 90 % synovial fluid), as well as a PBS (blank) measurement conducted before the A6-A7 measurement, for multiple time intervals. Those time intervals are 0.4 to 0.5 minutes, 0.5 to 0.65 minutes, 0.65 to 0.9 minutes, 3.3 to 3.5 minutes and 3.8 to 4 minutes.

To obtain further clues about the sample contents, the mass spectra can be analyzed. Figure 5.13 presents the obtained mass spectra for the blank measurement and fractions A6-A7 and C6-C7, for different time intervals; 0.4 to 0.5 minutes, 0.5 to 0.65 minutes, 0.65 to 0.9 minutes, 3.3 to 3.5 minutes and 3.8 to 4 minutes. Mass spectra, for additional time intervals, and all other cation-exchange chromatography fractions, can be found in Appendix E.

As expected based on the total ion chromatogram and UV-absorption at 280 nm, not much is detected for fraction A6-A7, despite the sample showing relatively high intensity between 0.5 and 0.65 minutes for detection at 280 nm. One possible explanation for this could be that the molecules that are detected through the UV-absorption spectroscopy have masses under 500 Da, a mass range where the mass detector is not as sensitive.

5.3 Combined discussion

The synovial samples examined in this project are biological fluids, and each patient has a unique synovial fluid composition. Synovial fluids from only two different patients were investigated in this study, meaning any conclusions about the specific synovial fluid contents drawn from the results presented in this report are not statistically supported. This would require a study involving a larger number of patients. However, regarding the methodological nature of this thesis, several conclusions can be made about the potential of the implemented methods in identifying neutrophil chemoattractants.

Continuing on the subject of discussing the biological aspects, there is of course the possibility of altering the biological function of sample compounds through the methods applied here. Even if the proteins themselves might not experience denaturing of three-dimensional structure, biological systems are complex and might sometimes be dependent on cooperation between different compounds. If this is the case here, that several chemoattractants rely on other chemoattractants to carry out their own function, separating the synovial fluid sample into fractions might interfere with this. However, to thoroughly investigate the process underlying inflamed synovial fluid in IA patients from scratch, this course of action is necessary, not least because of the potential of previously unknown chemoattractants playing their part in the recruitment of neutrophils.

To be able to fully analyze and evaluate the methods employed in this project, the different methods have to be discussed together, not just individually. Between the two different approaches – separation by gel electrophoresis and separation by liquid chromatography – the latter seems most promising. There are signs of both reagent contamination and insufficient extraction of proteins from the gels connected to gel electrophoresis separation. During this project, no conclusion can be made from the results of the methods belonging to this approach. In addition, the method itself includes many steps on the way to eventually identifying chemoattractants, since recombinant variants of identified compounds would have to be tested for chemo-

tactic ability. However, the method is not without its benefits, such as more control and knowledge over absolute sizes of the different size intervals compared to only knowing comparative sizes in SEC.

Considering the liquid chromatography approach, separation of components by IEC was more successful than by SEC, due to smaller molecules sticking to, and eluting together with, larger ones. Better separation with SEC could possibly be achieved through the addition of DTT to the sample and mobile phase, to break disulfide bonds in between proteins. Another possibility would be to run additional SEC measurements with the already obtained fractions from IEC, using a column that separates a shorter mass interval with higher sensitivity, to further separate the synovial fluid components.

Despite the successful separation with IEC, the high salt concentration seemed to interfere with the chemotactic potential of the sample fractions. To better evaluate the separation yielded with IEC and the chemotactic ability of the collected fractions, the fractions could be de-salted through for example dialysis. This would make their cellular environment more friendly, and allow for a more accurate chemotaxis assay measurement.

Due to the time limitation for this project, LC-MS measurements were only performed for fractions collected from the 90 % synovial fluid. However, comparing two different fluids is mostly of interest further down the search for chemoattractants, and not of the same importance during the development of method implementation. Comparing the total ion chromatograms between SEC and IEC for the 90 % synovial fluid, the cation-exchange chromatography fractions A6-A7 to B10-B11 exhibit the same shape as in principle all SEC fractions. However, some peaks are more distinct in some samples than others.

In addition, many samples do not display any visible differences from the blank measurements. The reason for this could be that they simply do not contain high enough concentrations of compounds. Comparing with the gel electrophoresis performed for these fractions (Figures 5.5 and 5.7), only very pale bands are visible. Fractions C2-C3 to C10-C11 from cation-exchange chromatography do display very distinct peaks, in line with the gel electrophoresis showing the most intensive bands for these fractions.

The A6-A7 cation-exchange chromatography fraction, as well as the C1 and C2 SEC fractions, exhibit quite high chemotactic capacity despite having a relatively low concentration of compounds – especially A6-A7 – as evidenced by gel electrophoresis and LC-MS. This fact could be a bit confusing. One explanation could be that chemoattractants elute together with the column contaminations at around 4.2 minutes, or in the injection peak at 0.5 minutes. In fact, chemoattractants in some of the samples could themselves be one source of the column contaminations. Another possibility could be that there is a very low concentrations of chemoattractants, too low for the sensitivity of the LC-MS detector and stain for the gel. Additionally,

the chemotactic ability could still be high even for very small chemoattractant concentrations.

Despite there being differences in the total ion chromatograms for the cation-exchange chromatography fractions, no conclusion regarding potential chemoattractants in these fractions can be made since there is no way of knowing if the fractions B10-B11 to C10-C11 possess any chemotactic activity, due to their high salt concentration seemingly interfering with the chemotaxis assay measurement. This also goes for the true strength of chemotactic capacity for fractions A6-A7 to B6-B7; which also to some degree might be influenced by the salt concentrations of the fractions.

To obtain a more detailed analysis of the detected components beyond the implemented LC-MS, liquid chromatography-tandem mass spectrometry (LC-MS/MS) measurements could be performed. Those results can be analyzed using software that compares the resulting mass spectra with a database. However, time was not sufficient to be able to implement these experiments during the scope of this project. Other ways to further analyze the samples could be more exploration of instrument conditions and settings to find parameters for optimal combination of separation and detection, since the choice of the column, column conditions, mobile phase composition and other instrument settings affects factors such as retention times, peak shape and peak resolution.

In general, for the gel electrophoresis measurements performed, silver stain could be used instead of staining buffers based on coomassie blue. While coomassie blue is easier and faster to use, silver staining is more sensitive for the detection of smaller amounts of protein [76]. Furthermore, it should be noted as a potential source of error for all employed methods that there is always the possibility of sample contamination during the different elements of the experimental work, as well as the chemicals and reagents used already being contaminated. Furthermore, some measurements, especially the chemotaxis assay, involve many sensitive technical steps.

6
Conclusion and future work

Separation by liquid chromatography and subsequent measurement of chemotactic ability is a promising method as a first step towards identifying the neutrophil chemoattractants in synovial fluid of IA patients. With this method, different compounds in the synovial fluid could be separated on the basis of size, while still preserving the chemotactic ability of the fractions (in most cases). Different fractions could be identified as of high interest in terms of the probable presence of neutrophil chemoattractants, and the data from the LC-MS measurements provided more insights into the components.

Some degree of separation was obtained with SEC without infringing on the chemotactic potential of the fractions. However, the most successful separation of components was achieved with IEC. Some impact on the chemotactic ability of fractions with high salt concentration was seen, but due to the exhibition of a high chemotactic potential of some low salt IEC fractions, this is most likely not caused by the method itself or addition by DTT, but by the high salt concentration. To expand the chemotaxis assay for those fractions, they could be desalted and re-run.

Furthermore, the SEC method might be improved upon by investigating if the addition of DTT to the sample and mobile phase would yield better size separation by breaking disulfide bonds between proteins. Another possibility would be to run additional SEC measurements with the already obtained fractions from IEC, using a column that separates a shorter mass interval with higher sensitivity, to further separate the synovial fluid components.

To provide more statistically certain results regarding chemotactic abilities, more repetitions of the chemotaxis assay measurements are needed. In combination with LC-MS/MS measurements, through which more detailed information about, or even exact identification of, molecules in the samples can be obtained, a more complex analysis could be performed.

The development of a methodology for characterizing neutrophil chemoattractants in synovial fluid in IA patients, and subsequent identification of the chemoattractants, would give further insight into the associated inflammatory process. All pieces of knowledge about this are of great importance in order to develop better treatment and improve life quality for those affected by IA. This thesis proposes the first steps of this methodology.

[1] M. A. Sugimoto, L. P. Sousa, V. Pinho, M. Perretti, and M. M. Teixeira, "Resolution of inflammation: What controls its onset?", *Frontiers in Immunology*, vol. 7, no. 160, Apr. 2016. DOI: 10.3389/fimmu.2016.00160.

[2] A. Abudukelimu, M. Barberis, F. A. Redegeld, N. Sahin, and H. V. Westerhoff, "Predictable irreversible switching between acute and chronic inflammation", *Frontiers in Immunology*, vol. 9, Aug. 2018. DOI: 10.3389/fimmu.2018.01596.

[3] L. Chen et al., "Inflammatory responses and inflammation-associated diseases in organs", *Oncotarget*, vol. 9, no. 6, pp. 7204–7218, Jan. 2018. DOI: 10.18632/oncotarget.23208.

[4] D. Furman et al., "Chronic inflammation in the etiology of disease across the life span", *Nature Medicine*, vol. 25, no. 12, pp. 1822–1832, Dec. 2019. DOI: 10.1038/s41591-019-0675-0.

[5] A. S. Canada, *Inflammatory arthritis*, Available at https://arthritis.ca/about-arthritis/arthritis-types-(a-z)/types/inflammatory-arthritis (2023/06/18).

[6] A.-F. Radu and S. G. Bungau, "Management of rheumatoid arthritis: An overview", *Cells*, vol. 10, no. 11, Oct. 2021. DOI: 10.3390/cells10112857.

[7] A. J. Sankowski, U. M. Łebkowska, J. Ćwikła, I. Walecka, and J. Walecki, "Psoriatic arthritis", *Polish journal of radiology*, vol. 78, no. 1, pp. 7–17, Jan. 2013. DOI: 10.12659/PJR.883763.

[8] J. Bullock et al., "Rheumatoid arthritis: A brief overview of the treatment", *Medical principles and practice*, vol. 27, no. 6, pp. 501–507, Sep. 2018. DOI: 10.1159/000493390.

[9] F. Verhoeven, C. Prati, C. Demougeot, and D. Wendling, "Cardiovascular risk in psoriatic arthritis, a narrative review", *Joint Bone Spine*, vol. 87, no. 5, pp. 413–418, Jan. 2020. DOI: 10.1016/j.jbspin.2019.12.004.

[10] C. S. Crowson et al., "Rheumatoid arthritis and cardiovascular disease", *American Heart Journal*, vol. 166, no. 4, pp. 622–628, Oct. 2013. DOI: 10.1016/j.ahj.2013.07.010.

[11] Socialstyrelsen, "Nationella riktlinjer för rörelseorganens sjukdomar reumatoid artrit, axial spondylartrit, psoriasisartrit, artros och osteoporos", Tech. Rep., 2021.

[12] J.-T. Liu, H.-M. Yeh, S.-Y. Liu, and K.-T. Chen, "Psoriatic arthritis: Epidemiology, diagnosis, and treatment", *World journal of orthopedics*, vol. 5, no. 4, pp. 537–543, Sep. 2014. DOI: 10.5312/wjo.v5.i4.537.

[13] F. Brunello et al., "New insights on juvenile psoriatic arthritis", *Frontiers in Pediatrics*, vol. 10, May. 2022. DOI: 10.3389/fped.2022.884727.

[14] R. Burgos-Vargas and R. E. Petty, "Juvenile ankylosing spondylitis", *Rheumatic Disease Clinics of North America*, vol. 18, no. 1, pp. 123–142, 1992. DOI: https://doi.org/10.1016/S0889-857X(21)00713-4.

[15] N. D. Kim and A. D. Luster, "The role of tissue resident cells in neutrophil recruitment", *Trends in Immunology*, vol. 36, no. 9, pp. 547–555, Sep. 2015. DOI: 10.1016/j.it.2015.07.007.

[16] Z. Fan et al., "Neutrophil recruitment limited by high-affinity bent β_2 integrin binding ligand in cis", *Nature Communications*, vol. 7, Aug. 2016. DOI: 10.1038/ncomms12658.

[17] E. Kolaczkowska and P. Kubes, "Neutrophil recruitment and function in health and inflammation", *Nature Reviews Immunology*, vol. 13, no. 3, pp. 159–175, Feb. 2013. DOI: 10.1038/nri3399.

[18] I. Halilovic, J. Wu, M. Alexander, and F. Lin, "Neutrophil migration under spatially-varying chemoattractant gradient profiles", *Biomedical Microdevices*, vol. 17, no. 57, May 2015. DOI: 10.1007/s10544-015-9963-8.

[19] I. Miralda, S. M. Uriarte, and K. R. McLeish, "Multiple phenotypic changes define neutrophil priming", *Frontiers in Cellular and Infection Microbiology*, vol. 7, no. 217, May 2017. DOI: 10.3389/fcimb.2017.00217.

[20] L. Björkman et al., "Neutrophil recruitment to inflamed joints can occur without cellular priming", *Journal of Leukocyte Biology*, vol. 105, no. 6, pp. 1123–1130, Jun. 2019. DOI: 10.1002/JLB.3AB0918-369R.

[21] P. L. Yeagle, "Chapter 1 - introduction", in *The Membranes of Cells (Third Edition)*, P. L. Yeagle, Ed., Third Edition, Boston: Academic Press, 2016, pp. 1–25. DOI: https://doi.org/10.1016/B978-0-12-800047-2.00001-2.

[22] K. Radhakrishnan, Á. Halász, D. Vlachos, and J. S. Edwards, "Quantitative understanding of cell signaling: The importance of membrane organization", *Current opinion in biotechnology*, vol. 21, no. 5, pp. 677–682, Sep. 2010. DOI: 10.1016/j.copbio.2010.08.006.

[23] C.-H. Heldin, B. Lu, R. Evans, and J. S. Gutkind, "Signals and receptors", *Cold Spring Harbor perspectives in biology*, vol. 8, no. 4, Apr. 2016. DOI: 10.1101/cshperspect.a005900.

[24] D. D. Chaplin, "Overview of the immune response", *The Journal of allergy and clinical immunology*, vol. 125, no. 125(2 Suppl 2), pp. 3–23, 2010. DOI: 10.1016/j.jaci.2009.12.980.

[25] Britannica, *Antigen*, Available at https://www.britannica.com/science/antigen (2023/06/16).

[26] B. Alberts, A. Johnson, J. Lewis, M. Raff, K. Roberts, and P. Walter., "Chapter 24. the adaptive immune system", in *Molecular Biology of the Cell (Fourth Edition)*, Fourth Edition, New York: Garland Science, 2002.

[27] J. S. Marshall, R. Warrington, W. Watson, and H. L. Kim, "An introduction to immunology and immunopathology", *Allergy, Asthma Clinical Immunology volume*, vol. 14, no. 49, Sep. 2018. DOI: 10.1186/s13223-018-0278-1.

[28] C. Rosales, "Neutrophil: A cell with many roles in inflammation or several cell types?", *Frontiers in Physiology*, vol. 9, no. 113, Feb. 2018. DOI: 10.3389/fphys.2018.00113.

[29] R. C. Furze and S. M. Rankin, "Neutrophil mobilization and clearance in the bone marrow", *Immunology*, vol. 125, no. 3, pp. 281–288, Nov. 2008. DOI: 10.1111/j.1365-2567.2008.02950.x.

[30] T. Németh, M. Sperandio, and A. Mócsai, "Neutrophils as emerging therapeutic targets", *Nature Reviews Drug Discovery*, vol. 19, no. 4, pp. 253–275, Jan. 2020. DOI: 10.1038/s41573-019-0054-z.

[31] K. R. Eichelberger and W. E. Goldman, "Manipulating neutrophil degranulation as a bacterial virulence strategy", *PLOS Pathogens*, vol. 16, no. 12, Dec. 2020. DOI: 10.1371/journal.ppat.1009054.

[32] B. M. Skinner and E. E. P. Johnson, "Nuclear morphologies: Their diversity and functional relevance", *Chromosoma*, vol. 126, no. 2, pp. 195–212, Mar. 2017. DOI: 10.1007/s00412-016-0614-5.

[33] M. Lázaro-Díez et al., "Human neutrophils phagocytose and kill acinetobacter baumannii and a. pittii", *Scientific Reports*, vol. 7, no. 1, Jul. 2017. DOI: 10.1038/s41598-017-04870-8.

[34] V. Brinkmann et al., "Neutrophil extracellular traps kill bacteria", *Science*, vol. 303, no. 5663, pp. 1532–1535, Mar. 2004. DOI: 10.1126/science.1092385.

[35] P. X. Liew and P. Kubes, "The neutrophil's role during health and disease", *Physiological Reviews*, vol. 99, no. 2, pp. 1223–1248, Feb. 2019. DOI: 10.1152/physrev.00012.2018.

[36] M.-D. Filippi, "Neutrophil transendothelial migration: Updates and new perspectives", *Blood*, vol. 133, no. 20, pp. 2149–2158, May. 2019. DOI: 10.1182/blood-2018-12-844605.

[37] H. L. Wright, R. J. Moots, R. C. Bucknall, and S. W. Edwards, "Neutrophil function in inflammation and inflammatory diseases", *Rheumatology*, vol. 49, no. 9, pp. 1618–1631, Sep. 2010. DOI: 10.1093/rheumatology/keq045.

[38] M. Metzemaekers, M. Gouwy, and P. Proost, "Neutrophil chemoattractant receptors in health and disease: Double-edged swords", *Cellular & Molecular Immunology*, vol. 17, no. 5, pp. 433–450, Apr. 2020. DOI: 10.1038/s41423-020-0412-0.

[39] I. Miralda, S. M. Uriarte, and K. R. McLeish, "Multiple phenotypic changes define neutrophil priming", *Frontiers in cellular and infection microbiology*, vol. 7, no. 217, May 2017. DOI: 10.3389/fcimb.2017.00217.

[40] D. S. Pisetskya and M. M. Ward, "Advances in the treatment of inflammatory arthritis", *Best Practice Research: Clinical Rheumatology*, vol. 26, no. 2, pp. 251–261, Apr. 2012. DOI: 10.1016/j.berh.2012.03.001.

[41] T. Bennike et al., "A normative study of the synovial fluid proteome from healthy porcine knee joints", *Journal of Proteome research*, vol. 13, no. 10, pp. 4377–4387, Aug. 2014. DOI: 10.1021/pr500587x.

[42] JH. Lee et al., "Proteomic analysis of human synovial fluid reveals potential diagnostic biomarkers for ankylosing spondylitis", *Clinical Proteomics*, vol. 17, no. 20, Jun. 2020. DOI: 10.1186/s12014-020-09281-y.

[43] J. al-Mughales, T. H. Blyth, J. A. Hunter, and P. C. Wilkinson, "The chemoattractant activity of rheumatoid synovial fluid for human lymphocytes is due to multiple cytokines", *Clinical and Experimental Immunology*, vol. 106, no. 2, pp. 230–236, Nov. 1996. DOI: 10.1046/j.1365-2249.1996.d01-836.x.

[44] S. Carnevale, I. D. Ceglie, G. Grieco, A. Rigatelli, E. Bonavita, and S. Jaillon, "Neutrophil diversity in inflammation and cancer", *Frontiers in Immunology*, vol. 14, Apr. 2023. DOI: 10.3389/fimmu.2023.1180810.

[45] H. L. Wright, M. Lyon, E. A. Chapman, R. J. Moots, and S. W. Edwards, "Rheumatoid arthritis synovial fluid neutrophils drive inflammation through production of chemokines, reactive oxygen species, and neutrophil extracellular traps", *Frontiers in Immunology*, vol. 11, Jan. 2021. DOI: 10.3389/fimmu.2020.584116.

[46] A. B. Nowakowski, W. J. Wobig, and D. H. Petering, "Native sds-page: High resolution electrophoretic separation of proteins with retention of native properties including bound metal ions", *Metallomics : integrated biometal science*, vol. 6, no. 5, pp. 1068–1078, May 2014. DOI: 10.1039/c4mt00033a.

[47] R. Wiesner, C. Scheller, F. Krebs, H. Wätzig, and I. Oltmann-Norden, "A comparative study of ce-sds, sds-page, and simple western: Influences of sample preparation on molecular weight determination of proteins", *Electrophoresis*, vol. 42, no. 3, pp. 206–218, Feb. 2021. DOI: 10.1002/elps.202000199.

[48] W.-H. Dong, T.-Y. Wang, F. Wang, and J.-H. Zhang, "Simple, time-saving dye staining of proteins for sodium dodecyl sulfate–polyacrylamide gel electrophoresis using coomassie blue", *PLOS ONE*, vol. 6, no. 8, Aug. 2011. DOI: 10.1371/journal.pone.0022394.

[49] A. Rodger and K. Sanders, "Biomacromolecular applications of uv-visible absorption spectroscopy*", in *Encyclopedia of Spectroscopy and Spectrometry (Second Edition)*, J. C. Lindon, Ed., Second Edition, Oxford: Academic Press, 1999, pp. 166–173. DOI: https://doi.org/10.1016/B978-0-12-374413-5.00108-1.

[50] C. Ó'Fágáin, P. M. Cummins, and B. F. O'Connor, *Gel-Filtration Chromatography* (Methods in molecular biology). Humana Press, 2017, vol. 1485. DOI: 10.1007/978-1-4939-6412-3_2.

[51] J. B. Ngere, K. H. Ebrahimi, R. Williams, E. Pires, J. Walsby-Tickle, and J. S. O. McCullagh, "Ion-exchange chromatography coupled to mass spectrometry in life science, environmental, and medical research", *Analytical Chemistry*, vol. 95, no. 1, pp. 152–166, Jan. 2023. DOI: 10.1021/acs.analchem.2c04298.

[52] M. Schauperl, M. Podewitz, B. J. Waldner, and K. R. Liedl, "Enthalpic and entropic contributions to hydrophobicity", *Journal of Chemical Theory and Computation*, vol. 12, no. 9, pp. 4600–4610, Jul. 2016. DOI: 10.1021/acs.jctc.6b00422.

[53] R. Malviya, V. Bansal, O. Pal, and P. Sharma, "High performance liquid chromatography: A short review", *Journal of Global Pharma Technology*, vol. 2, no. 5, pp. 22–26, Jun. 2010.

[54] J. G. McDonald, P. T. Ivanova, and H. A. Brown, "Chapter 2 - approaches to lipid analysis", in *Biochemistry of Lipids, Lipoproteins and Membranes*, N. D. Ridgway and R. S. McLeod, Eds., Sixth Edition, Boston: Elsevier, 2016, pp. 41–72. DOI: 10.1016/B978-0-444-63438-2.00002-X.

[55] M. Imran, M. S. Butt, S. Akhtar, M. Riazi, M. J. Iqbal, and H. A. R. Suleria, "Quantification of mangiferin by high pressure liquid chromatography; physicochemical and sensory evaluation of functional mangiferin drink", *Journal of Food Processing and Preservation*, vol. 40, no. 4, pp. 760–769, Nov. 2015. DOI: 10.1111/jfpp.12657.

[56] M. A. Skidmore and J. E. Turnbull, "Chapter 6 - separation and sequencing of heparin and heparan sulphate saccharides", in *Chemistry and Biology of Heparin and Heparan Sulfate*, H. G. Garg, R. J. Linhardt, and C. A. Hales, Eds., Amsterdam: Elsevier Science, 2005, pp. 179–201. DOI: https://doi.org/10.1016/B978-008044859-6/50007-1.

[57] K. Robards and D. Ryan, "Chapter 5 - high performance liquid chromatography: Instrumentation and techniques", in *Principles and Practice of Modern Chromatographic Methods (Second Edition)*, K. Robards and D. Ryan, Eds., Second Edition, Academic Press, 2022, pp. 247–282. DOI: https://doi.org/10.1016/B978-0-12-822096-2.00009-8.

[58] K. Robards, P. Haddad, and P. Jackson, "5 - high-performance liquid chromatography—instrumentation and techniques", in *Principles and Practice of Modern Chromatographic Methods*, K. Robards, P. Haddad, and P. Jackson, Eds., Boston: Academic Press, 2004, pp. 227–303. DOI: https://doi.org/10.1016/B978-0-08-057178-2.50008-X.

[59] V. S. Joshi, V. Kumar, and A. S. Rathore, "Role of organic modifier and gradient shape in rp-hplc separation: Analysis of gcsf variants", *Journal of Chromatographic Science*, vol. 53, no. 3, pp. 417–423, Jan. 2015. DOI: 10.1093/chromsci/bmu222.

[60] M. Mamouei, K. Budidha, N. Baishya, M. Qassem, and P. A. Kyriacou, "An empirical investigation of deviations from the beer–lambert law in optical estimation of lactate", *Scientific Reports*, vol. 11, no. 13734, Jul. 2021. DOI: 10.1038/s41598-021-92850-4.

[61] J. E. Noble, "Chapter two - quantification of protein concentration using uv absorbance and coomassie dyes", in *Laboratory Methods in Enzymology: Protein Part A*, ser. Methods in Enzymology, J. Lorsch, Ed., vol. 536, Academic Press, 2014, pp. 17–26. DOI: https://doi.org/10.1016/B978-0-12-420070-8.00002-7.

[62] J. Z. Porterfield and A. Zlotnick, "A simple and general method for determining the protein and nucleic acid content of viruses by uv absorbance", *Virology*, vol. 407, no. 2, pp. 281–288, Nov. 2010. DOI: 10.1016/j.virol.2010.08.015.

[63] B. J. H. Kuipers and H. Gruppen, "Prediction of molar extinction coefficients of proteins and peptides using uv absorption of the constituent amino acids at 214 nm to enable quantitative reverse phase high-performance liquid chromatographymass spectrometry analysis", *Journal of Agricultural and Food Chemistry*, vol. 55, no. 14, pp. 5445–5451, Jun. 2007. DOI: 10.1021/jf0703371.

[64] S. Boyden, "The chemotactic effect of mixtures of antibody and antigen on polymorphonuclear leukocytes", *Journal of Experimental Medicine*, vol. 115, no. 3, pp. 453–466, Feb. 1962. DOI: 10.1084/jem.115.3.453.

[65] Katarina Wolf et al., "Physical limits of cell migration: Control by ecm space and nuclear deformation and tuning by proteolysis and traction force", *Journal of Cell Biology*, vol. 201, no. 7, pp. 1069–1084, Jun. 2013. DOI: 10.1083/jcb.201210152.

[66] S. Wickramasinghe and W. Erber, "Chapter 1 - normal blood cells", in *Blood and Bone Marrow Pathology (Second Edition)*, A. Porwit, J. McCullough, and W. N. Erber, Eds., Second Edition, Edinburgh: Churchill Livingstone, 2011, pp. 3–18. DOI: https://doi.org/10.1016/B978-0-7020-3147-2.00001-8.

[67] H. Drescher, S. Weiskirchen, and R. Weiskirchen, "Flow cytometry: A blessing and a curse", *Biomedicines*, vol. 9, no. 11, Nov. 2021. DOI: 10.3390/biomedicines9111613.

[68] A. Adan, G. Alizada, Y. Kiraz, Y. Baran, and A. Nalbant, "Flow cytometry: Basic principles and applications", *Critical Reviews in Biotechnology*, vol. 37, no. 2, pp. 163–176, Mar. 2016. DOI: 10.3109/07388551.2015.1128876.

[69] H. Brouwers et al., "Hyaluronidase treatment of synovial fluid is required for accurate detection of inflammatory cells and soluble mediators", *Arthritis research therapy*, vol. 24, no. 18, Jan. 2022. DOI: 10.1186/s13075-021-02696-4.

[70] H. Brouwers et al., "Hyaluronidase treatment of synovial fluid is required for accurate detection of inflammatory cells and soluble mediators", *Arthritis Research and Therapy*, vol. 24, no. 1, Jan. 2022. DOI: 10.1186/s13075-021-02696-4.

[71] H. S. Jónasdóttir et al., "Targeted lipidomics reveals activation of resolution pathways in knee osteoarthritis in humans", *Osteoarthritis and Cartilage*, vol. 25, no. 7, pp. 1150–1160, Jul. 2017. DOI: 10.1016/j.joca.2017.01.018.

[72] A. Pribush, D. Zilberman-Kravits, and N. Meyerstein, "The mechanism of the dextran-induced red blood cell aggregation", *European Biophysics Journal*, vol. 36, no. 2, pp. 85–94, Feb. 2007. DOI: 10.1007/s00249-006-0107-1.

[73] S. A. H. M. van den Tillaart, M. P. H. Busard, and J. B. M. Z. Trimbos, "The use of distilled water in the achievement of local hemostasis during surgery", *Gynecological surgery*, vol. 6, no. 3, pp. 255–259, Jan. 2009. DOI: 10.1007/s10397-008-0464-0.

[74] S.-O. Kim, J. Kim, T. Okajima, and N.-J. Cho, "Mechanical properties of paraformaldehyde-treated individual cells investigated by atomic force microscopy and scanning ion conductance microscopy", *Nano convergence*, vol. 4, no. 1, Mar. 2017. DOI: 10.1186/s40580-017-0099-9.

[75] O. Núñez and P. Lucci, "Applications and uses of formic acid in liquid chromatography-mass spectrometry analysis", in Jan. 2014, pp. 71–86, ISBN: 978-1-62948-275-0.

[76] J. Sasse and S. R. Gallagher, "Staining proteins in gels", *Current Protocols in Molecular Biology*, Jan. 2009. DOI: 10.1002/0471142727.mb1006s85.

A

Flow cytometry plots for the synovial fluids

A.1 Synovial fluid with 90 % neutrophils before cell removal

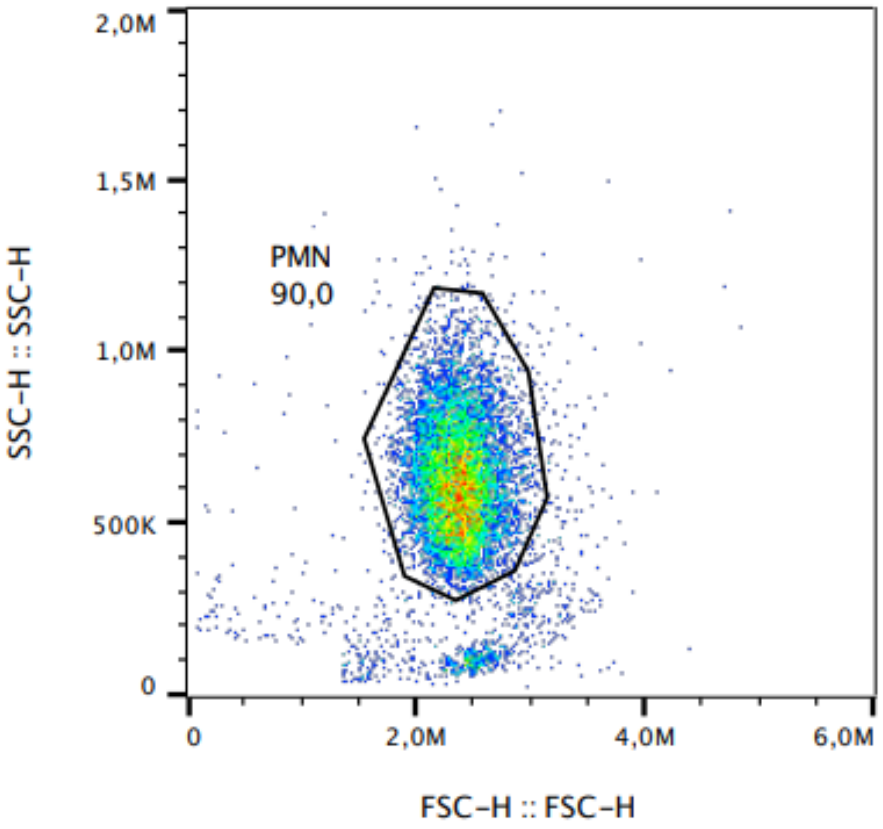

Figure A.1: A scatter plot of counts from flow cytometry of the 90 % synovial fluid (as determined by the neutrophil gate applied), with SSC plotted versus FSC. The total number of counts detected for this sample is 10267.

A.2 Synovial fluid with 5 % neutrophils before cell removal

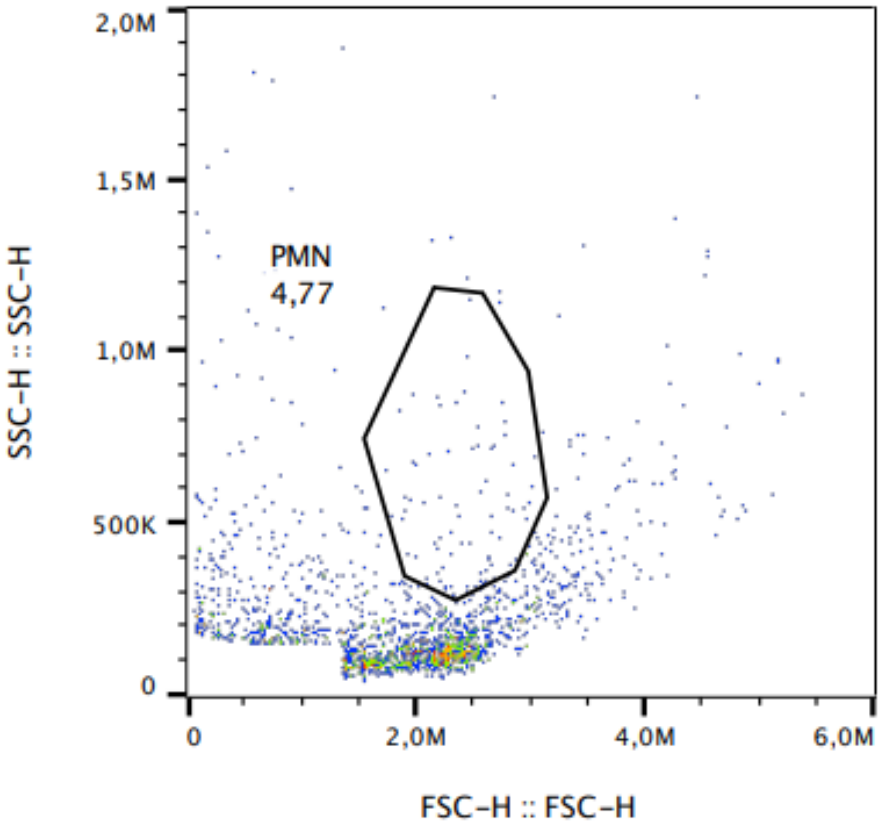

Figure A.2: A scatter plot of counts from flow cytometry of the 5 % synovial fluid (as determined by the neutrophil gate applied), with SSC plotted versus FSC. The total number of counts detected for this sample is 1676.

B

Liquid chromatography-mass spectrometry of fractions from gel electrophoresis

B.1 Extracted proteins of sizes <15 kDa

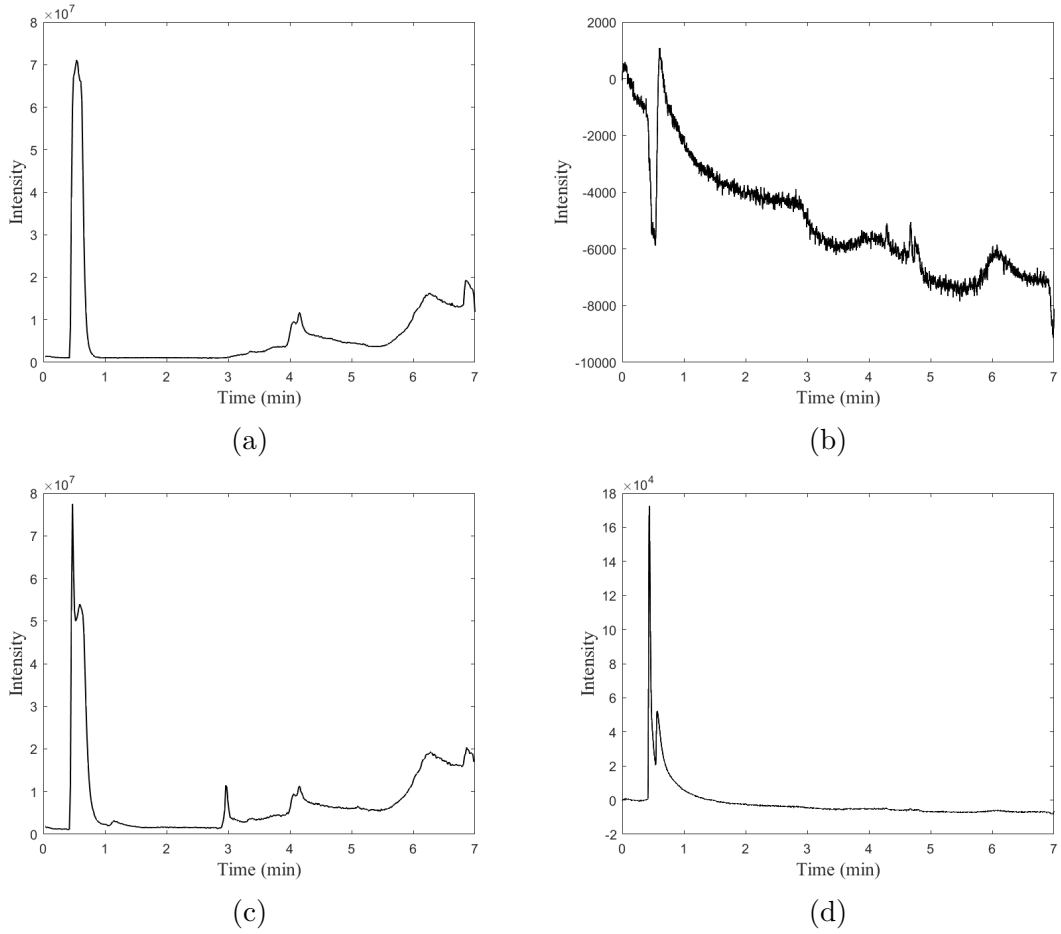

Figure B.1: The total ion chromatogram and UV-absorption at 280 nm for the extracted 90 % synovial fluid proteins from gel with sizes <15 kDa in (a) and (b), respectively, and for the PBS (blank) measurement run before that in (a) and (b).

B.2 Extracted proteins of sizes 15-25 kDa

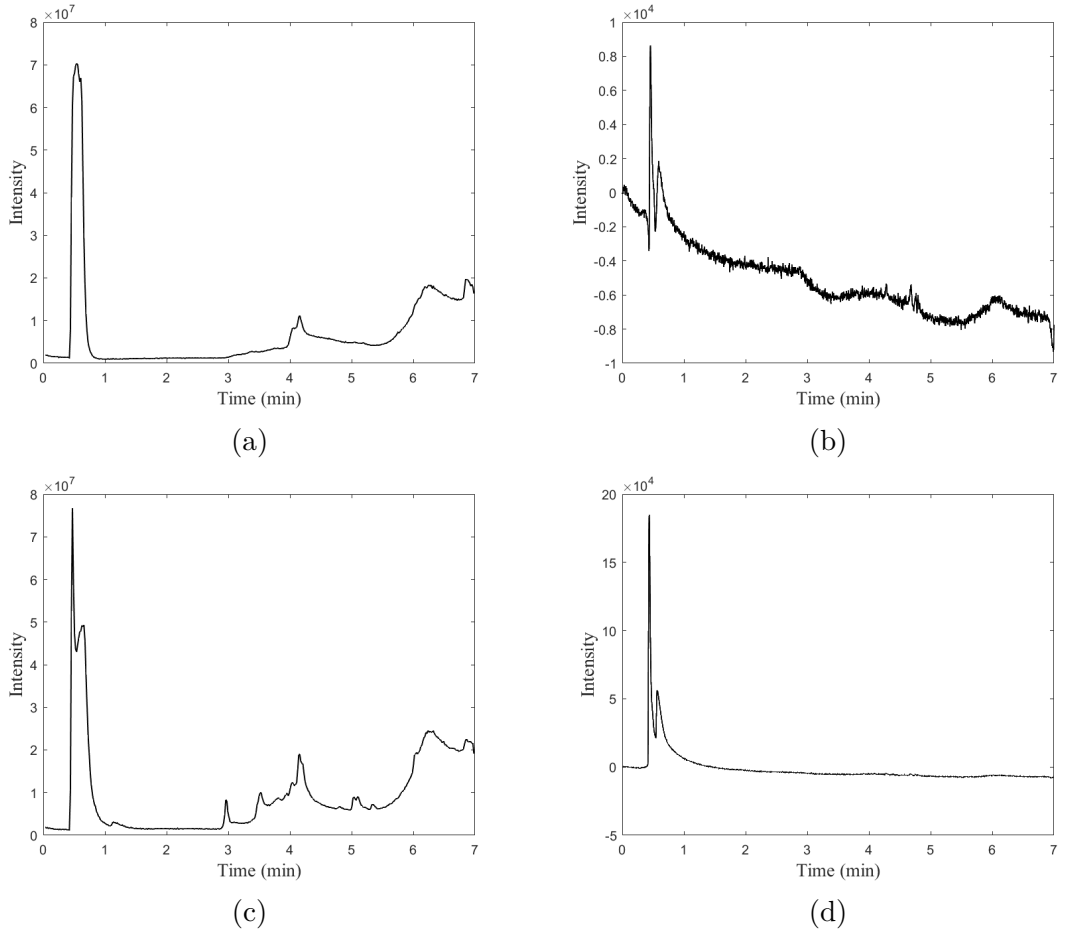

Figure B.2: The total ion chromatogram and UV-absorption at 280 nm for the extracted 90 % synovial fluid proteins from gel with sizes 15-25 kDa in (a) and (b), respectively, and for the PBS (blank) measurement run before that in (a) and (b).

B.3 Extracted proteins of sizes 25-37 kDa

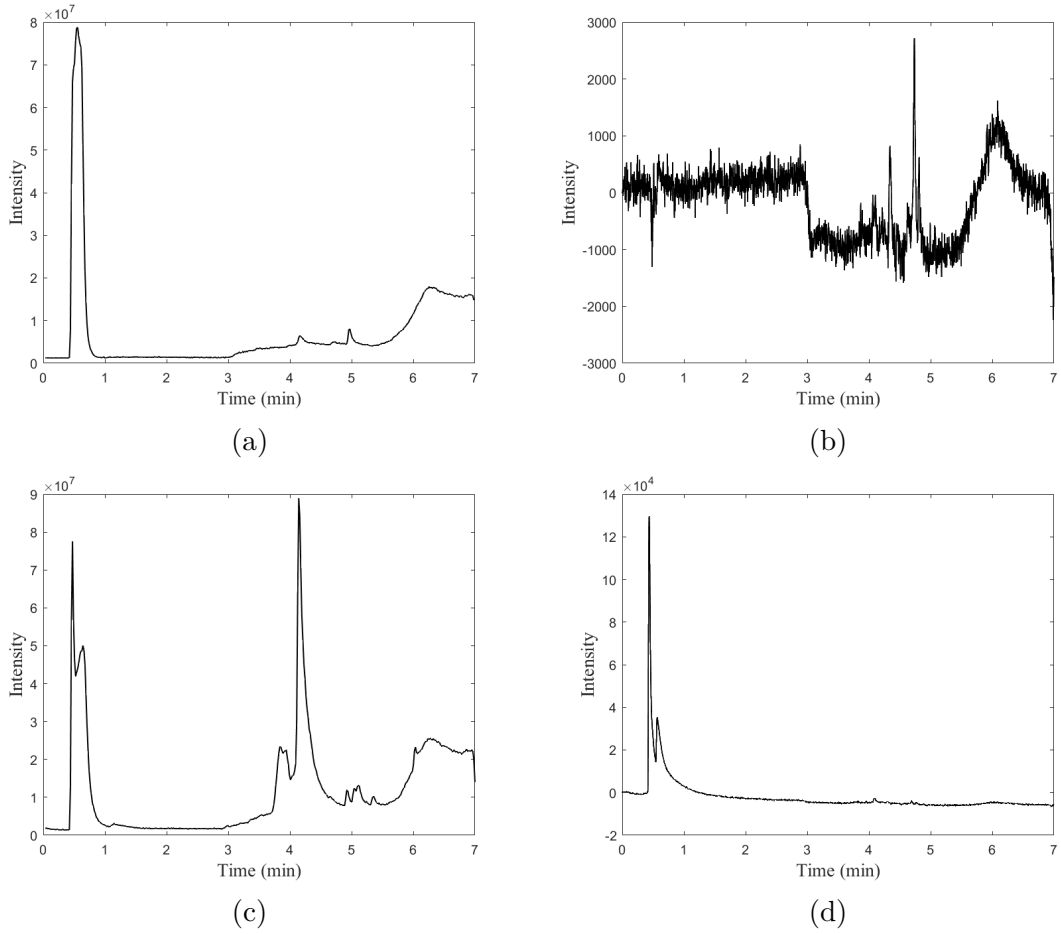

Figure B.3: The total ion chromatogram and UV-absorption at 280 nm for the extracted 90 % synovial fluid proteins from gel with sizes 25-37 kDa in (c) and (d), respectively, and for the PBS (blank) measurement run before that in (a) and (b).

B.4 Extracted proteins of sizes 37-50 kDa

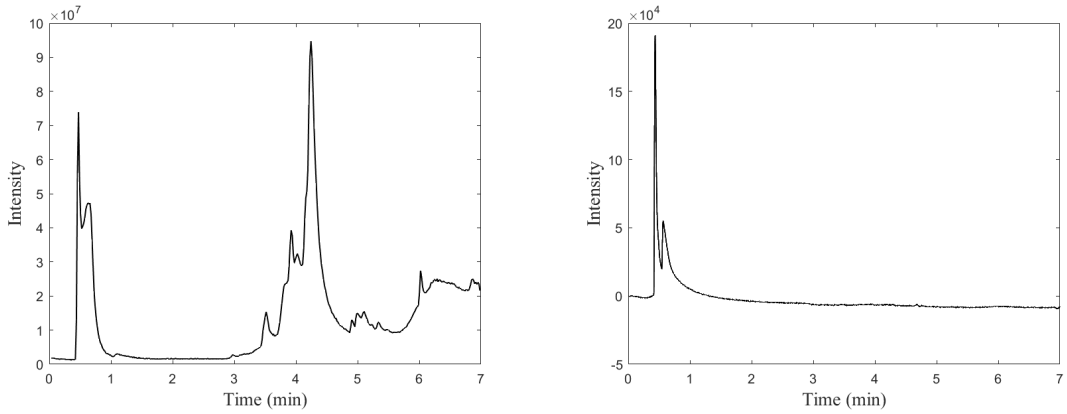

(a) (b)

Figure B.4: The total ion chromatogram and UV-absorption at 280 nm for the extracted 90 % synovial fluid proteins from gel with sizes 37-50 kDa in (a) and (b), respectively, and for the PBS (blank) measurement run before that in (a) and (b).

C

Flow cytometry measurements of samples applied in chemotaxis assay

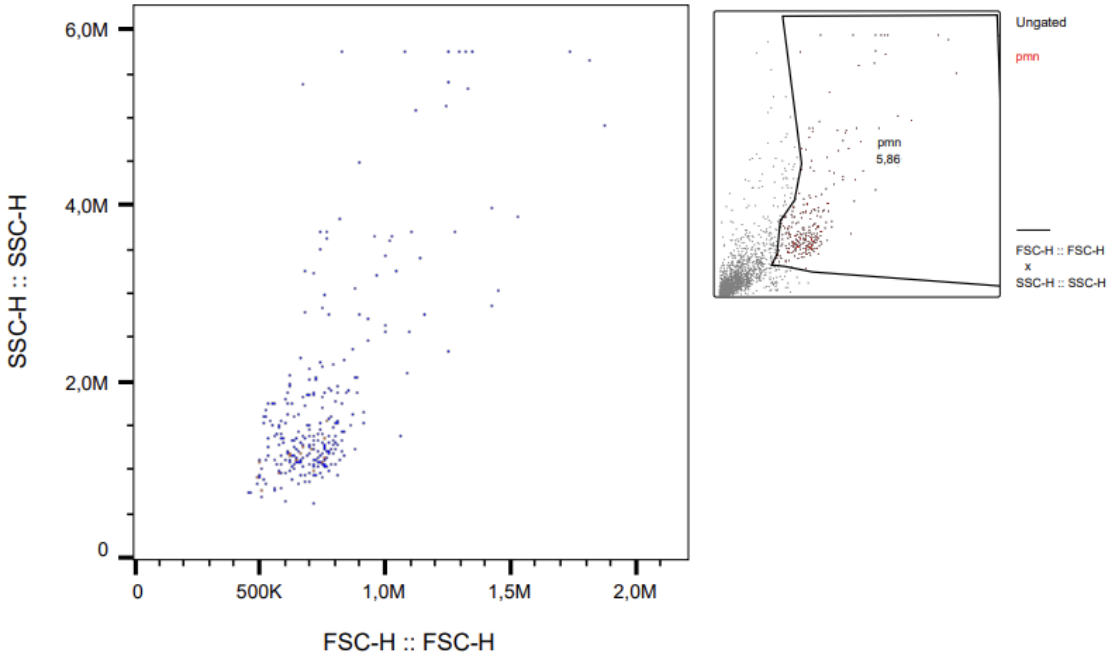

Figure C.1: A scatterplot of counts from flow cytometry of migrated cells from chemotaxis of the negative control (spontaneous migration) from the first chemotaxis set-up is plotted, with SSC versus FSC. The upper right figure displays the original plot and the neutrophil gate used, while the center figure exclusively shows the counts within the gate.

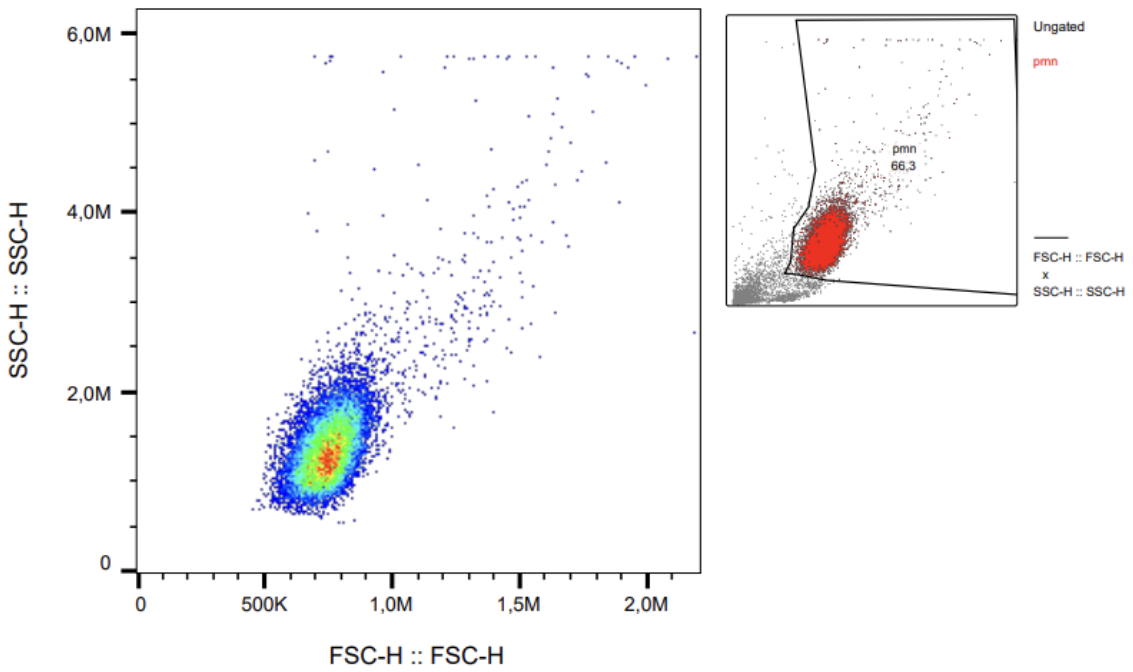

Figure C.2: A scatterplot of counts from flow cytometry of migrated cells from chemotaxis of the positive control from the first chemotaxis set-up is plotted, with SSC versus FSC. The upper right figure displays the original plot and the neutrophil gate used, while the center figure exclusively shows the counts within the gate.

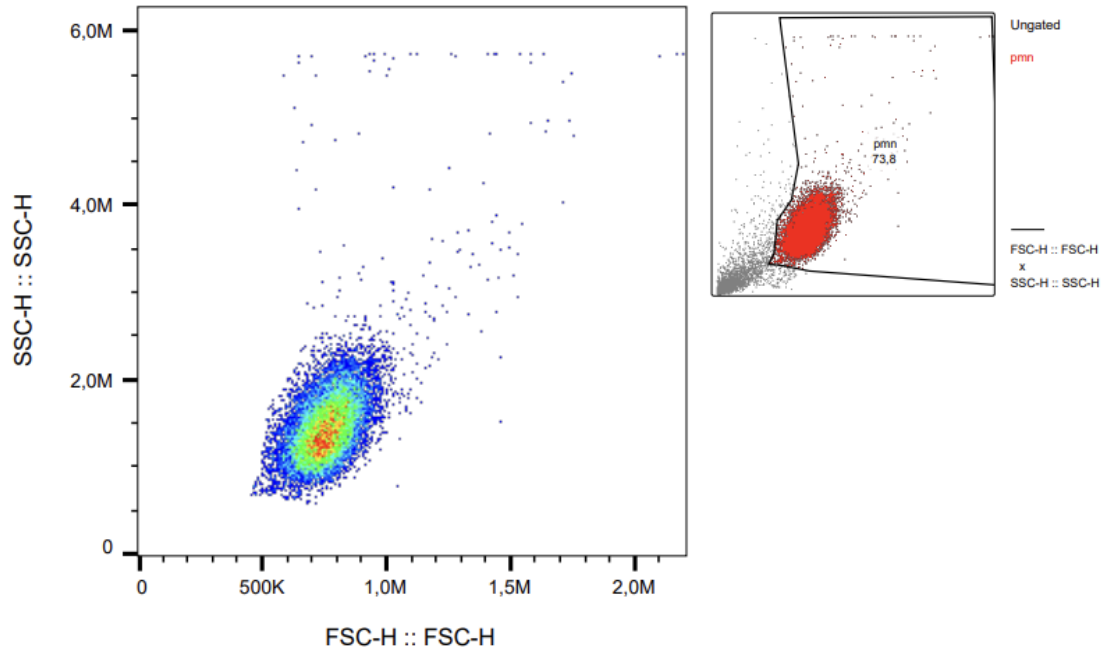

Figure C.3: A scatterplot of counts from flow cytometry of migrated cells from chemotaxis of the fMLF control from the first chemotaxis set-up is plotted, with SSC versus FSC. The upper right figure displays the original plot and the neutrophil gate used, while the center figure exclusively shows the counts within the gate.

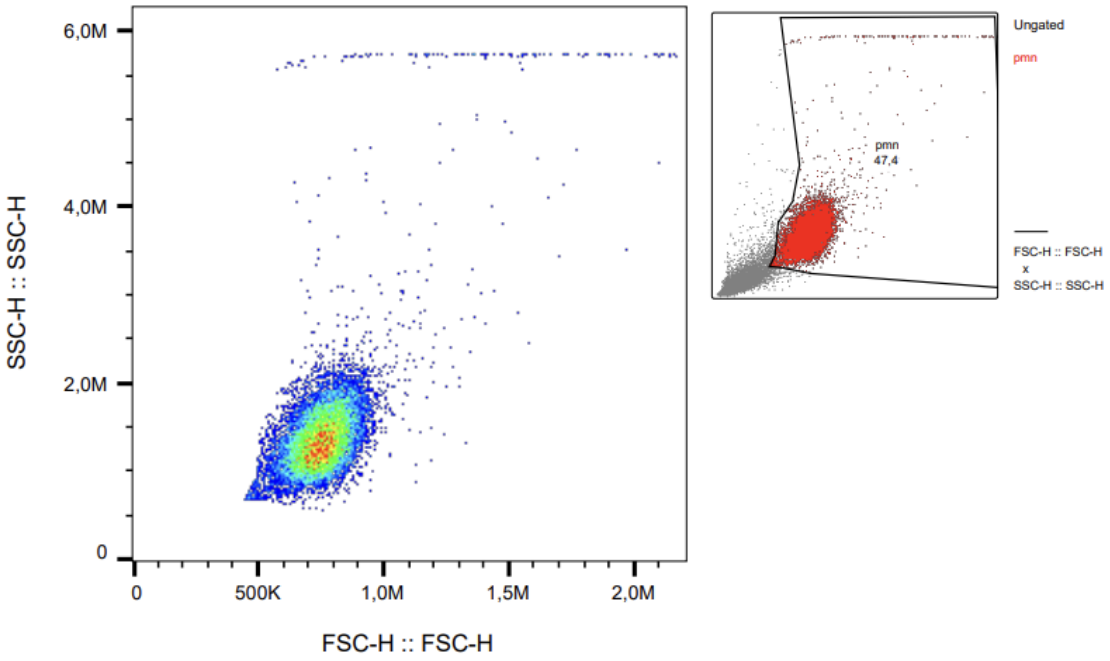

Figure C.4: A scatterplot of counts from flow cytometry of migrated cells from chemotaxis set-up one of the 90 % synovial fluid is plotted, with SSC versus FSC. The upper right figure displays the original plot and the neutrophil gate used, while the center figure exclusively shows the counts within the gate.

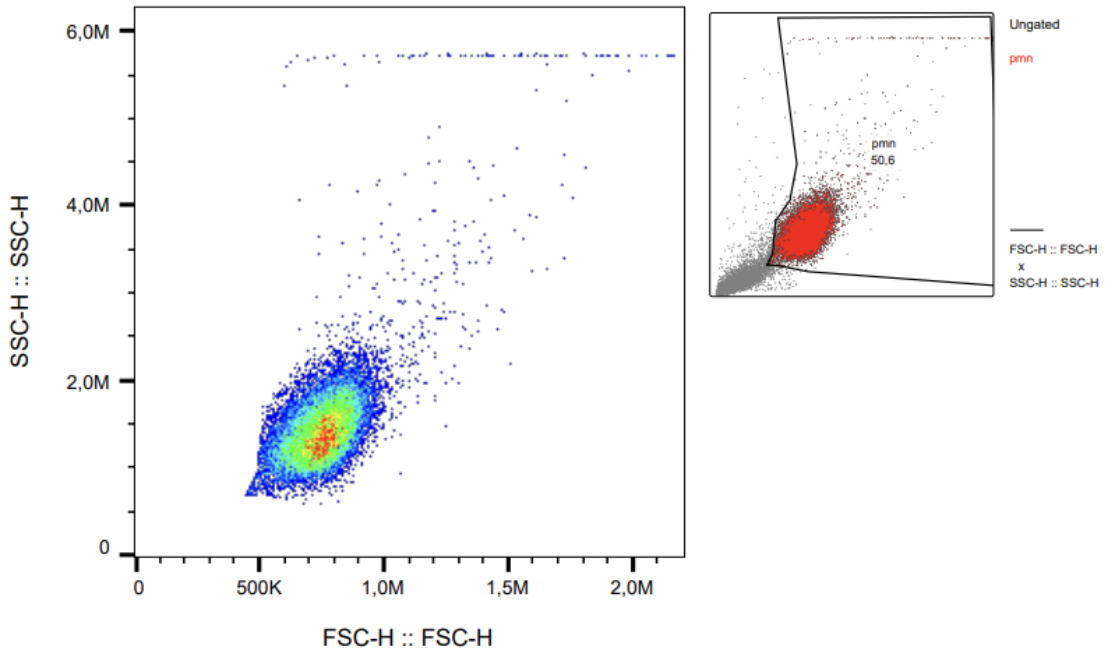

Figure C.5: A scatterplot of counts from flow cytometry of migrated cells from chemotaxis set-up one of hyaluronidase treated 90 % synovial fluid is plotted, with SSC versus FSC. The upper right figure displays the original plot and the neutrophil gate used, while the center figure exclusively shows the counts within the gate.

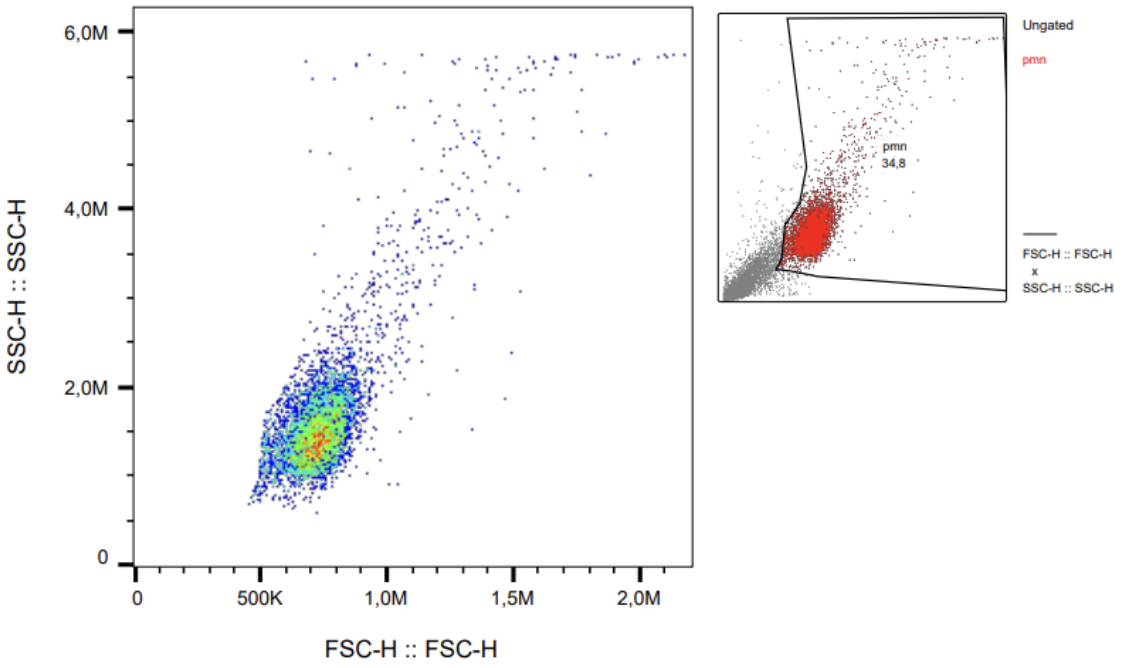

Figure C.6: A scatterplot of counts from flow cytometry of migrated cells from chemotaxis set-up ine of fractions B6-B7 collected from SEC of the 90 % synovial fluid is plotted, with SSC versus FSC. The upper right figure displays the original plot and the neutrophil gate used, while the center figure exclusively shows the counts within the gate.

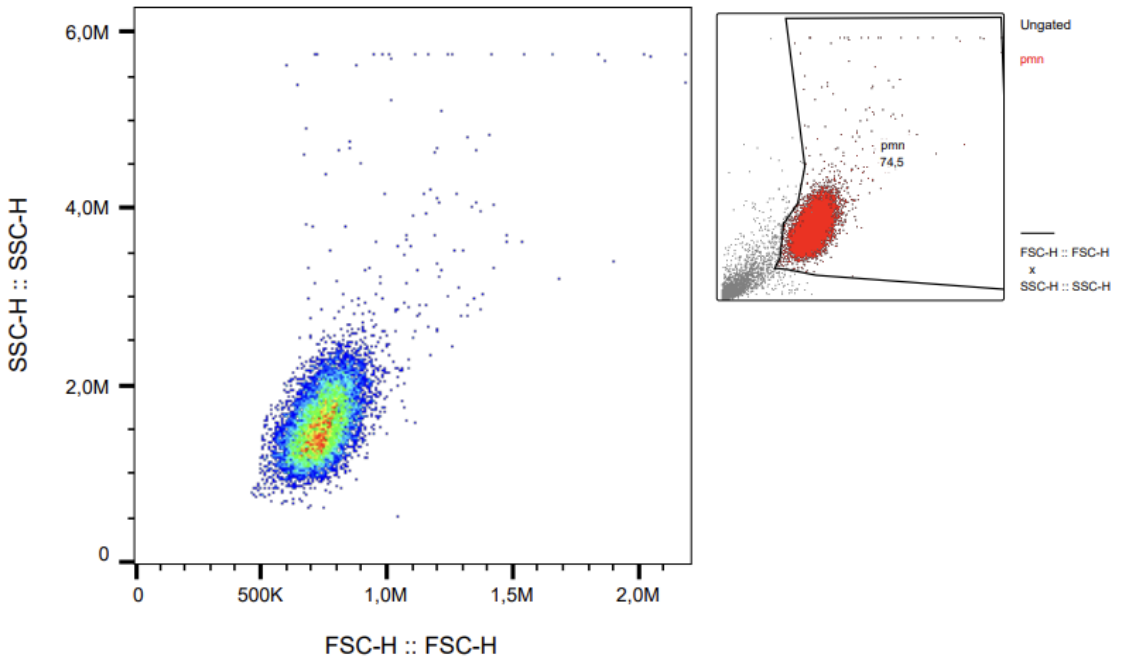

Figure C.7: A scatterplot of counts from flow cytometry of migrated cells from chemotaxis set-up one of fraction B8 collected from SEC of the 90 % synovial fluid is plotted, with SSC versus FSC. The upper right figure displays the original plot and the neutrophil gate used, while the center figure exclusively shows the counts within the gate.

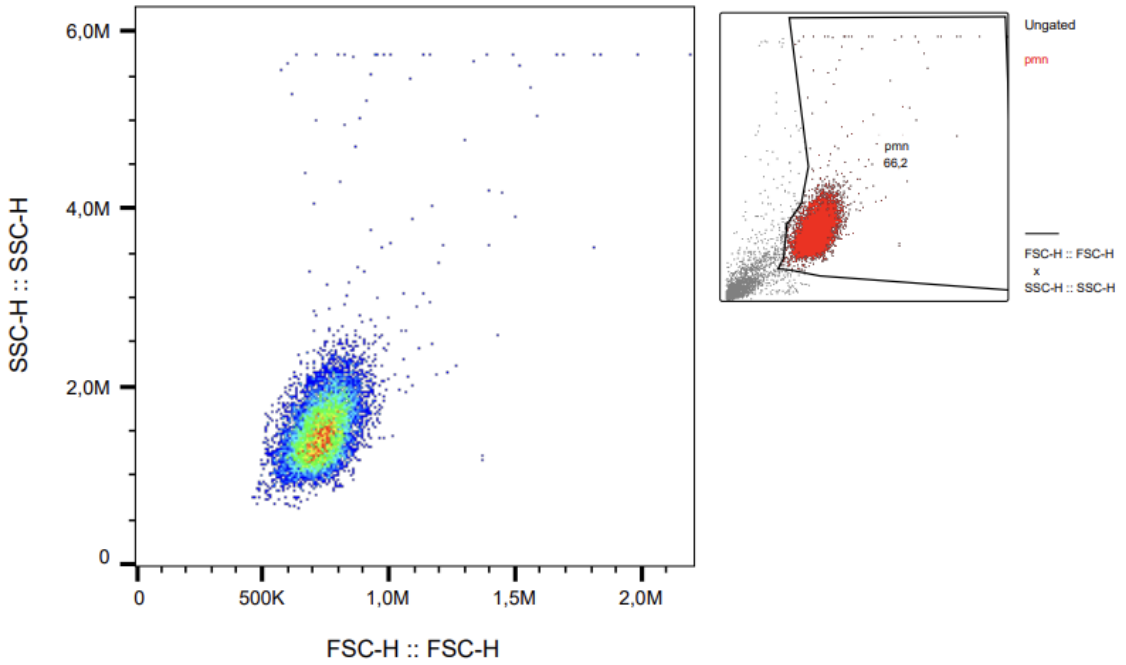

Figure C.8: A scatterplot of counts from flow cytometry of migrated cells from chemotaxis set-up one of fractions B9-B10 collected from SEC of the 90 % synovial fluid is plotted, with SSC versus FSC. The upper right figure displays the original plot and the neutrophil gate used, while the center figure exclusively shows the counts within the gate.

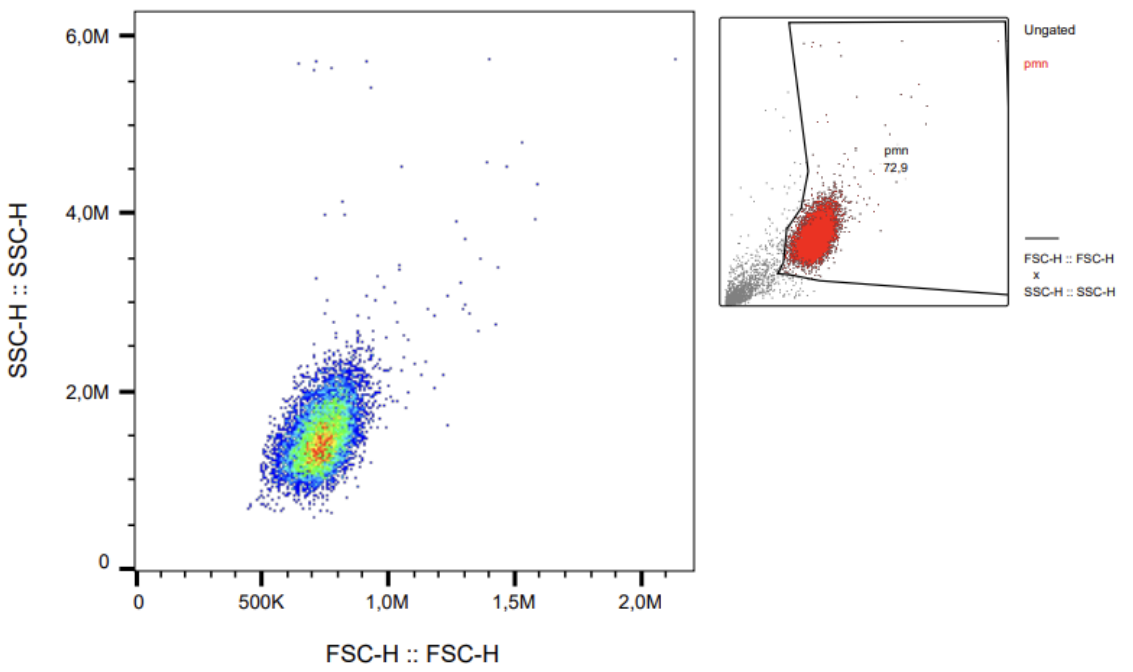

Figure C.9: A scatterplot of counts from flow cytometry of migrated cells from chemotaxis set-up one of fraction B11 collected from SEC of the 90 % synovial fluid is plotted, with SSC versus FSC. The upper right figure displays the original plot and the neutrophil gate used, while the center figure exclusively shows the counts within the gate.

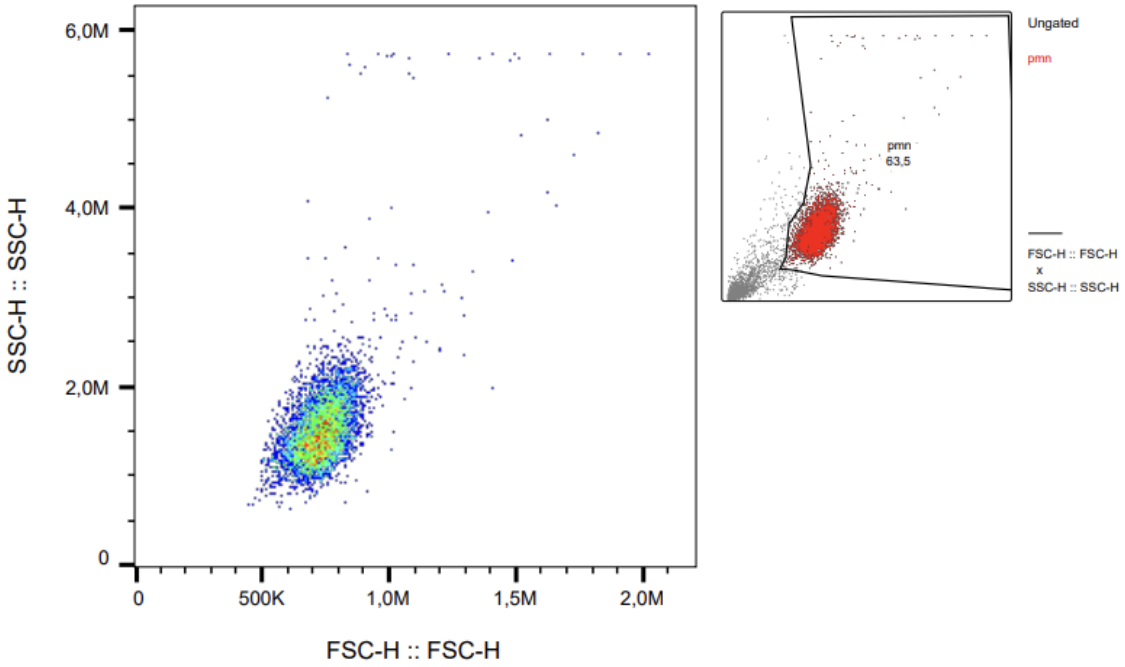

Figure C.10: A scatterplot of counts from flow cytometry of migrated cells from chemotaxis set-up one of fraction B12 collected from SEC of the 90 % synovial fluid is plotted, with SSC versus FSC. The upper right figure displays the original plot and the neutrophil gate used, while the center figure exclusively shows the counts within the gate.

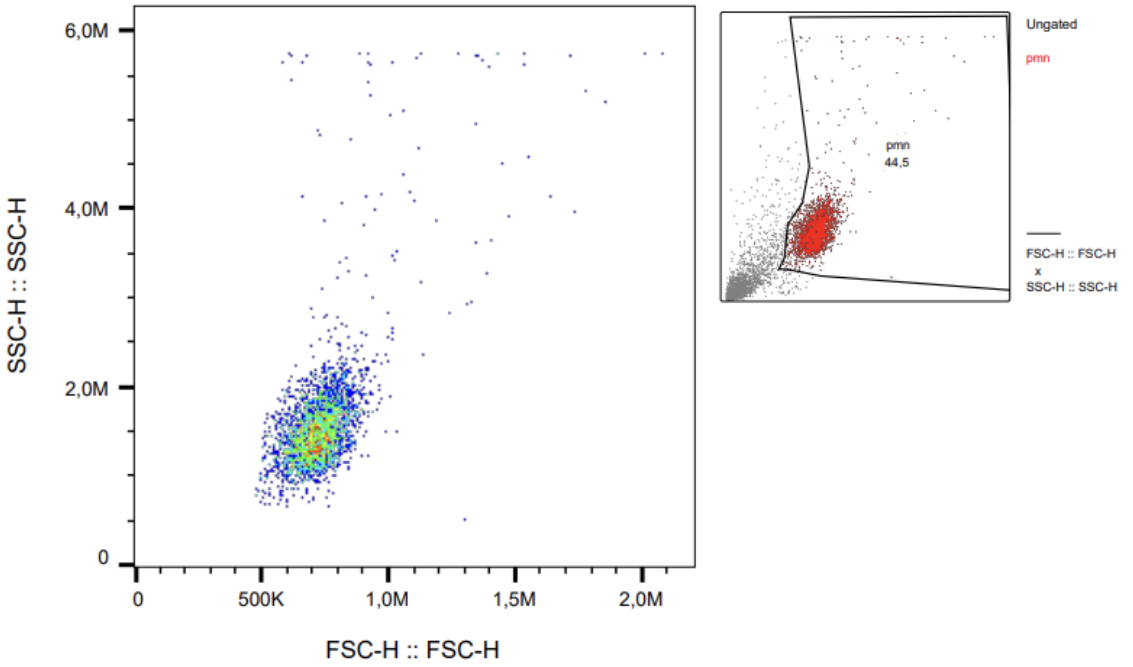

Figure C.11: A scatterplot of counts from flow cytometry of migrated cells from chemotaxis set-up one of fraction C1 collected from SEC of the 90 % synovial fluid is plotted, with SSC versus FSC. The upper right figure displays the original plot and the neutrophil gate used, while the center figure exclusively shows the counts within the gate.

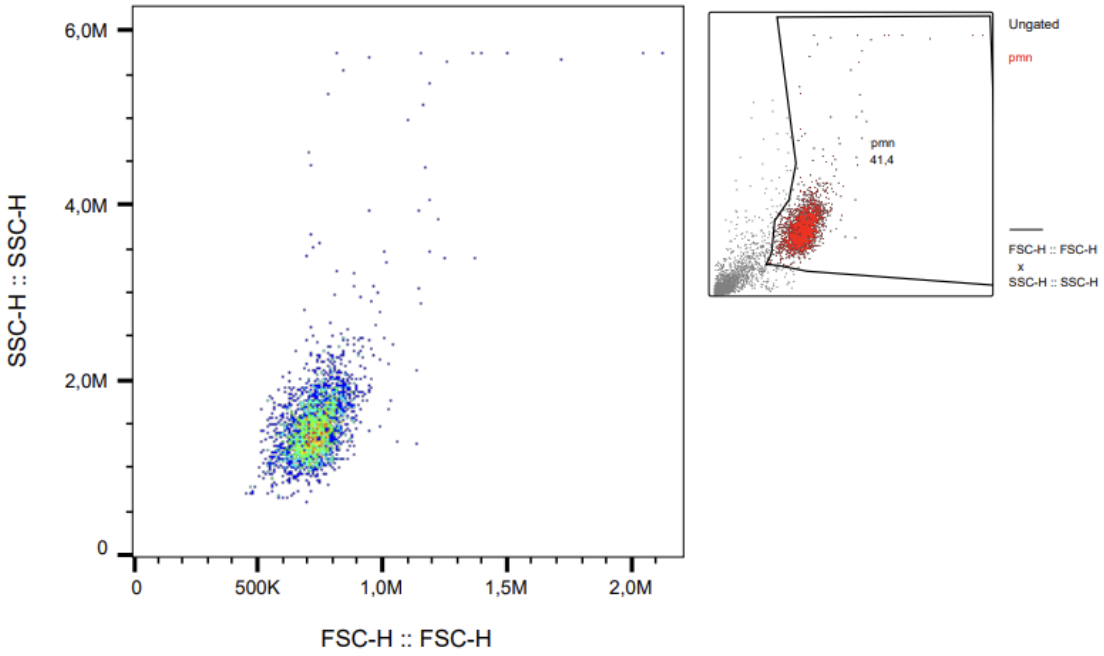

Figure C.12: A scatterplot of counts from flow cytometry of migrated cells from chemotaxis set-up one of fraction C2 collected from SEC of the 90 % synovial fluid is plotted, with SSC versus FSC. The upper right figure displays the original plot and the neutrophil gate used, while the center figure exclusively shows the counts within the gate.

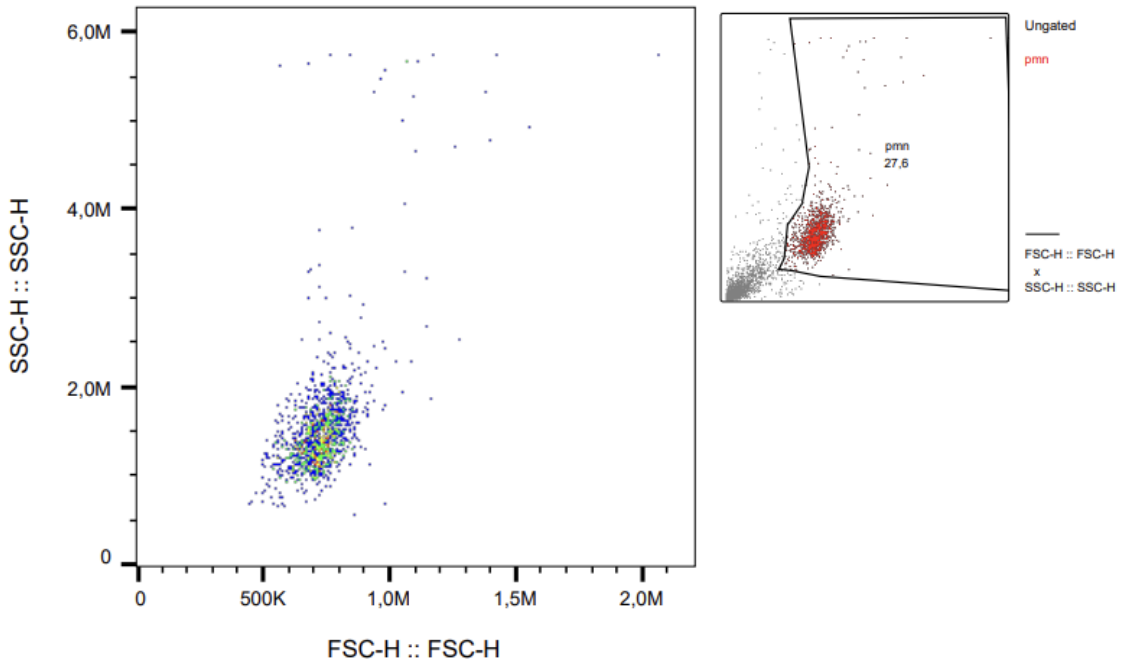

Figure C.13: A scatterplot of counts from flow cytometry of migrated cells from chemotaxis set-up one of fractions C3-C6 collected from SEC of the 90 % synovial fluid is plotted, with SSC versus FSC. The upper right figure displays the original plot and the neutrophil gate used, while the center figure exclusively shows the counts within the gate.

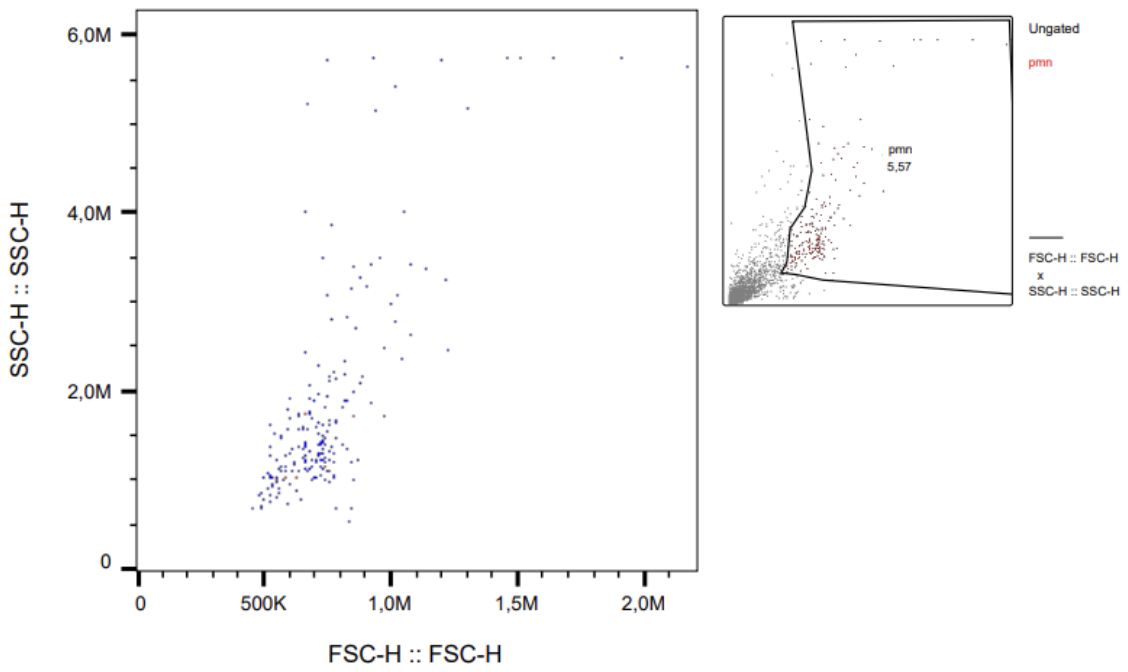

Figure C.14: A scatterplot of counts from flow cytometry of migrated cells from chemotaxis set-up one of fractions C7-C12 collected from SEC of the 90 % synovial fluid is plotted, with SSC versus FSC. The upper right figure displays the original plot and the neutrophil gate used, while the center figure exclusively shows the counts within the gate.

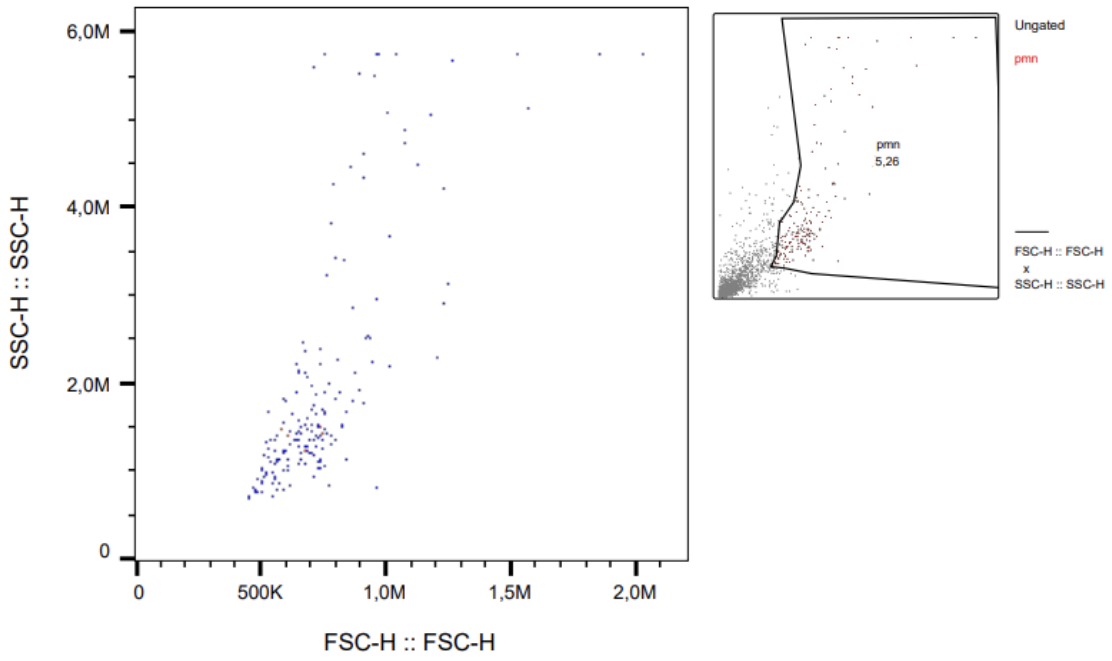

Figure C.15: A scatterplot of counts from flow cytometry of migrated cells from chemotaxis set-up one of fraction D1 collected from SEC of the 90 % synovial fluid is plotted, with SSC versus FSC. The upper right figure displays the original plot and the neutrophil gate used, while the center figure exclusively shows the counts within the gate.

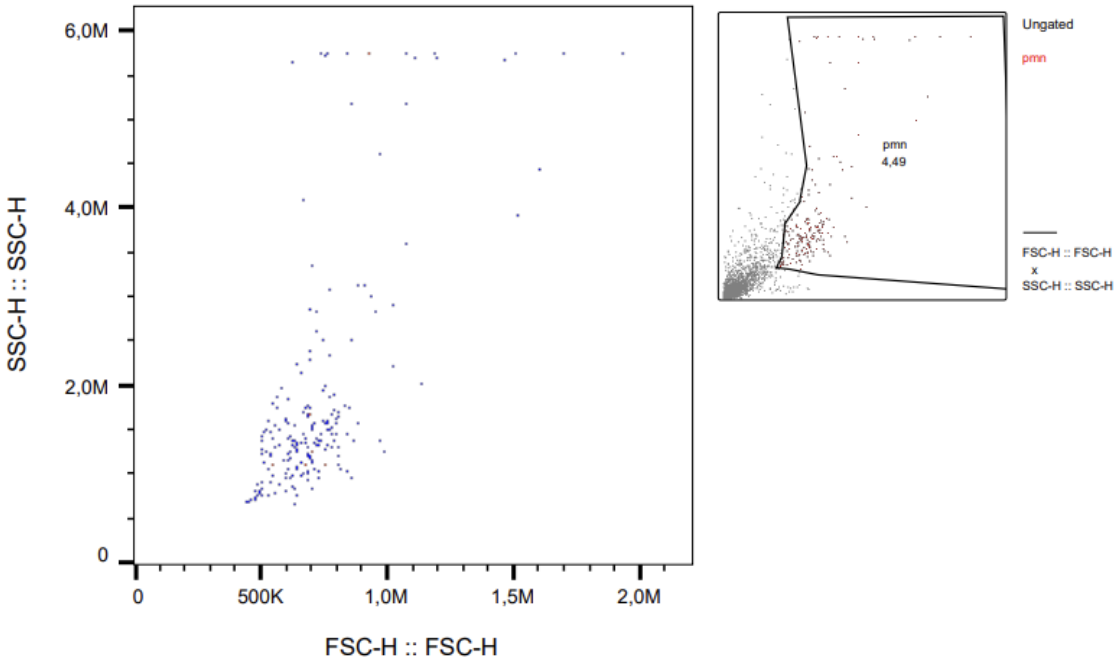

Figure C.16: A scatterplot of counts from flow cytometry of migrated cells from chemotaxis set-up one of fractions D2-D4 collected from SEC of the 90 % synovial fluid is plotted, with SSC versus FSC. The upper right figure displays the original plot and the neutrophil gate used, while the center figure exclusively shows the counts within the gate.

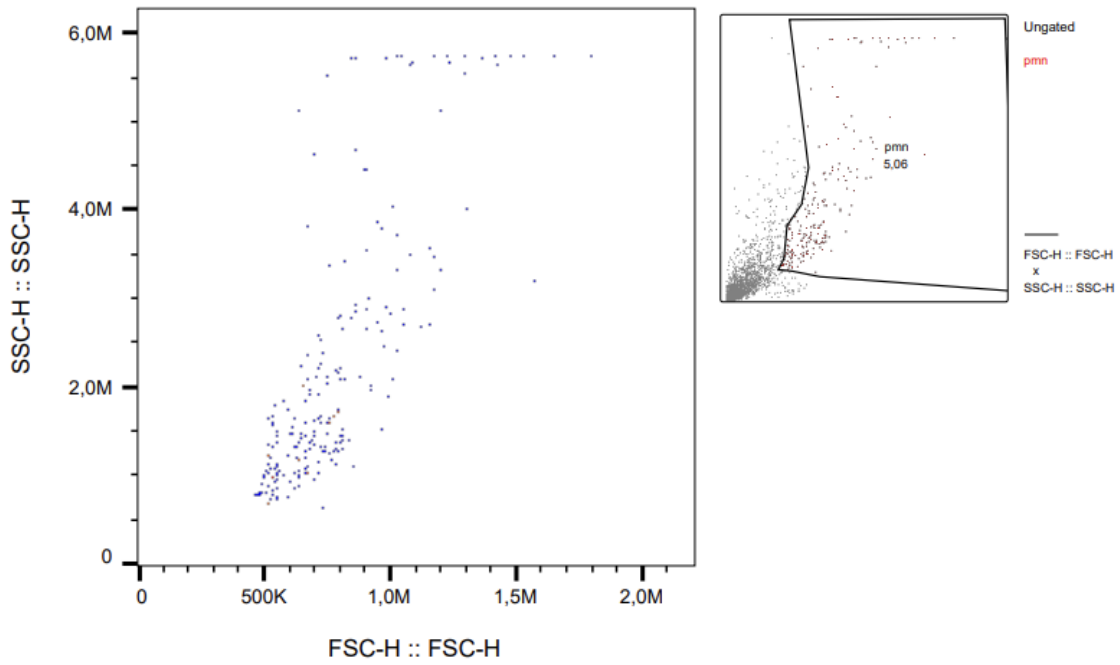

Figure C.17: A scatterplot of counts from flow cytometry of migrated cells from chemotaxis set-up one of fraction D5 collected from SEC of the 90 % synovial fluid is plotted, with SSC versus FSC. The upper right figure displays the original plot and the neutrophil gate used, while the center figure exclusively shows the counts within the gate.

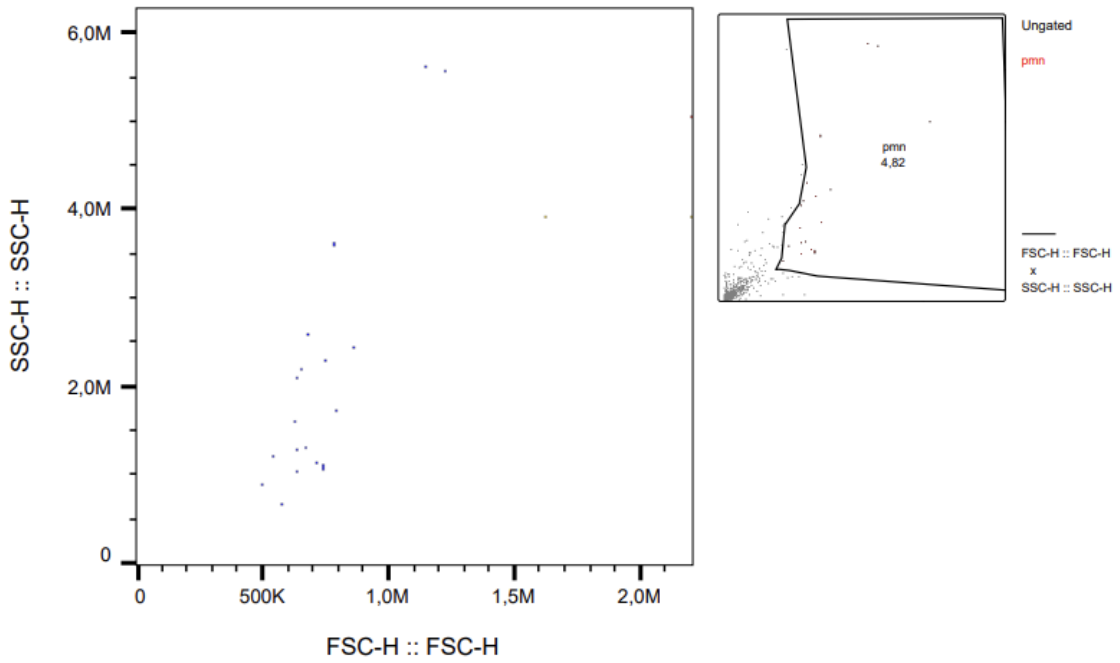

Figure C.18: A scatterplot of counts from flow cytometry of migrated cells from chemotaxis set-up one of fractions D6-D7 collected from SEC of the 90 % synovial fluid is plotted, with SSC versus FSC. The upper right figure displays the original plot and the neutrophil gate used, while the center figure exclusively shows the counts within the gate.

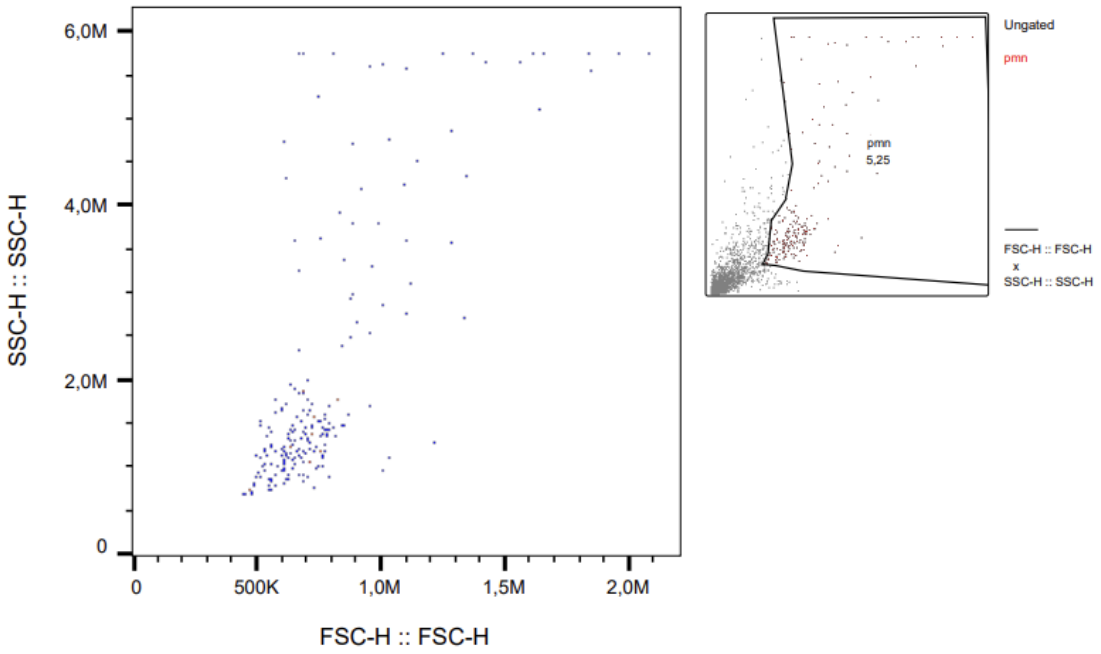

Figure C.19: A scatterplot of counts from flow cytometry of migrated cells from chemotaxis set-up one of fractions D8-D10 collected from SEC of the 90 % synovial fluid is plotted, with SSC versus FSC. The upper right figure displays the original plot and the neutrophil gate used, while the center figure exclusively shows the counts within the gate.

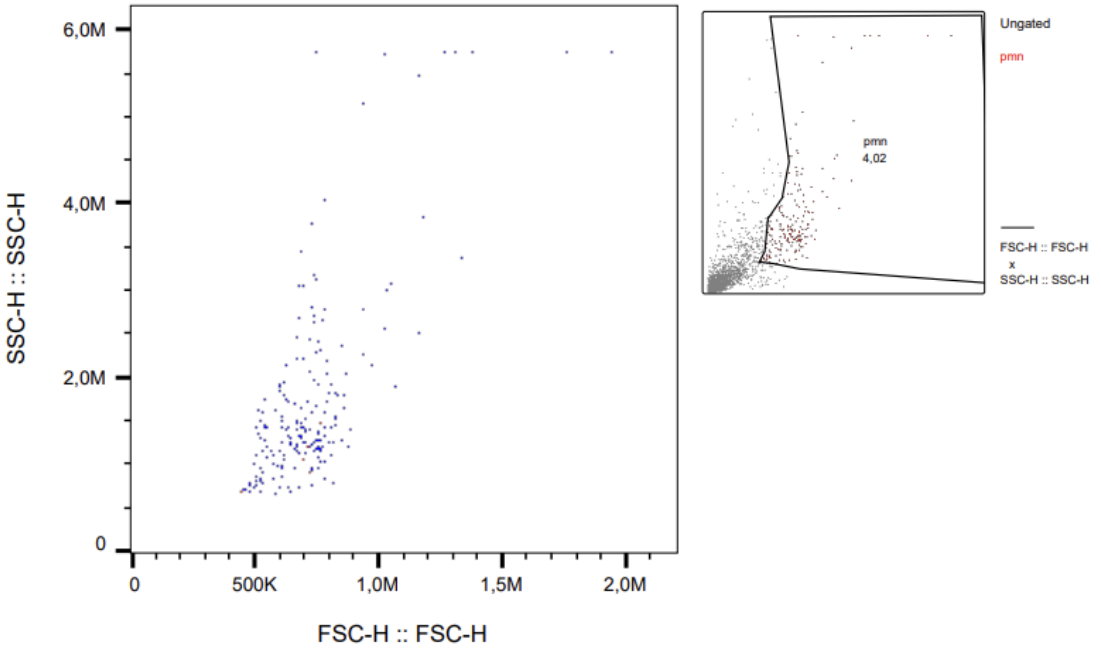

Figure C.20: A scatterplot of counts from flow cytometry of migrated cells from chemotaxis set-up one of fraction D11 collected from SEC of the 90 % synovial fluid is plotted, with SSC versus FSC. The upper right figure displays the original plot and the neutrophil gate used, while the center figure exclusively shows the counts within the gate.

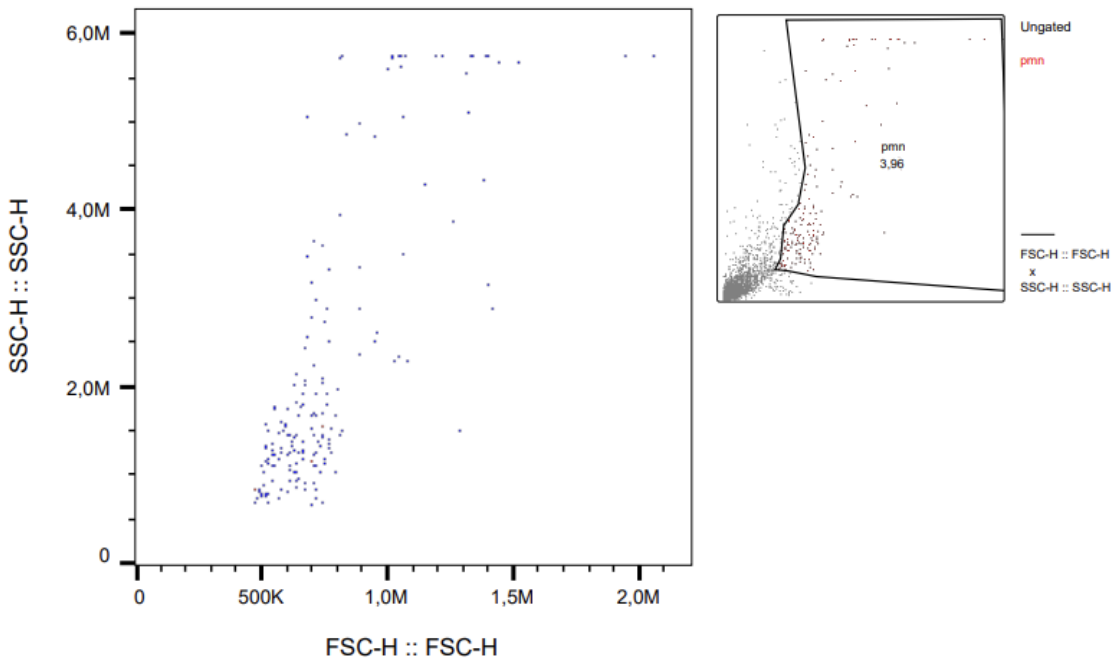

Figure C.21: A scatterplot of counts from flow cytometry of migrated cells from chemotaxis set-up one of fraction D12 collected from SEC of the 90 % synovial fluid is plotted, with SSC versus FSC. The upper right figure displays the original plot and the neutrophil gate used, while the center figure exclusively shows the counts within the gate.

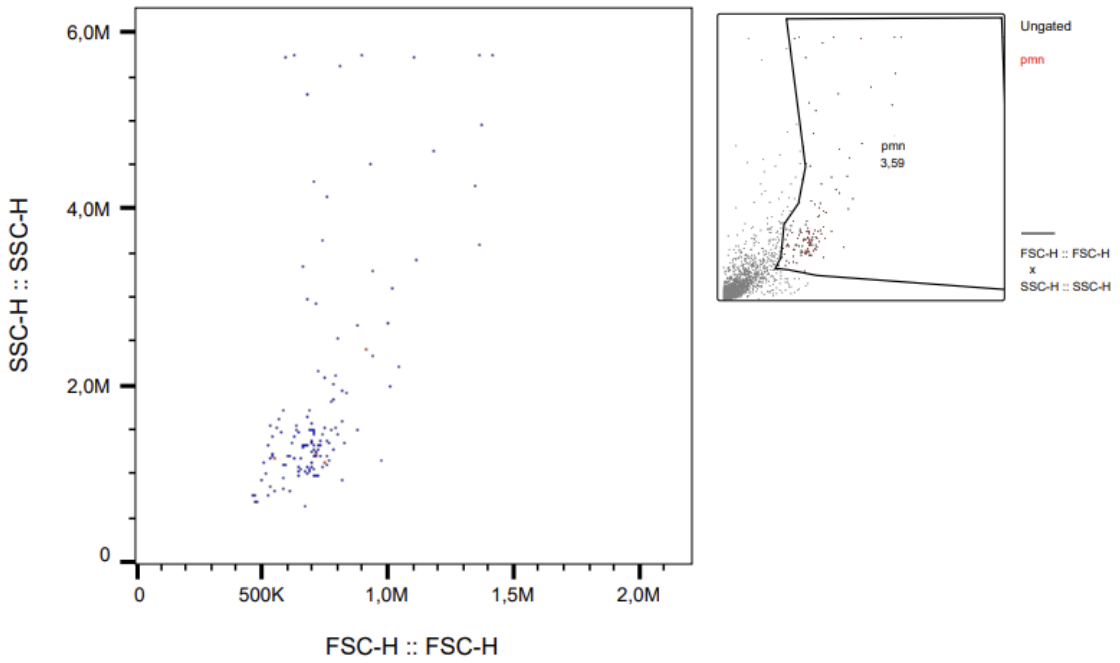

Figure C.22: A scatterplot of counts from flow cytometry of migrated cells from chemotaxis set-up one of fractions E1-E2 collected from SEC of the 90 % synovial fluid is plotted, with SSC versus FSC. The upper right figure displays the original plot and the neutrophil gate used, while the center figure exclusively shows the counts within the gate.

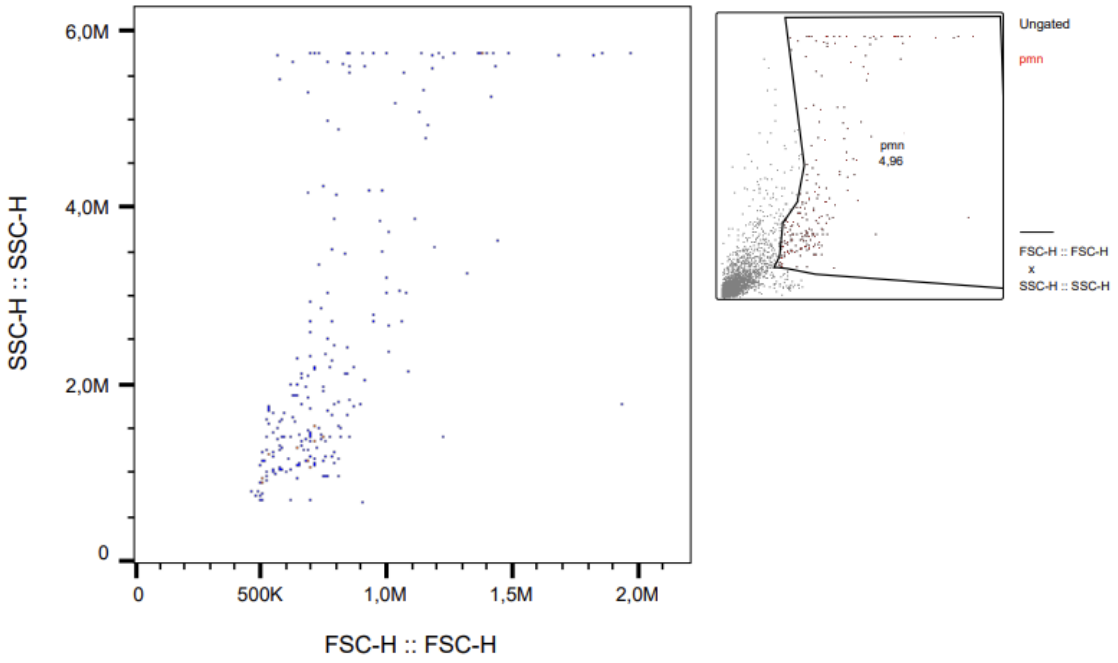

Figure C.23: A scatterplot of counts from flow cytometry of migrated cells from chemotaxis set-up one of fractions E3-E4 collected from SEC of the 90 % synovial fluid is plotted, with SSC versus FSC. The upper right figure displays the original plot and the neutrophil gate used, while the center figure exclusively shows the counts within the gate.

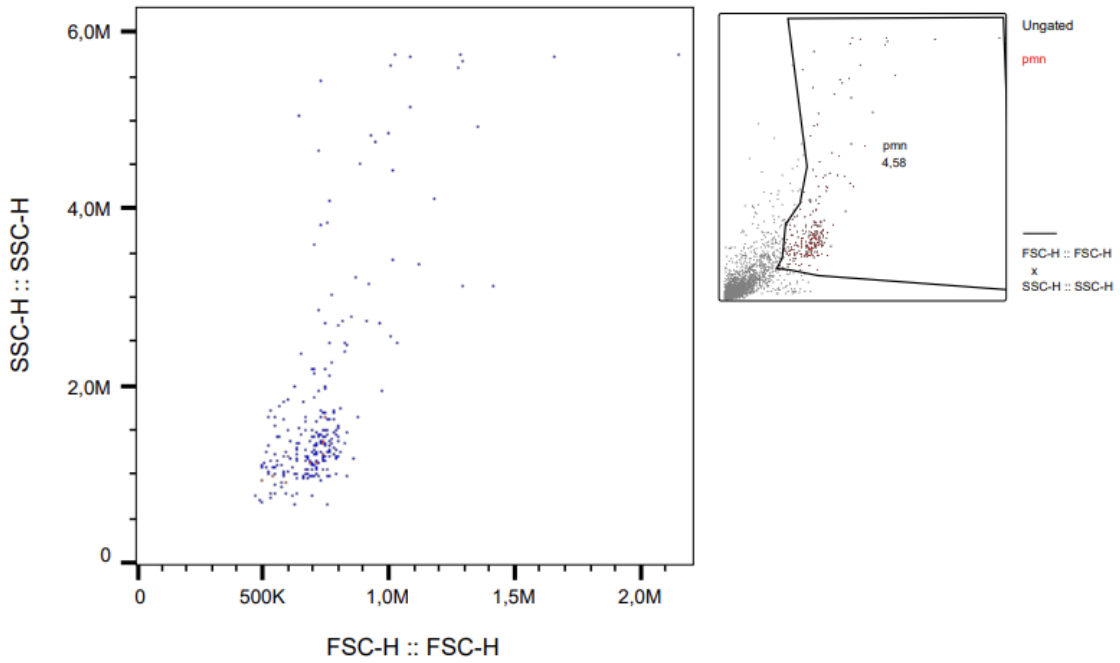

Figure C.24: A scatterplot of counts from flow cytometry of migrated cells from chemotaxis set-up one of fractions E5-E8 collected from SEC of the 90 % synovial fluid is plotted, with SSC versus FSC. The upper right figure displays the original plot and the neutrophil gate used, while the center figure exclusively shows the counts within the gate.

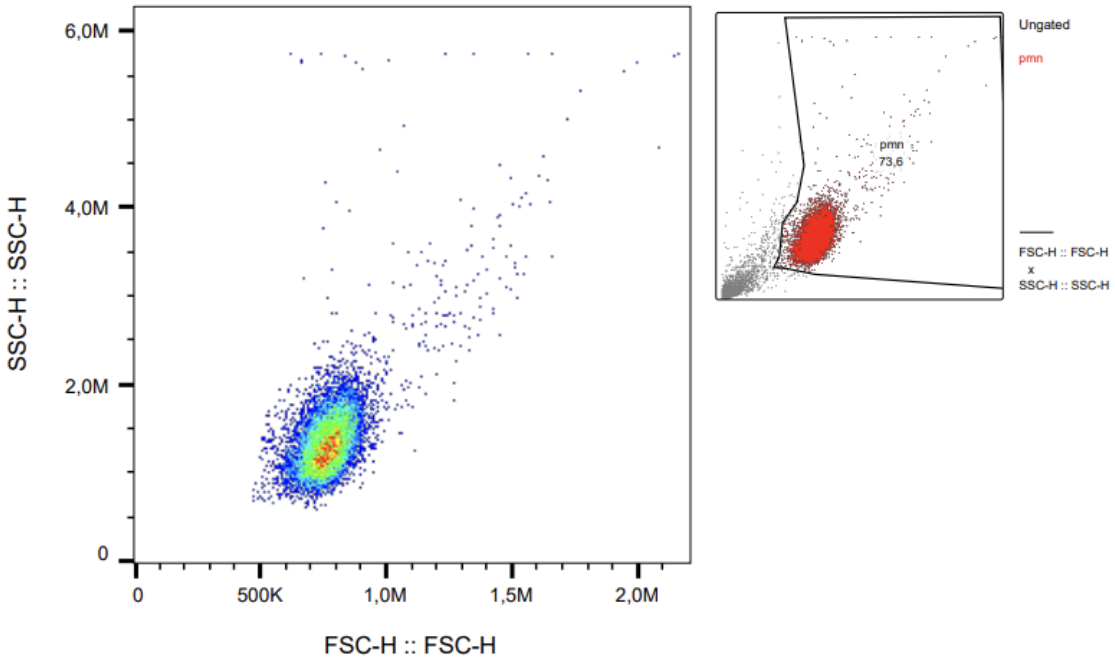

Figure C.25: A scatterplot of counts from flow cytometry of migrated cells from chemotaxis set-up one of fractions A6-A7 collected from cation-exchange chromatography of the 90 % synovial fluid is plotted, with SSC versus FSC. The upper right figure displays the original plot and the neutrophil gate used, while the center figure exclusively shows the counts within the gate.

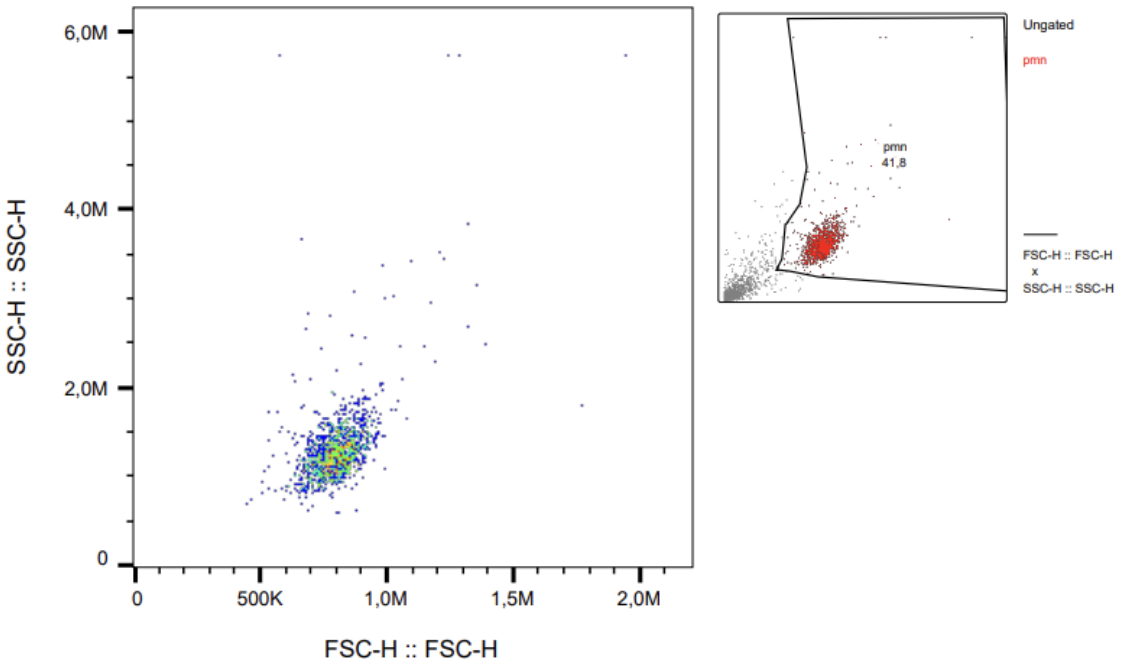

Figure C.26: A scatterplot of counts from flow cytometry of migrated cells from chemotaxis set-up one of fractions A10-A11 collected from cation-exchange chromatography of the 90 % synovial fluid is plotted, with SSC versus FSC. The upper right figure displays the original plot and the neutrophil gate used, while the center figure exclusively shows the counts within the gate.

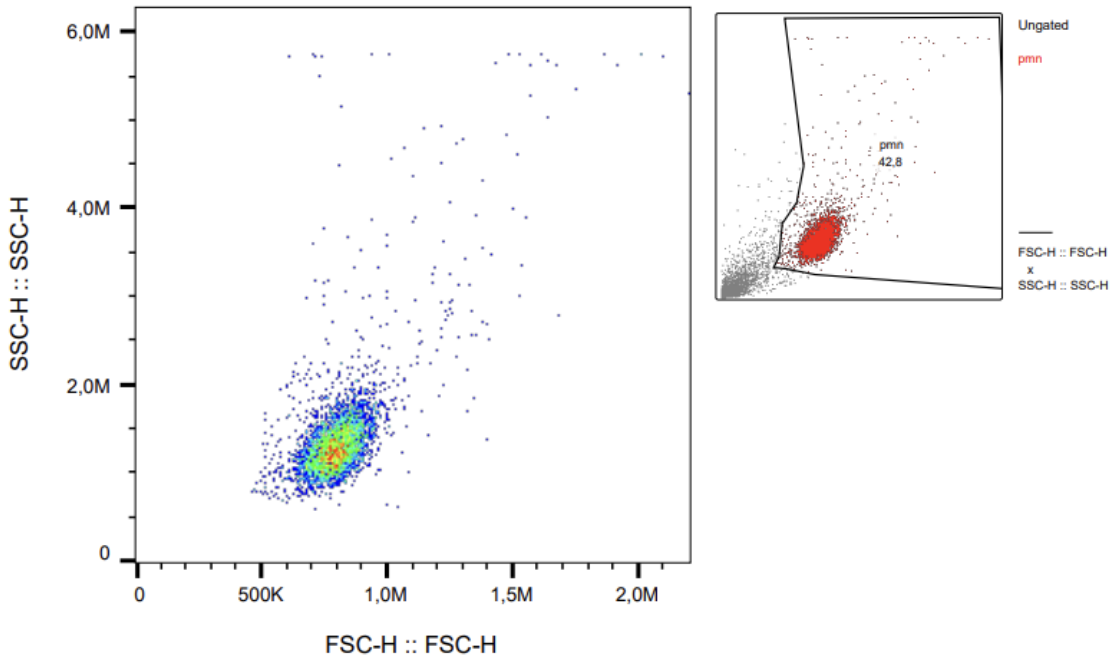

Figure C.27: A scatterplot of counts from flow cytometry of migrated cells from chemotaxis set-up one of fractions B2-B3 collected from cation-exchange chromatography of the 90 % synovial fluid is plotted, with SSC versus FSC. The upper right figure displays the original plot and the neutrophil gate used, while the center figure exclusively shows the counts within the gate.

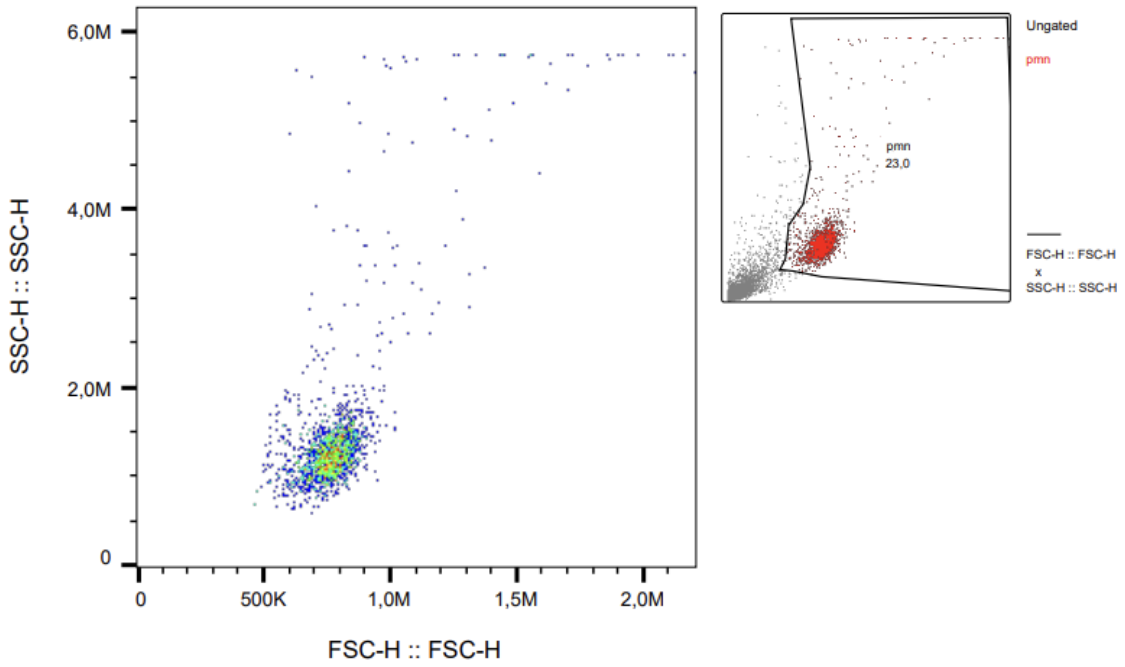

Figure C.28: A scatterplot of counts from flow cytometry of migrated cells from chemotaxis set-up one of fractions B6-B7 collected from cation-exchange chromatography of the 90 % synovial fluid is plotted, with SSC versus FSC. The upper right figure displays the original plot and the neutrophil gate used, while the center figure exclusively shows the counts within the gate.

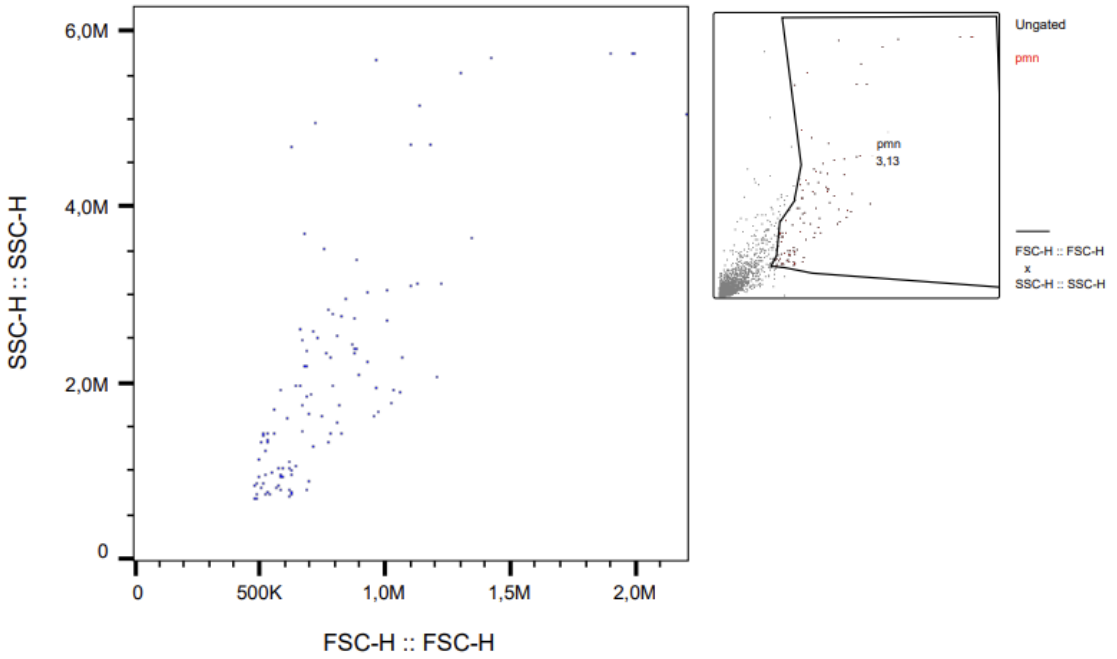

Figure C.29: A scatterplot of counts from flow cytometry of migrated cells from chemotaxis setup one of fractions B10-B11 collected from cation-exchange chromatography of the 90 % synovial fluid is plotted, with SSC versus FSC. The upper right figure displays the original plot and the neutrophil gate used, while the center figure exclusively shows the counts within the gate.

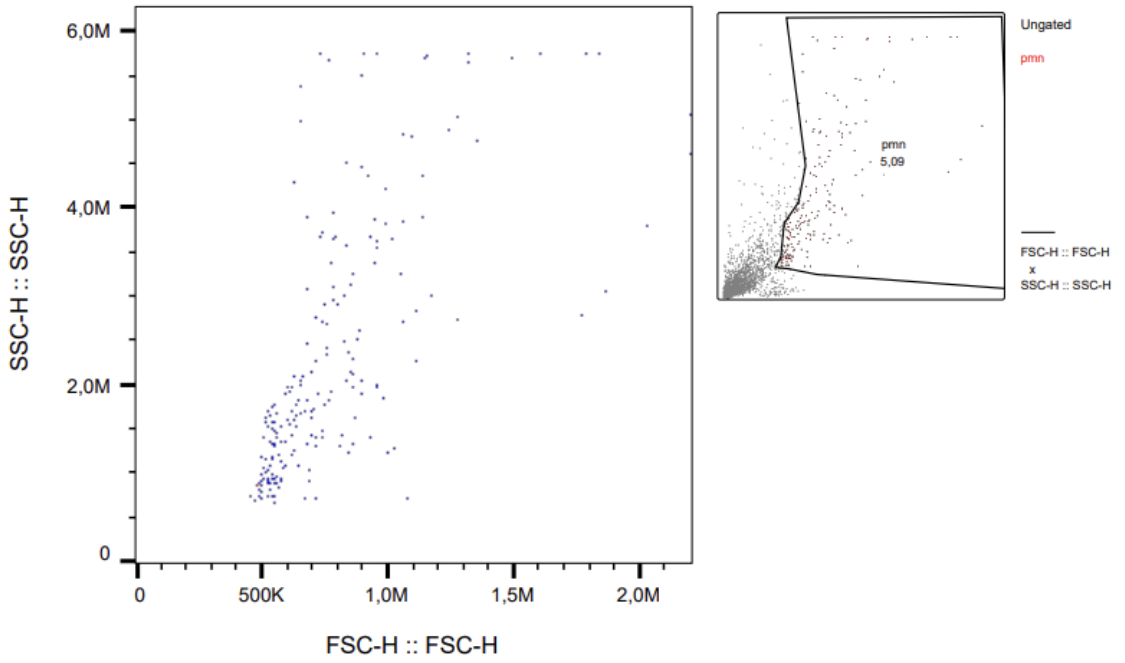

Figure C.30: A scatterplot of counts from flow cytometry of migrated cells from chemotaxis set-up one of fractions C2-C3 collected from cation-exchange chromatography of the 90 % synovial fluid is plotted, with SSC versus FSC. The upper right figure displays the original plot and the neutrophil gate used, while the center figure exclusively shows the counts within the gate.

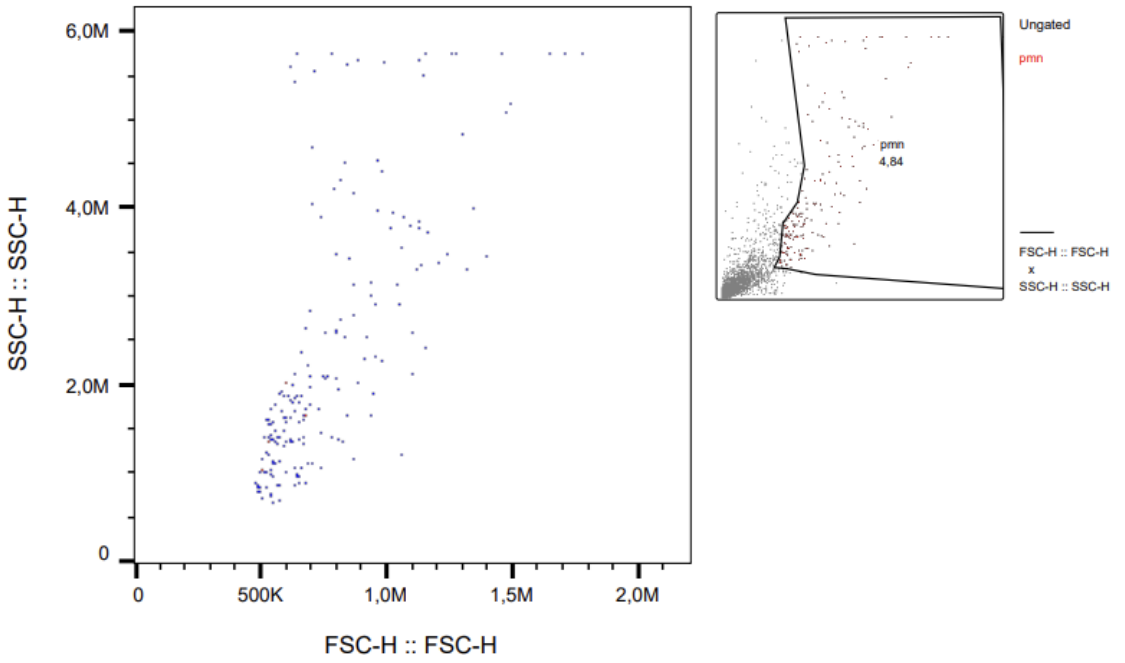

Figure C.31: A scatterplot of counts from flow cytometry of migrated cells from chemotaxis set-up one of fractions C6-C7 collected from cation-exchange chromatography of the 90 % synovial fluid is plotted, with SSC versus FSC. The upper right figure displays the original plot and the neutrophil gate used, while the center figure exclusively shows the counts within the gate.

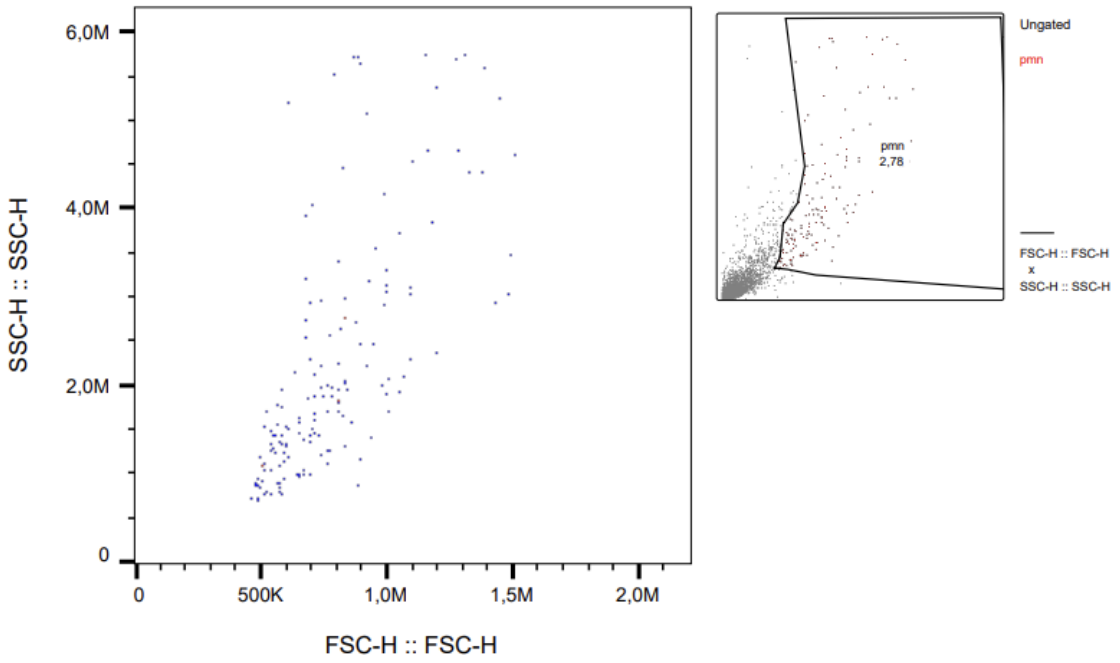

Figure C.32: A scatterplot of counts from flow cytometry of migrated cells from chemotaxis set-up one of fractions C10-C11 collected from cation-exchange chromatography of the 90 % synovial fluid is plotted, with SSC versus FSC. The upper right figure displays the original plot and the neutrophil gate used, while the center figure exclusively shows the counts within the gate.

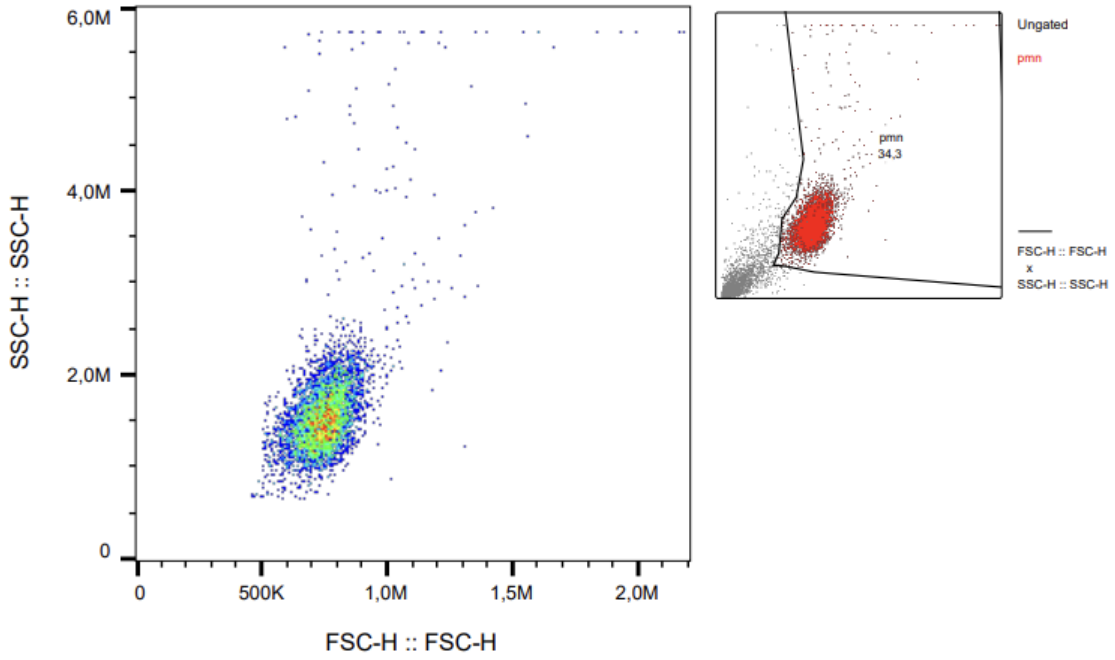

Figure C.33: A scatterplot of counts from flow cytometry of migrated cells from chemotaxis of the negative control (spontaneous migration) from the second chemotaxis set-up is plotted, with SSC versus FSC. The upper right figure displays the original plot and the neutrophil gate used, while the center figure exclusively shows the counts within the gate.

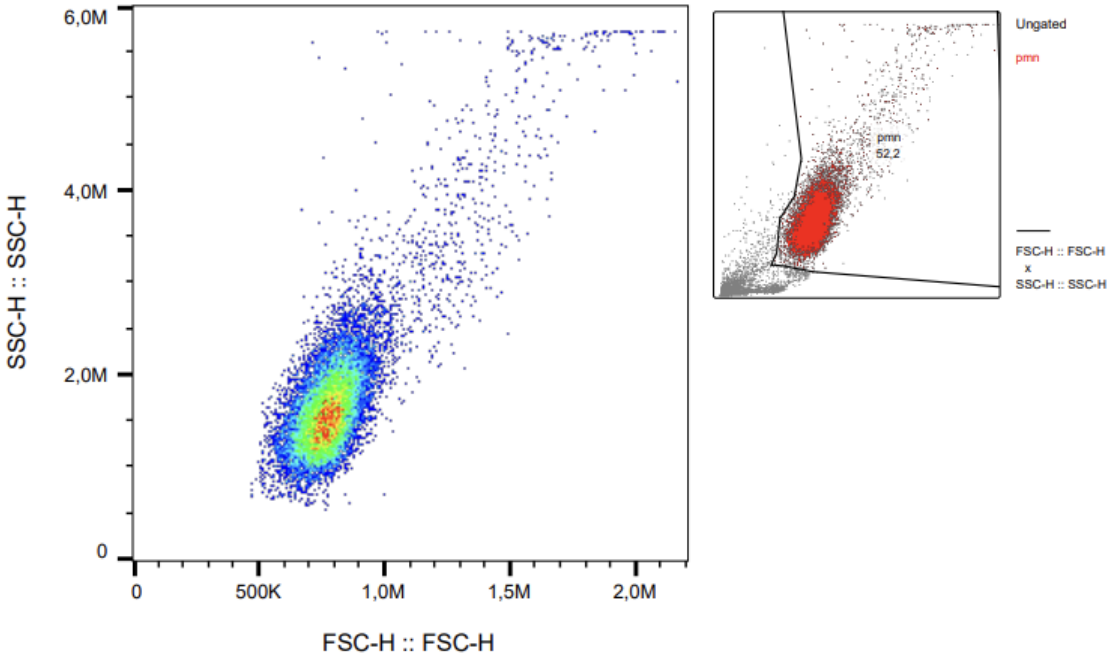

Figure C.34: A scatterplot of counts from flow cytometry of migrated cells from chemotaxis of the positive control from the second chemotaxis set-up is plotted, with SSC versus FSC. The upper right figure displays the original plot and the neutrophil gate used, while the center figure exclusively shows the counts within the gate.

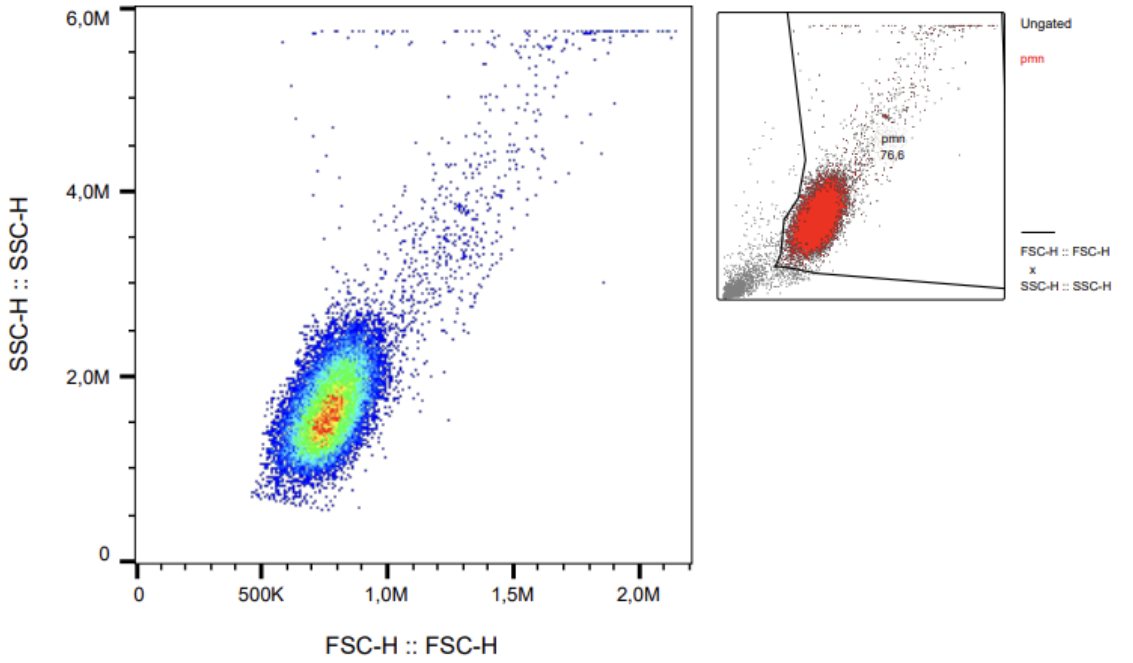

Figure C.35: A scatterplot of counts from flow cytometry of migrated cells from chemotaxis of the fMLF control from the second chemotaxis set-up is plotted, with SSC versus FSC. The upper right figure displays the original plot and the neutrophil gate used, while the center figure exclusively shows the counts within the gate.

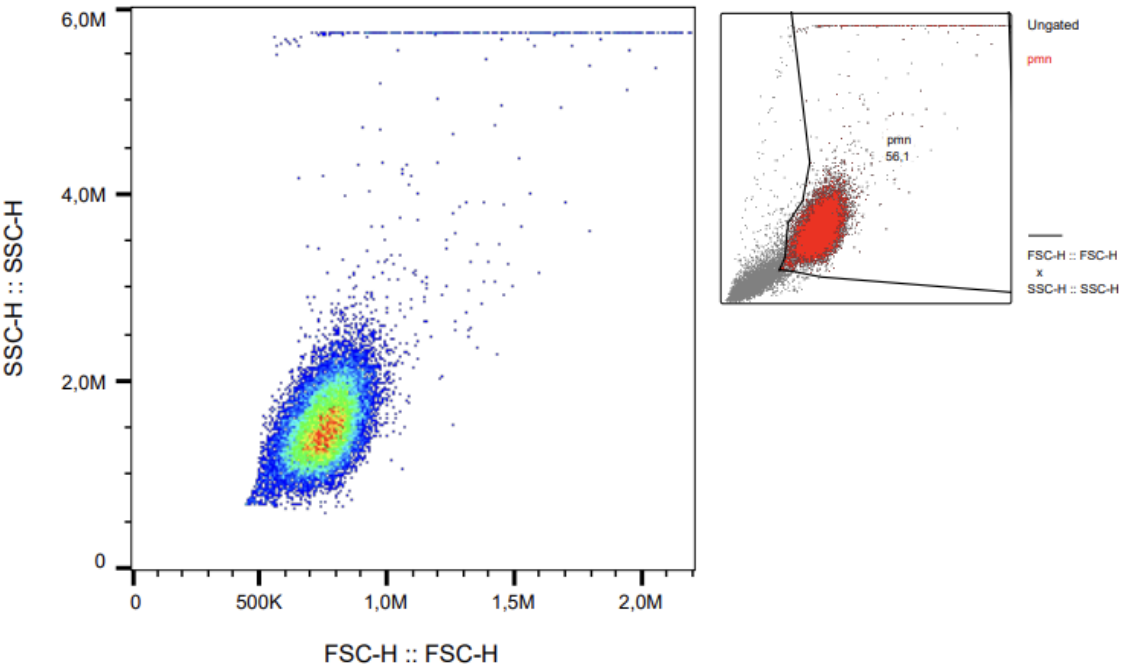

Figure C.36: A scatterplot of counts from flow cytometry of migrated cells from chemotaxis set-up two of the 90 % synovial fluid is plotted, with SSC versus FSC. The upper right figure displays the original plot and the neutrophil gate used, while the center figure exclusively shows the counts within the gate.

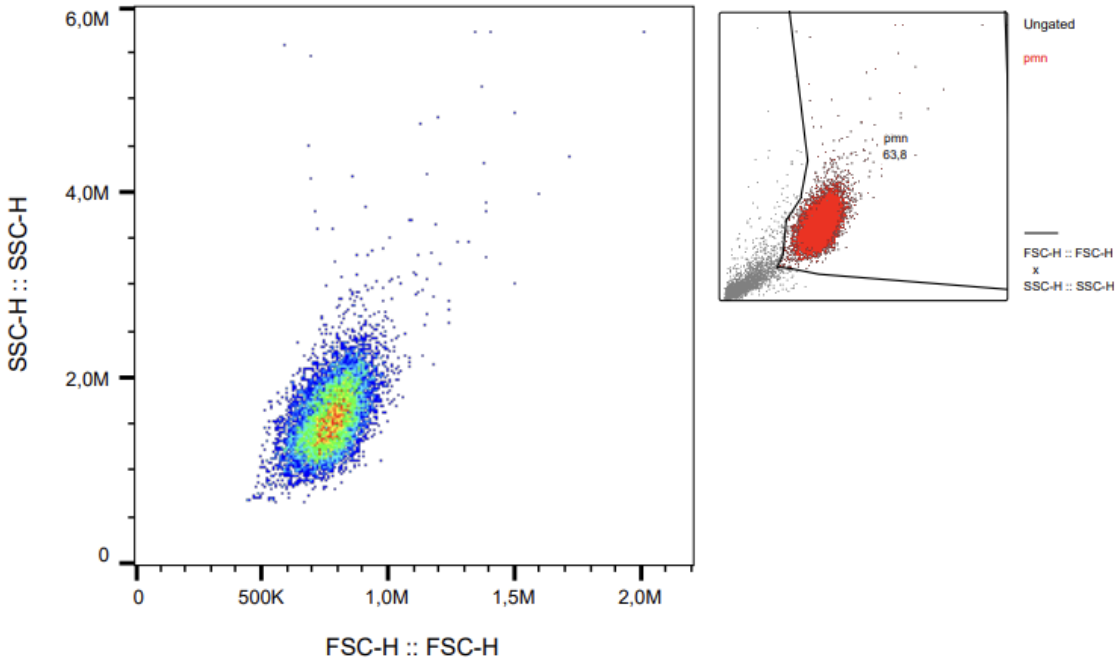

Figure C.37: A scatterplot of counts from flow cytometry of migrated cells from chemotaxis set-up two of hyaluronidase treated 90 % synovial fluid is plotted, with SSC versus FSC. The upper right figure displays the original plot and the neutrophil gate used, while the center figure exclusively shows the counts within the gate.

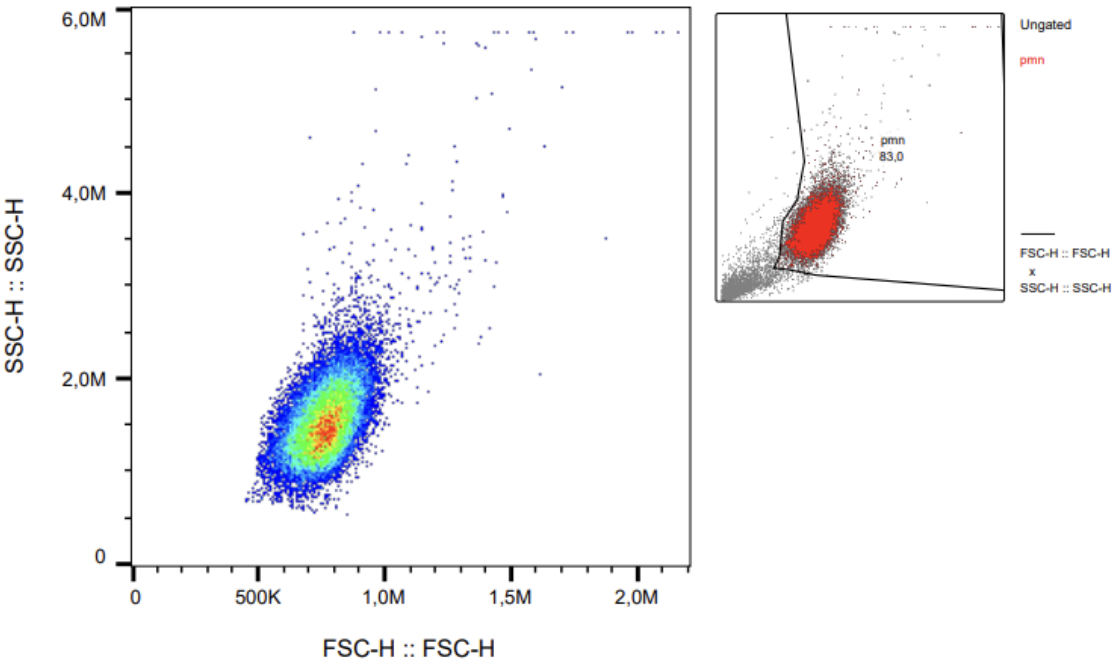

Figure C.38: A scatterplot of counts from flow cytometry of migrated cells from chemotaxis set-up two of the 5 % synovial fluid is plotted, with SSC versus FSC. The upper right figure displays the original plot and the neutrophil gate used, while the center figure exclusively shows the counts within the gate.

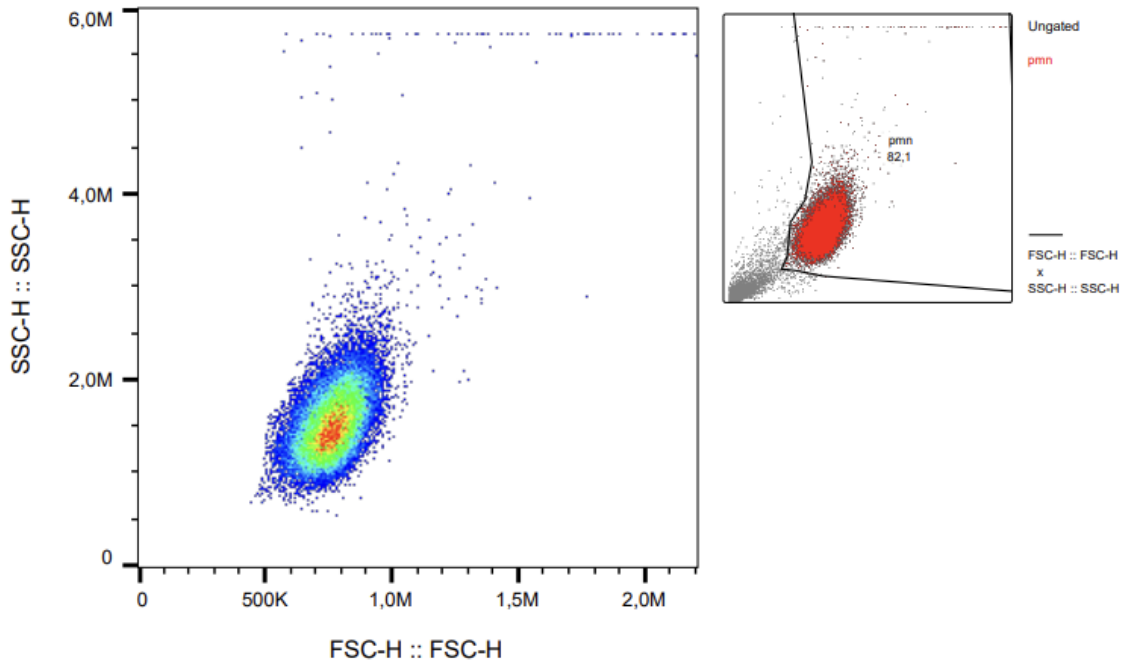

Figure C.39: A scatterplot of counts from flow cytometry of migrated cells from chemotaxis set-up two of hyaluronidase treated 5 % synovial fluid is plotted, with SSC versus FSC. The upper right figure displays the original plot and the neutrophil gate used, while the center figure exclusively shows the counts within the gate.

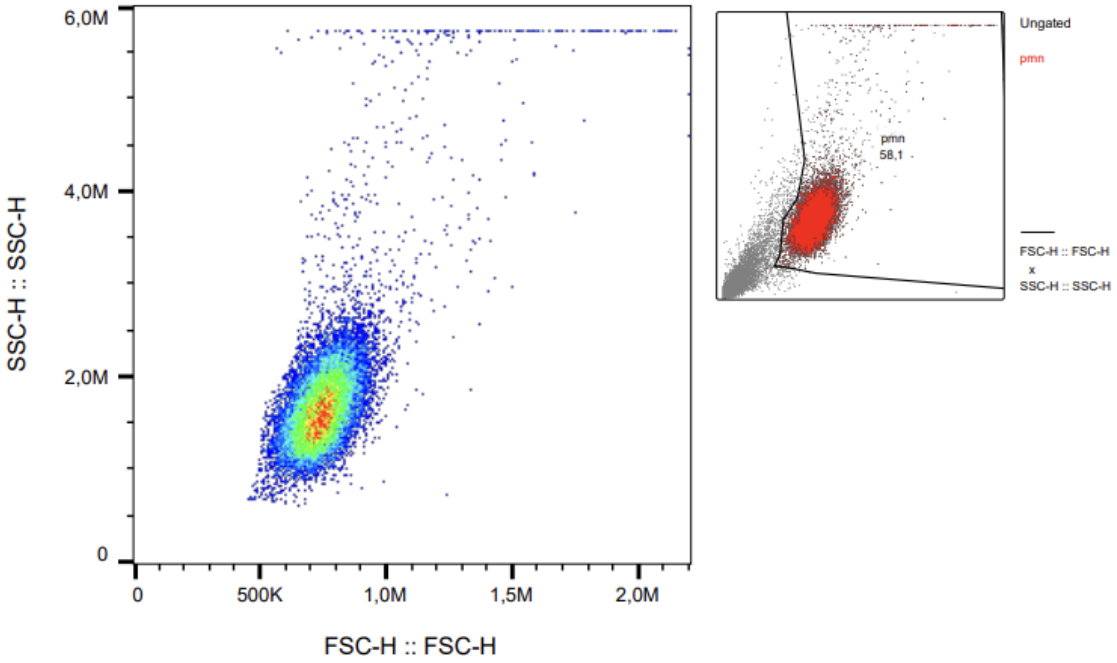

Figure C.40: A scatterplot of counts from flow cytometry of migrated cells from chemotaxis set-up two of fractions B4-B5 collected from SEC of the 5 % synovial fluid is plotted, with SSC versus FSC. The upper right figure displays the original plot and the neutrophil gate used, while the center figure exclusively shows the counts within the gate.

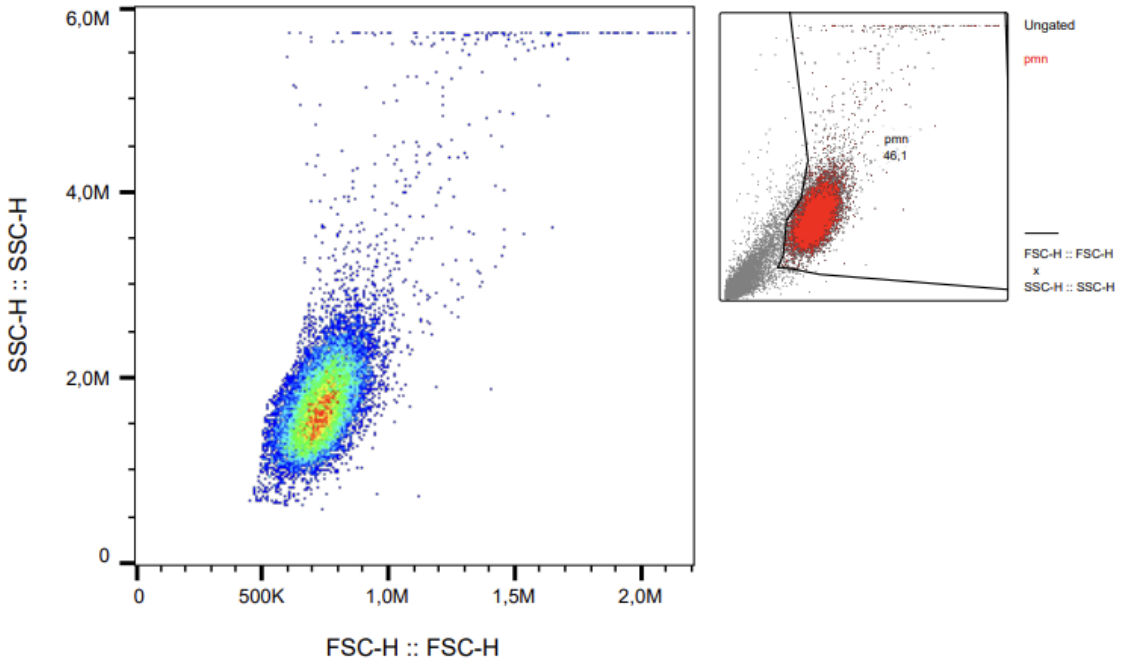

Figure C.41: A scatterplot of counts from flow cytometry of migrated cells from chemotaxis set-up two of fraction B6 collected from SEC of the 5 % synovial fluid is plotted, with SSC versus FSC. The upper right figure displays the original plot and the neutrophil gate used, while the center figure exclusively shows the counts within the gate.

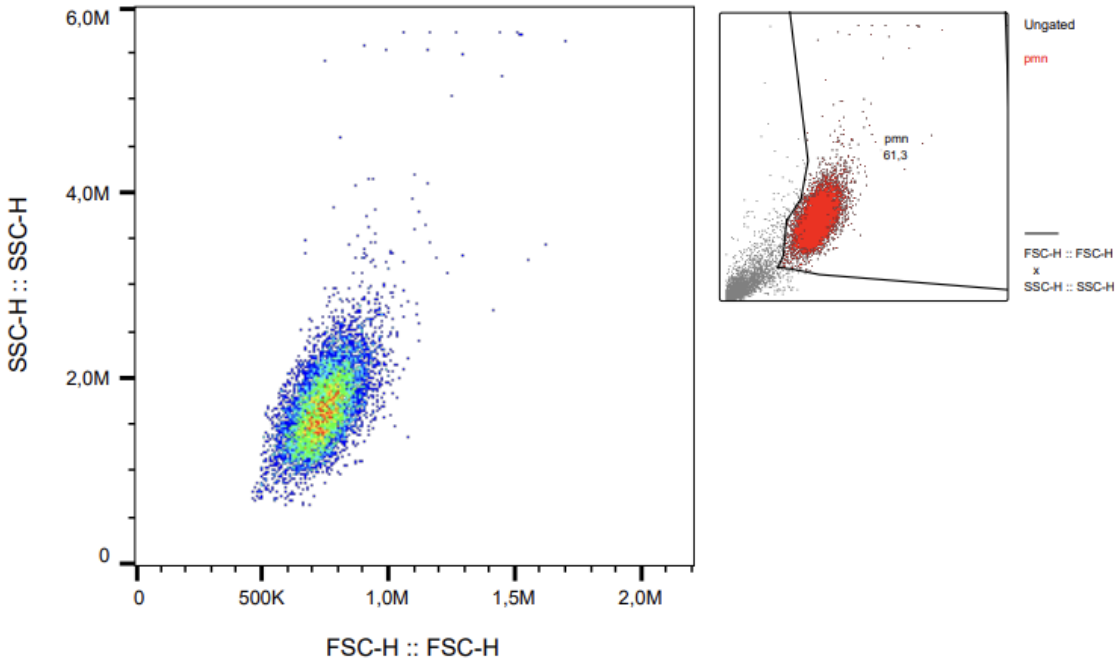

Figure C.42: A scatterplot of counts from flow cytometry of migrated cells from chemotaxis set-up two of fraction B7 collected from SEC of the 5 % synovial fluid is plotted, with SSC versus FSC. The upper right figure displays the original plot and the neutrophil gate used, while the center figure exclusively shows the counts within the gate.

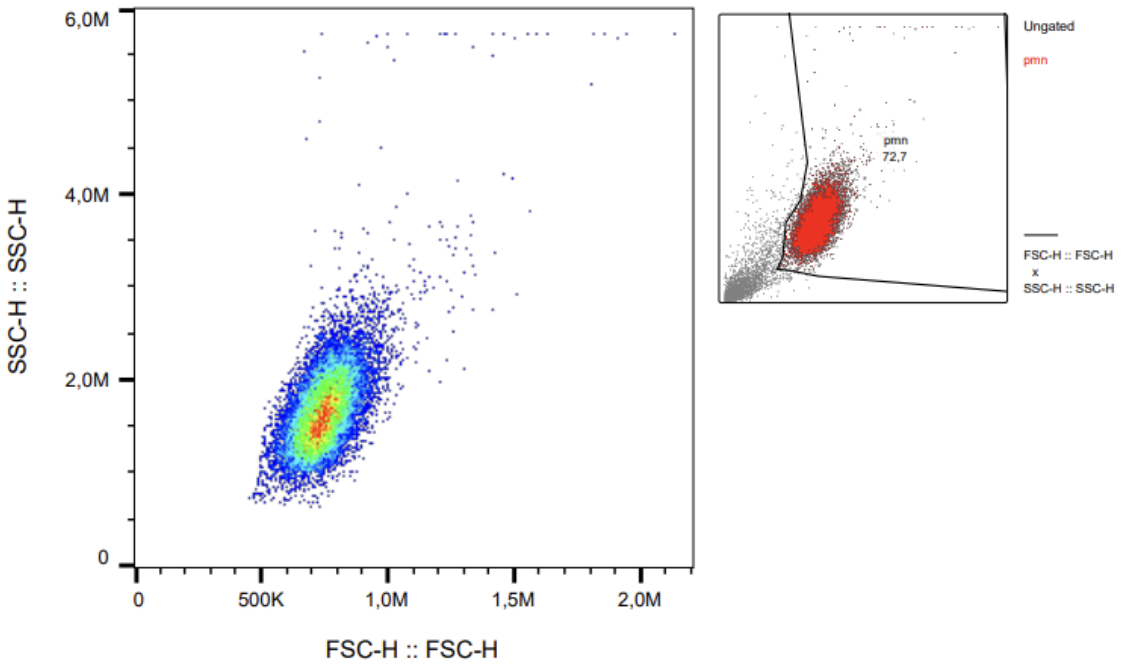

Figure C.43: A scatterplot of counts from flow cytometry of migrated cells from chemotaxis set-up two of fractions B8-B9 collected from SEC of the 5 % synovial fluid is plotted, with SSC versus FSC. The upper right figure displays the original plot and the neutrophil gate used, while the center figure exclusively shows the counts within the gate.

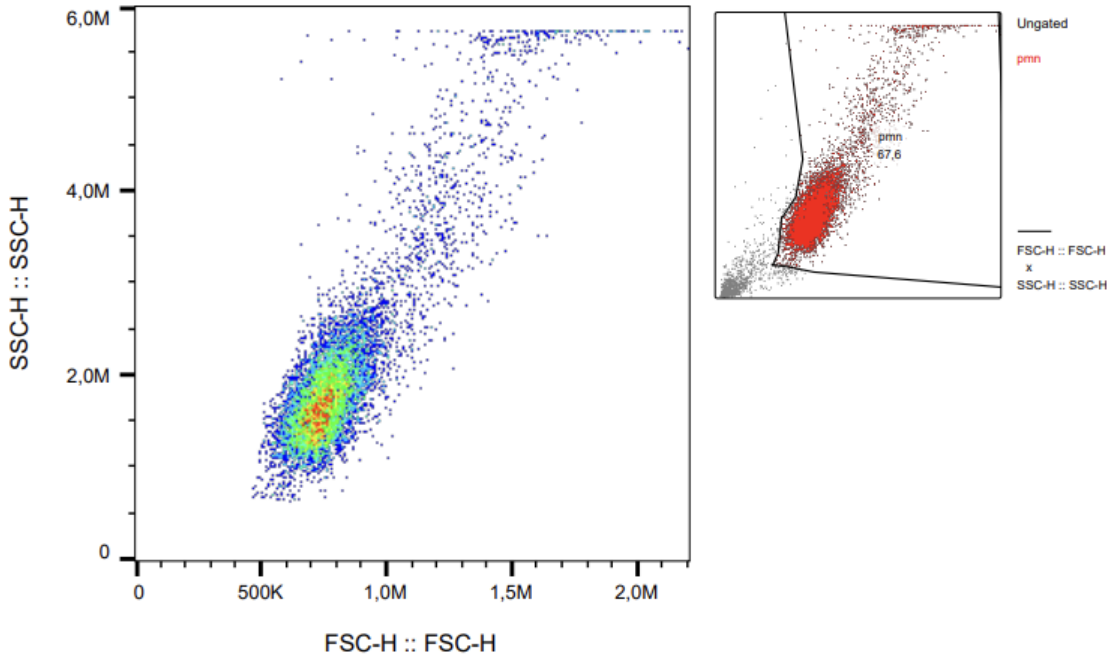

Figure C.44: A scatterplot of counts from flow cytometry of migrated cells from chemotaxis set-up two of fractions B10-C2 collected from SEC of the 5 % synovial fluid is plotted, with SSC versus FSC. The upper right figure displays the original plot and the neutrophil gate used, while the center figure exclusively shows the counts within the gate.

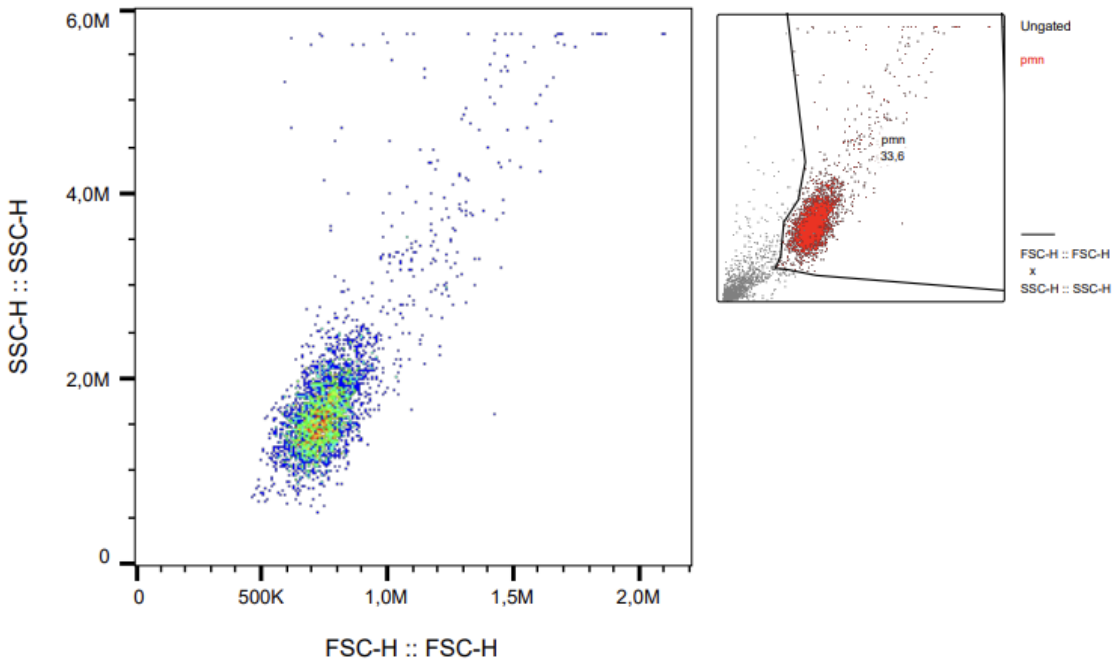

Figure C.45: A scatterplot of counts from flow cytometry of migrated cells from chemotaxis set-up two of fractions C3-C7 collected from SEC of the 5 % synovial fluid is plotted, with SSC versus FSC. The upper right figure displays the original plot and the neutrophil gate used, while the center figure exclusively shows the counts within the gate.

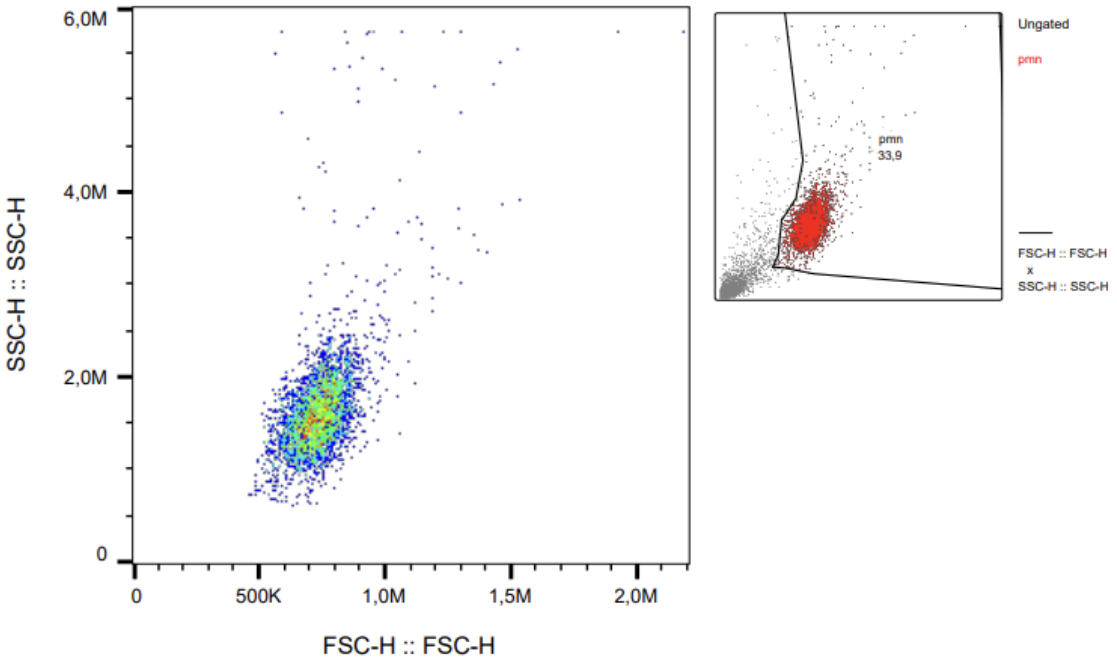

Figure C.46: A scatterplot of counts from flow cytometry of migrated cells from chemotaxis set-up two of fractions C8-C11 collected from SEC of the 5 % synovial fluid is plotted, with SSC versus FSC. The upper right figure displays the original plot and the neutrophil gate used, while the center figure exclusively shows the counts within the gate.

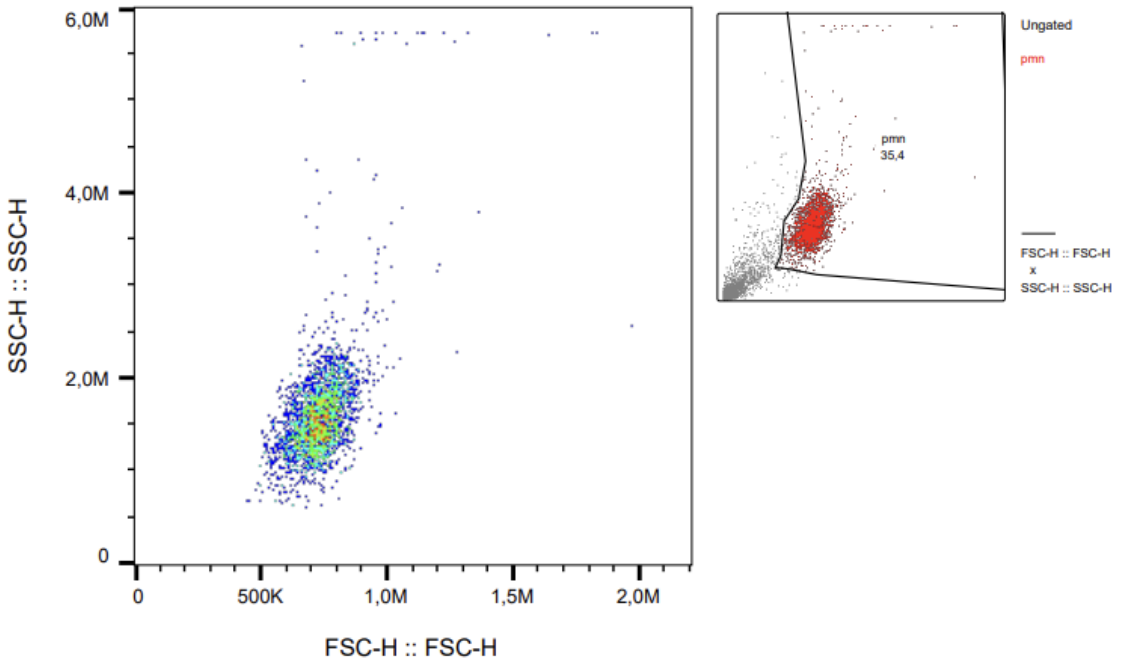

Figure C.47: A scatterplot of counts from flow cytometry of migrated cells from chemotaxis set-up two of fractions C12-D1 collected from SEC of the 5 % synovial fluid is plotted, with SSC versus FSC. The upper right figure displays the original plot and the neutrophil gate used, while the center figure exclusively shows the counts within the gate.

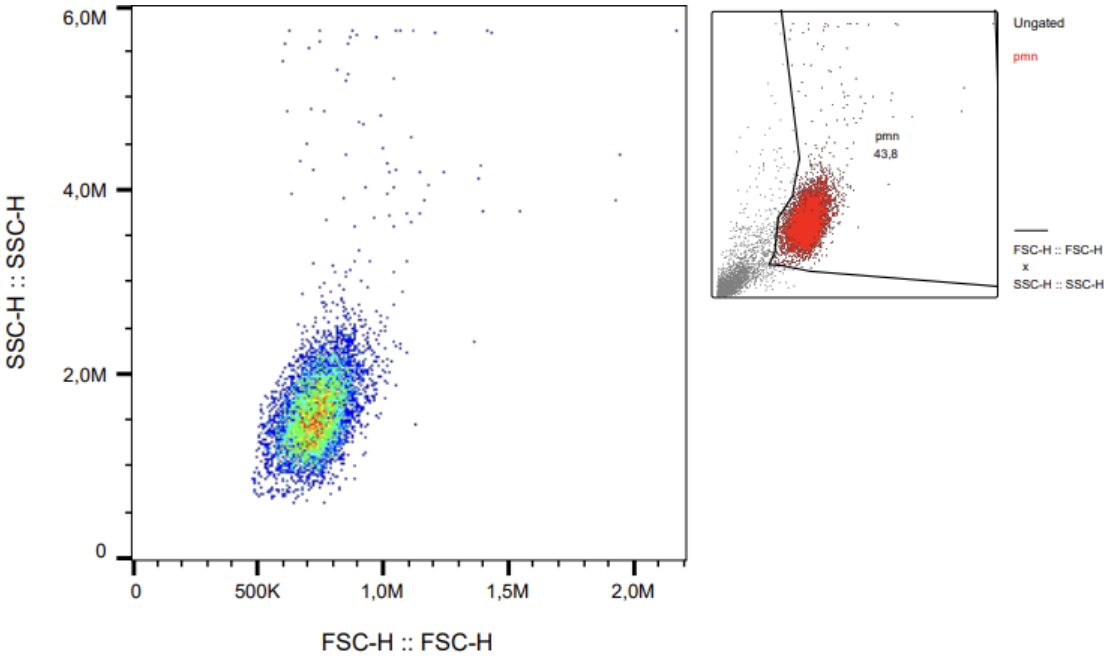

Figure C.48: A scatterplot of counts from flow cytometry of migrated cells from chemotaxis set-up two of fraction D2 collected from SEC of the 5 % synovial fluid is plotted, with SSC versus FSC. The upper right figure displays the original plot and the neutrophil gate used, while the center figure exclusively shows the counts within the gate.

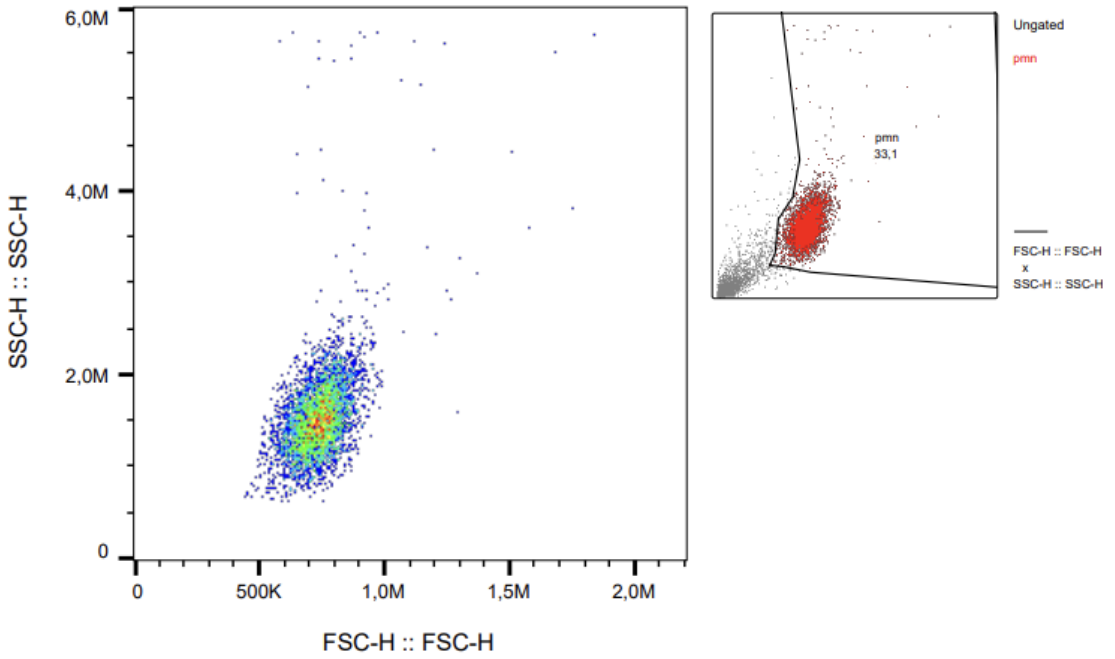

Figure C.49: A scatterplot of counts from flow cytometry of migrated cells from chemotaxis set-up two of fraction D3 collected from SEC of the 5 % synovial fluid is plotted, with SSC versus FSC. The upper right figure displays the original plot and the neutrophil gate used, while the center figure exclusively shows the counts within the gate.

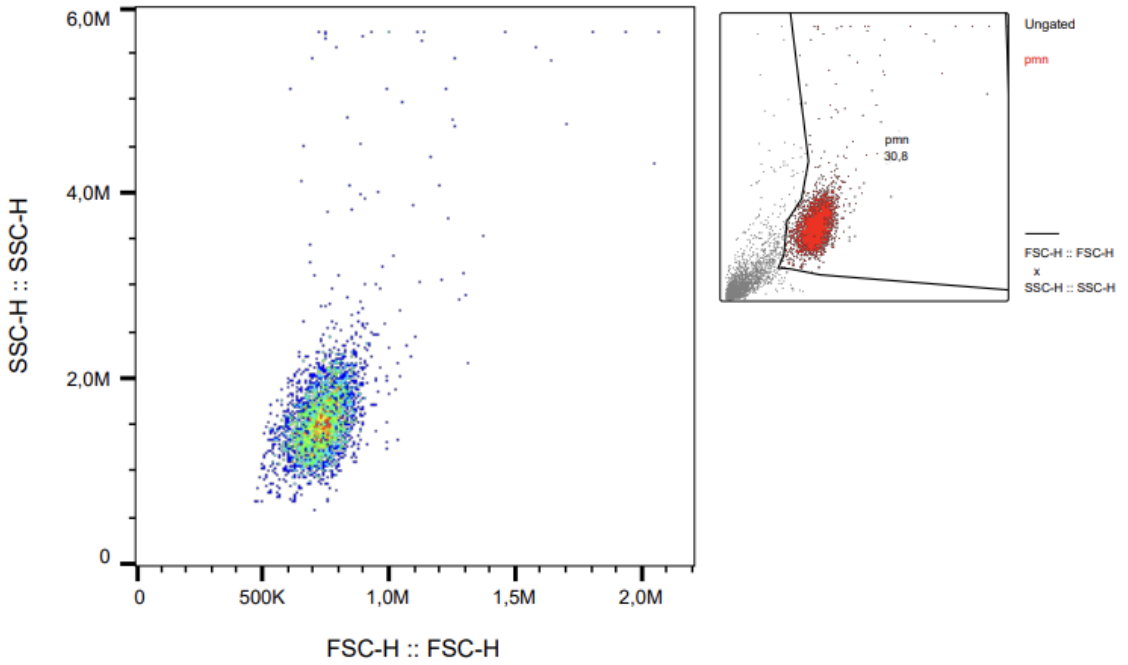

Figure C.50: A scatterplot of counts from flow cytometry of migrated cells from chemotaxis set-up two of fractions D4-D5 collected from SEC of the 5 % synovial fluid is plotted, with SSC versus FSC. The upper right figure displays the original plot and the neutrophil gate used, while the center figure exclusively shows the counts within the gate.

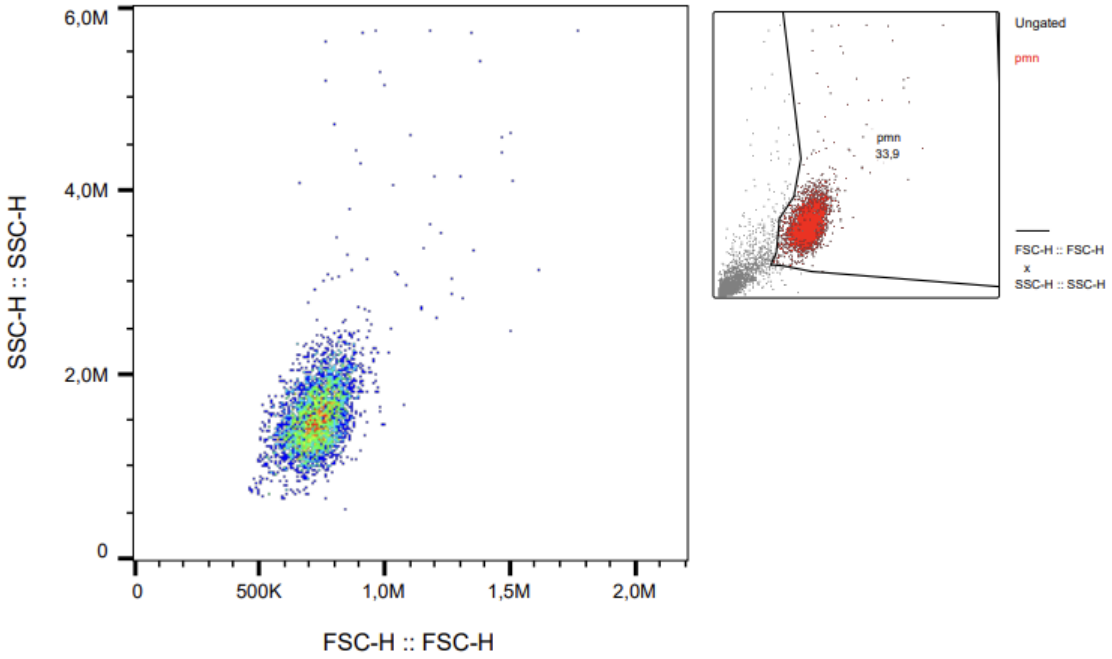

Figure C.51: A scatterplot of counts from flow cytometry of migrated cells from chemotaxis set-up two of fractions D6-D7 collected from SEC of the 5 % synovial fluid is plotted, with SSC versus FSC. The upper right figure displays the original plot and the neutrophil gate used, while the center figure exclusively shows the counts within the gate.

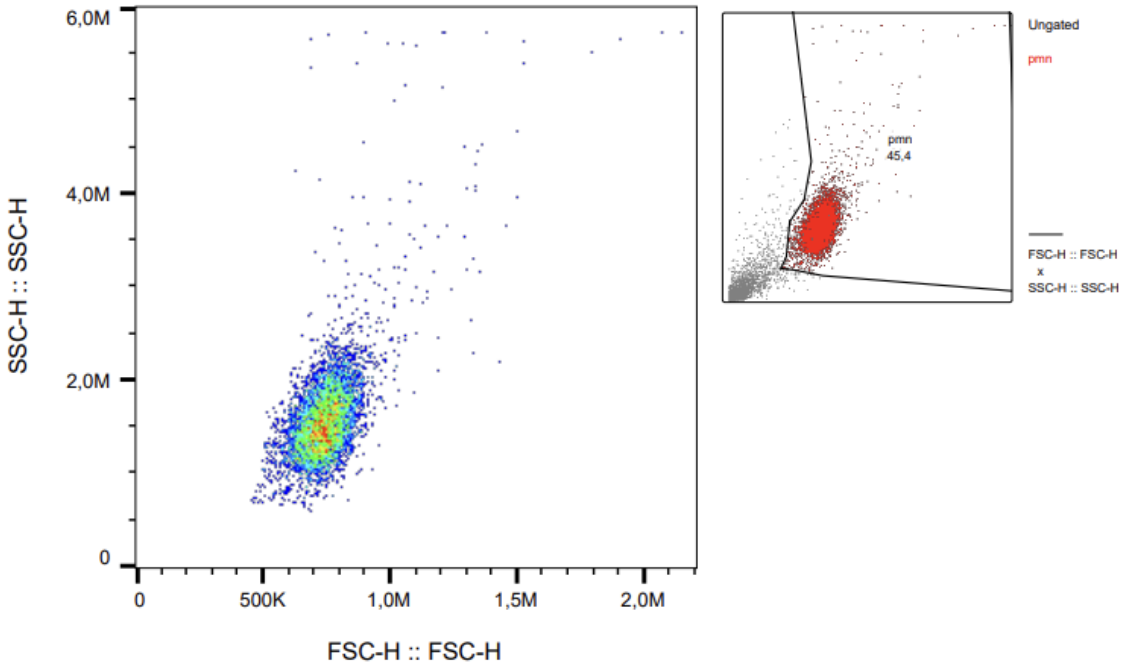

Figure C.52: A scatterplot of counts from flow cytometry of migrated cells from chemotaxis set-up two of fractions D8-D10 collected from SEC of the 5 % synovial fluid is plotted, with SSC versus FSC. The upper right figure displays the original plot and the neutrophil gate used, while the center figure exclusively shows the counts within the gate.

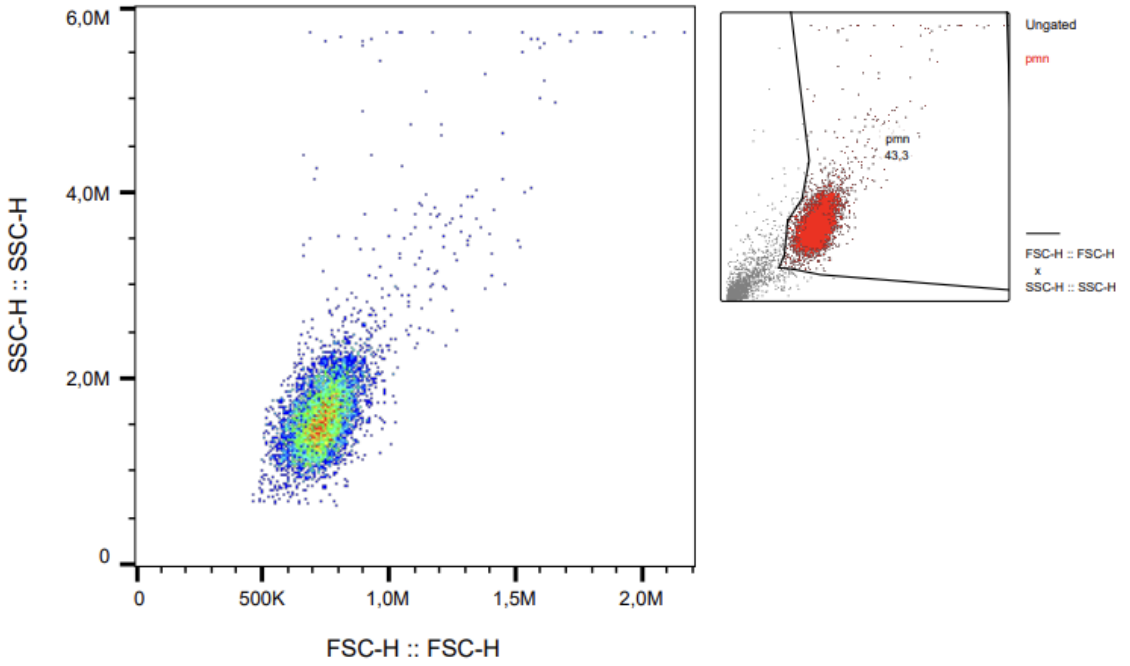

Figure C.53: A scatterplot of counts from flow cytometry of migrated cells from chemotaxis set-up two of fractions D11-E1 collected from SEC of the 5 % synovial fluid is plotted, with SSC versus FSC. The upper right figure displays the original plot and the neutrophil gate used, while the center figure exclusively shows the counts within the gate.

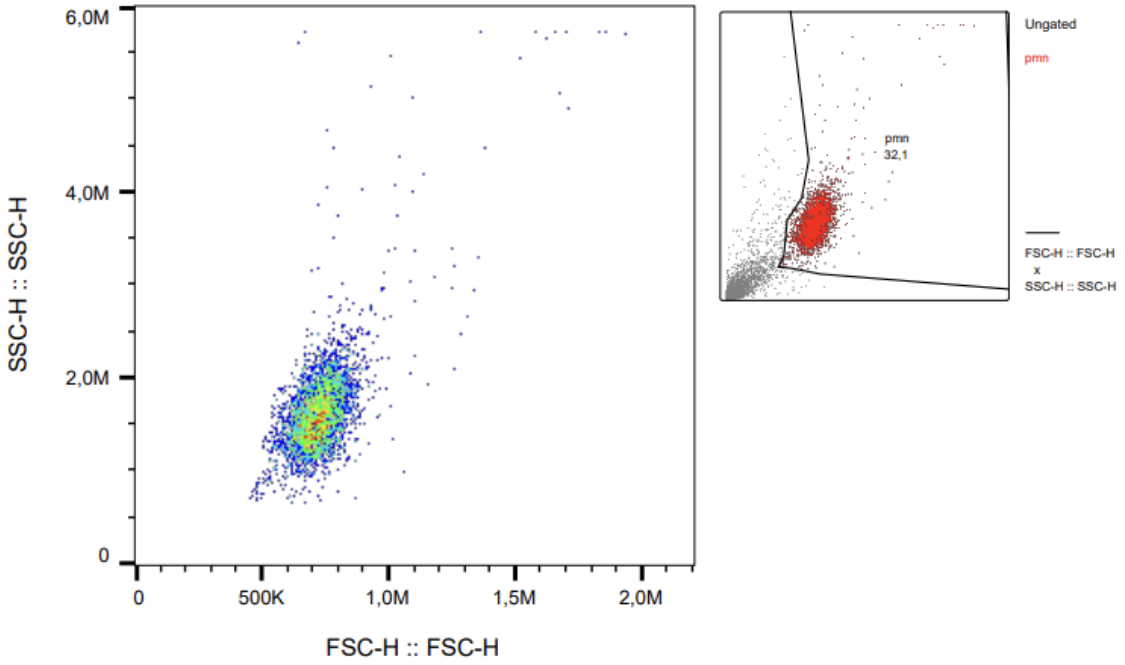

Figure C.54: A scatterplot of counts from flow cytometry of migrated cells from chemotaxis set-up two of fraction E2 collected from SEC of the 5 % synovial fluid is plotted, with SSC versus FSC. The upper right figure displays the original plot and the neutrophil gate used, while the center figure exclusively shows the counts within the gate.

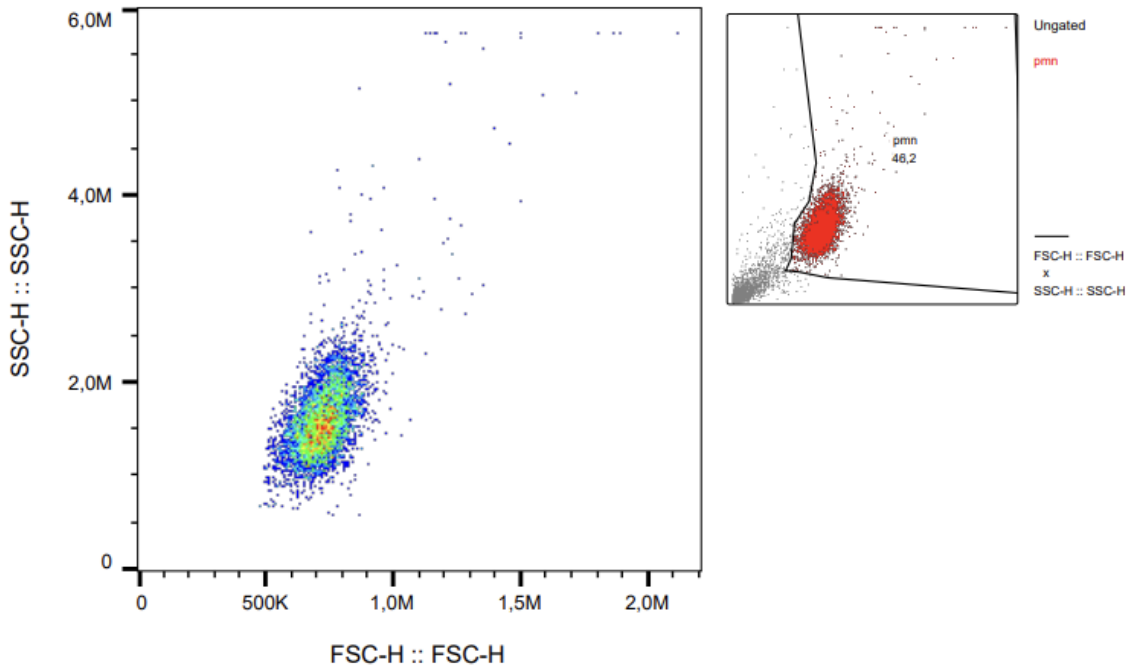

Figure C.55: A scatterplot of counts from flow cytometry of migrated cells from chemotaxis set-up two of fractions E3-E6 collected from SEC of the 5 % synovial fluid is plotted, with SSC versus FSC. The upper right figure displays the original plot and the neutrophil gate used, while the center figure exclusively shows the counts within the gate.

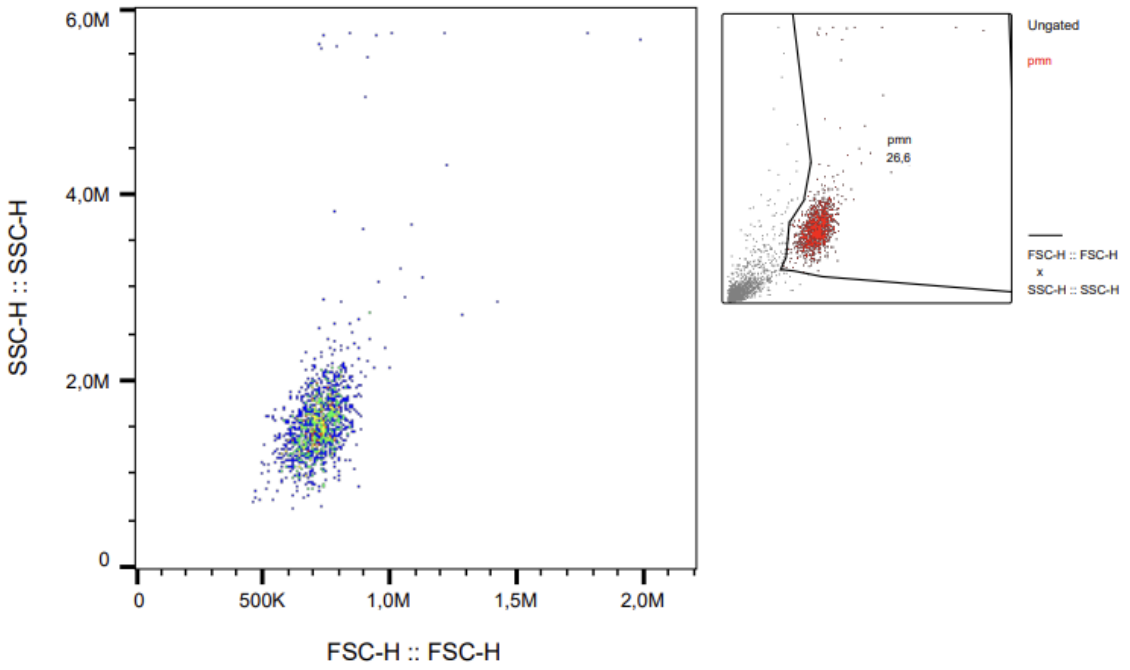

Figure C.56: A scatterplot of counts from flow cytometry of migrated cells from chemotaxis set-up two of fractions E7-E8 collected from SEC of the 5 % synovial fluid is plotted, with SSC versus FSC. The upper right figure displays the original plot and the neutrophil gate used, while the center figure exclusively shows the counts within the gate.

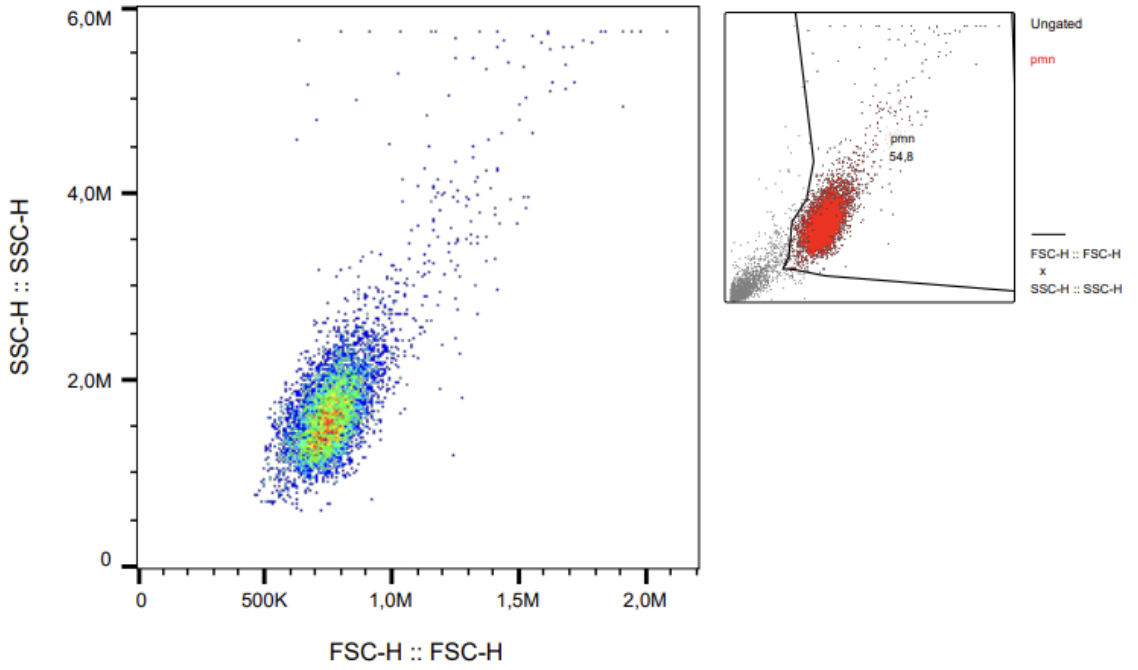

Figure C.57: A scatterplot of counts from flow cytometry of migrated cells from chemotaxis set-up two of elution collected from the loading step of IEC of the 90 % synovial fluid is plotted, with SSC versus FSC. The upper right figure displays the original plot and the neutrophil gate used, while the center figure exclusively shows the counts within the gate.

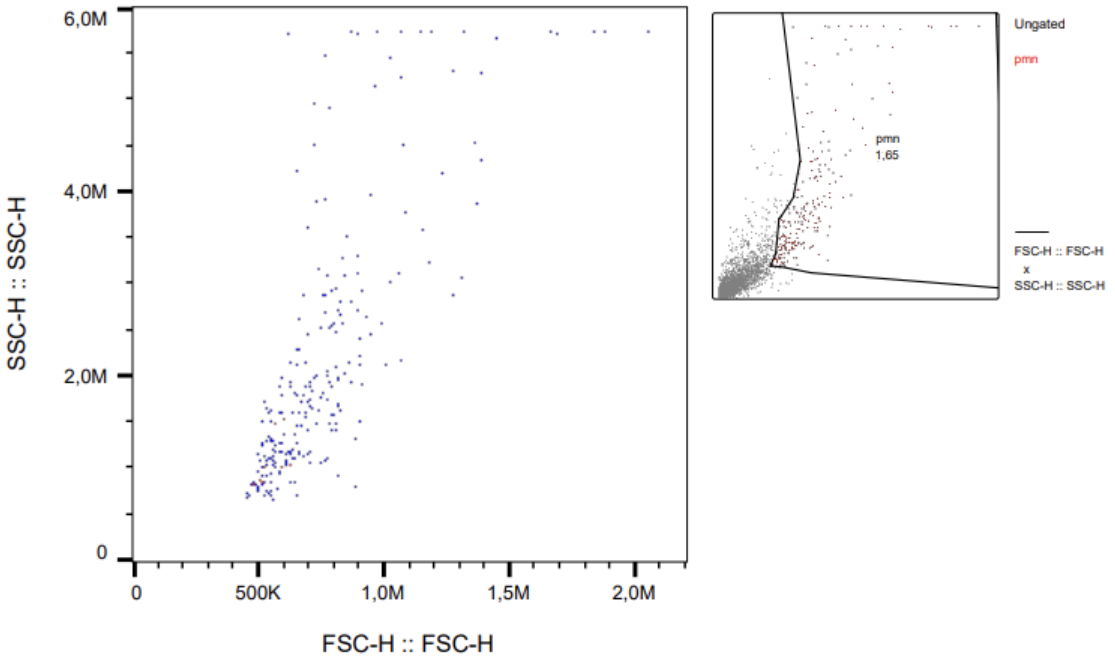

Figure C.58: A scatterplot of counts from flow cytometry of migrated cells from chemotaxis set-up two of fractions B6-B7 collected anion-exchange chromatography of the 90 % synovial fluid is plotted, with SSC versus FSC. The upper right figure displays the original plot and the neutrophil gate used, while the center figure exclusively shows the counts within the gate.

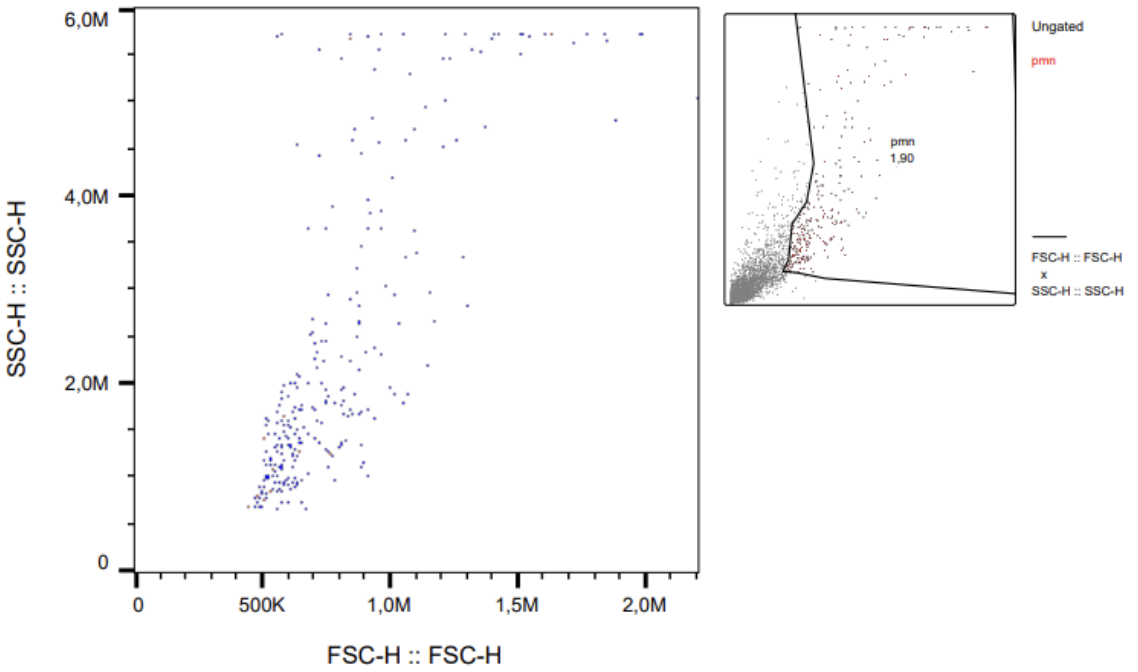

Figure C.59: A scatterplot of counts from flow cytometry of migrated cells from chemotaxis set-up two of fractions B8-B9 collected anion-exchange chromatography of the 90 % synovial fluid is plotted, with SSC versus FSC. The upper right figure displays the original plot and the neutrophil gate used, while the center figure exclusively shows the counts within the gate.

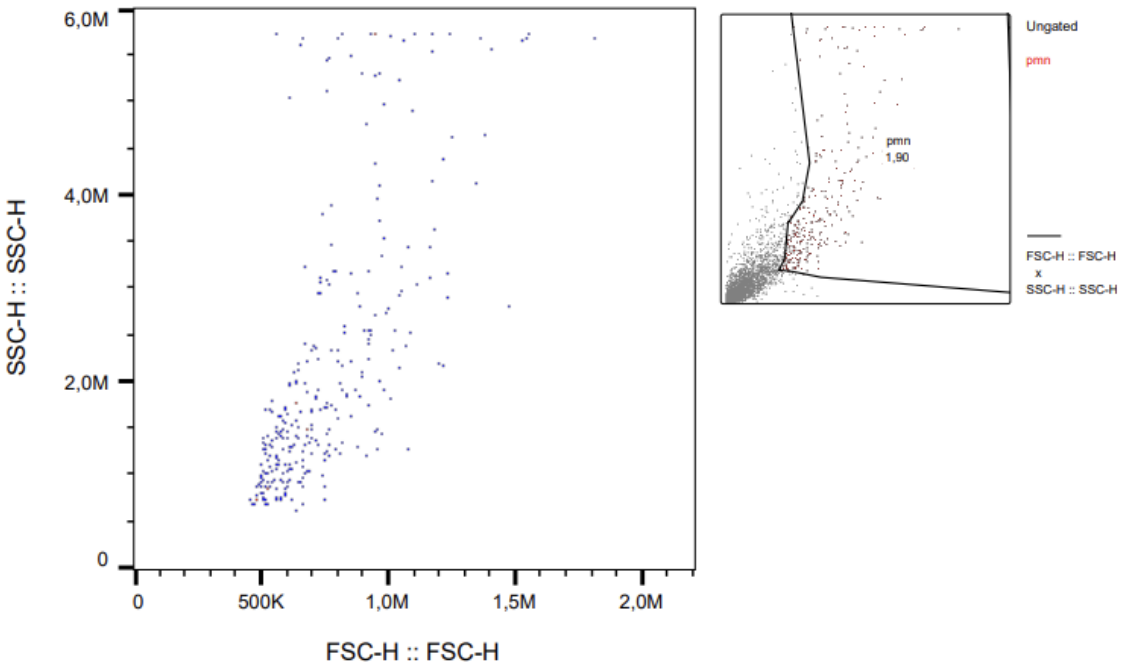

Figure C.60: A scatterplot of counts from flow cytometry of migrated cells from chemotaxis set-up two of fractions B10-B11 collected anion-exchange chromatography of the 90 % synovial fluid is plotted, with SSC versus FSC. The upper right figure displays the original plot and the neutrophil gate used, while the center figure exclusively shows the counts within the gate.

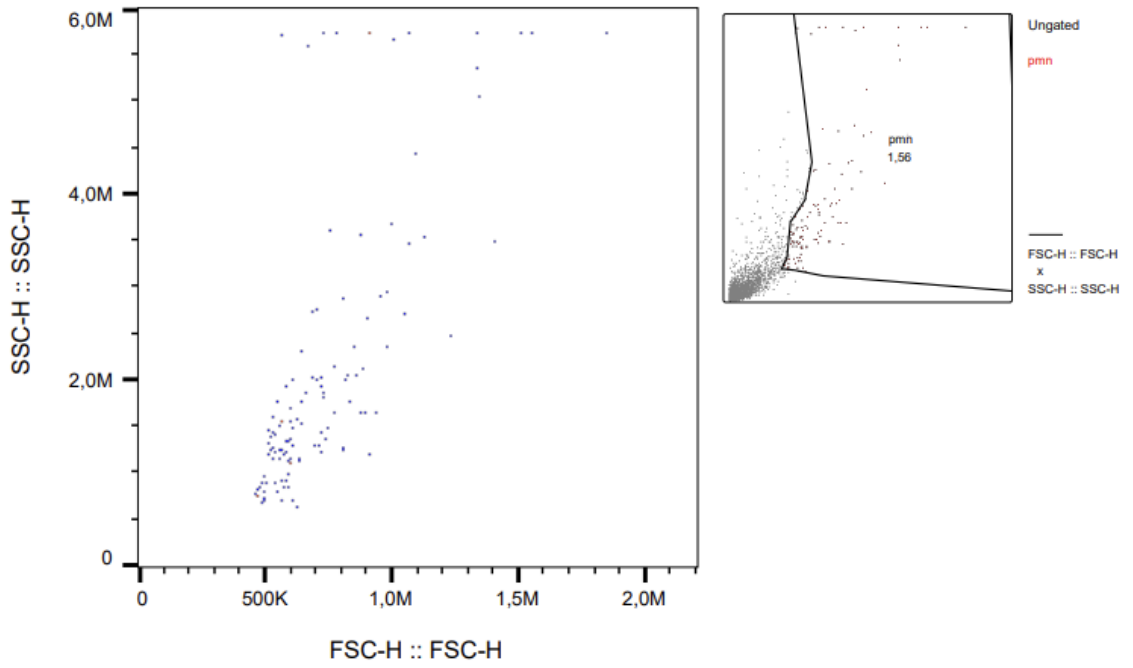

Figure C.61: A scatterplot of counts from flow cytometry of migrated cells from chemotaxis set-up two of fractions B12-C1 collected anion-exchange chromatography of the 90 % synovial fluid is plotted, with SSC versus FSC. The upper right figure displays the original plot and the neutrophil gate used, while the center figure exclusively shows the counts within the gate.

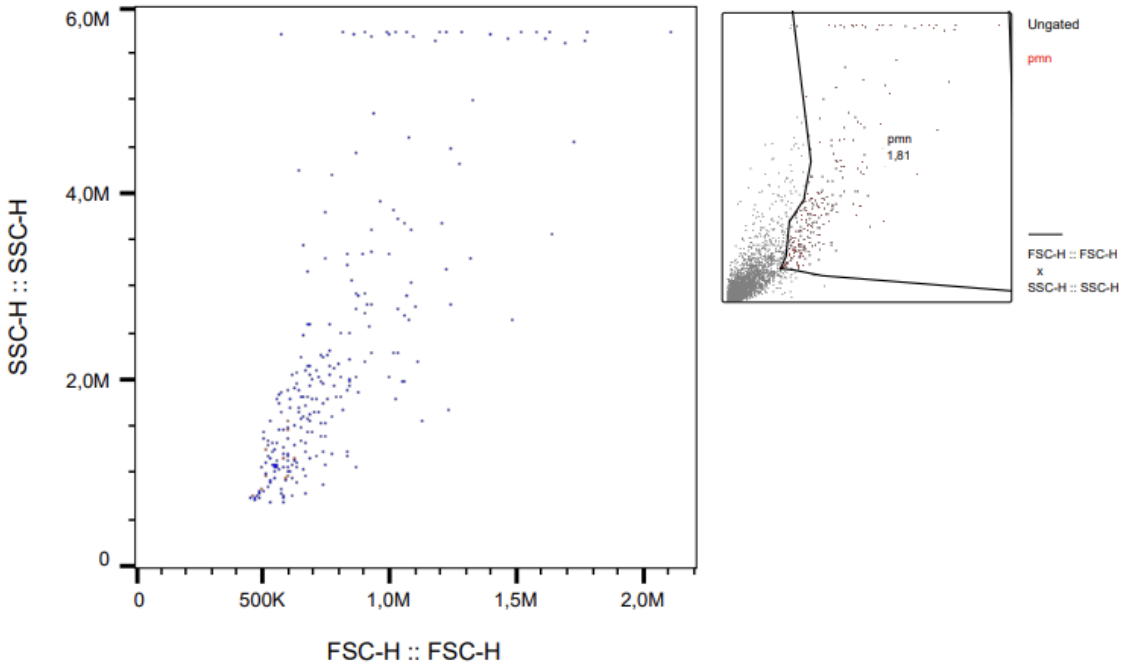

Figure C.62: A scatterplot of counts from flow cytometry of migrated cells from chemotaxis set-up two of fractions C2-C3 collected anion-exchange chromatography of the 90 % synovial fluid is plotted, with SSC versus FSC. The upper right figure displays the original plot and the neutrophil gate used, while the center figure exclusively shows the counts within the gate.

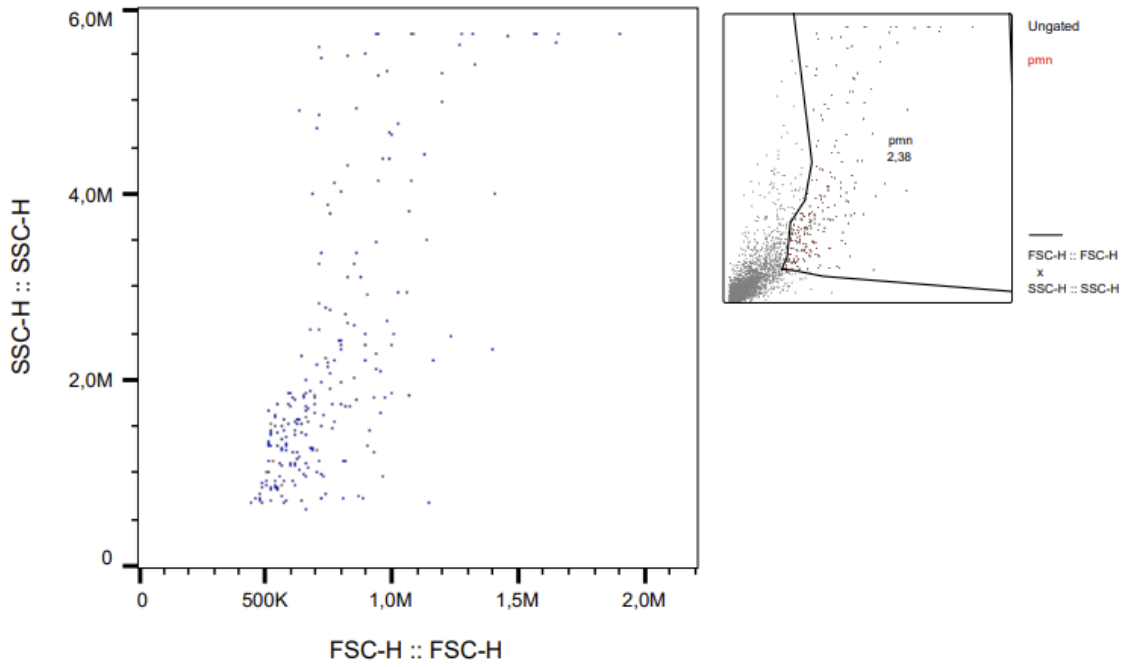

Figure C.63: A scatterplot of counts from flow cytometry of migrated cells from chemotaxis set-up two of fractions C4-C5 collected anion-exchange chromatography of the 90 % synovial fluid is plotted, with SSC versus FSC. The upper right figure displays the original plot and the neutrophil gate used, while the center figure exclusively shows the counts within the gate.

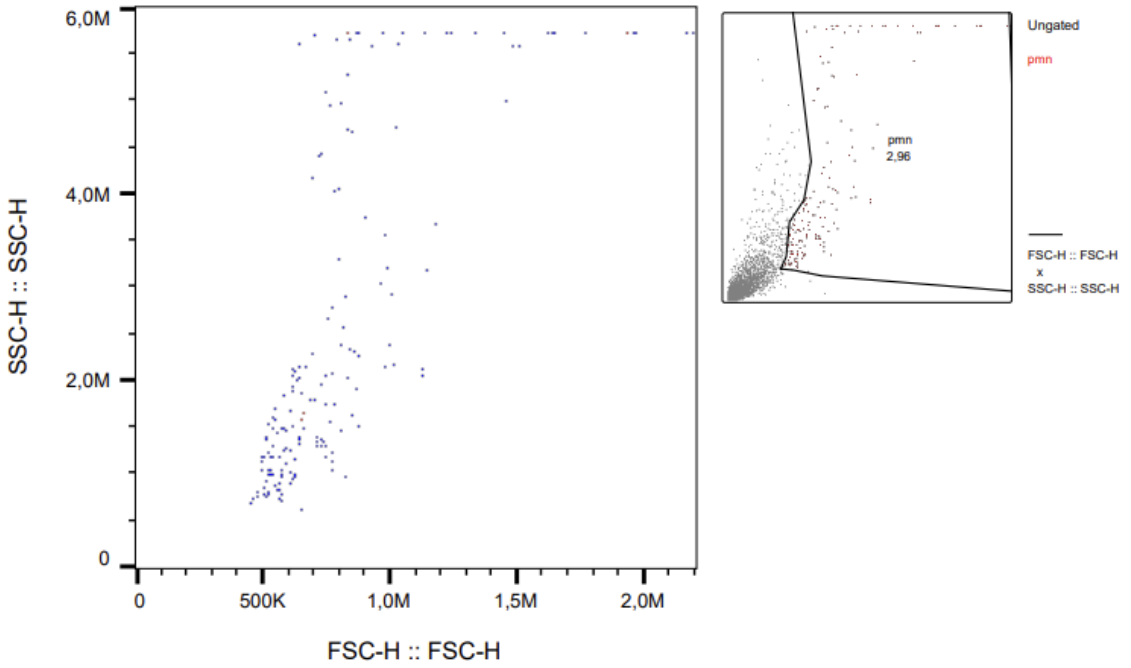

Figure C.64: A scatterplot of counts from flow cytometry of migrated cells from chemotaxis set-up two of fractions C6-C7 collected anion-exchange chromatography of the 90 % synovial fluid is plotted, with SSC versus FSC. The upper right figure displays the original plot and the neutrophil gate used, while the center figure exclusively shows the counts within the gate.

D

Liquid chromatography-mass spectrometry of fractions from size-exclusion chromatography

D.1 Fraction C1

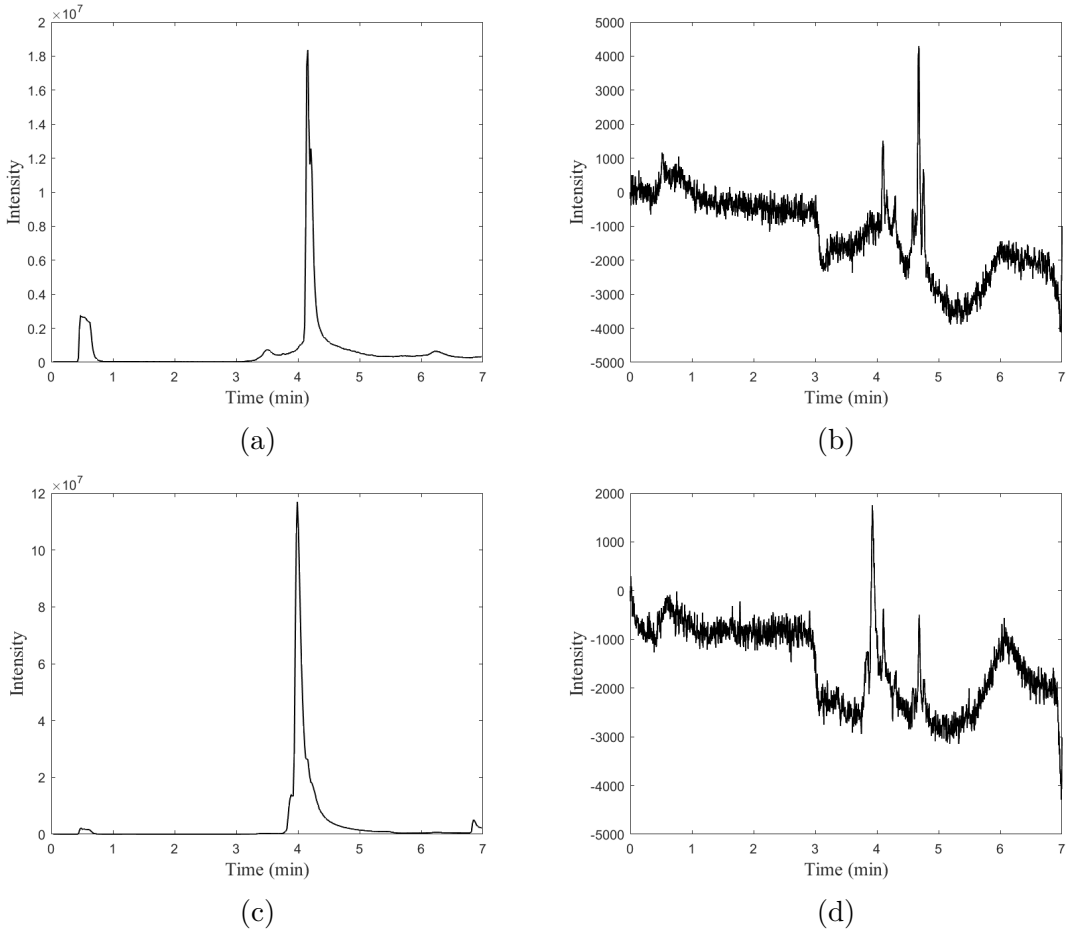

Figure D.1: The total ion chromatogram and UV-absorption at 280 nm for fraction C1 from SEC of the 90 % synovial fluid in (c) and (d), respectively, and for the PBS (blank) measurement run before that in (a) and (b).

D.2 Fraction C2

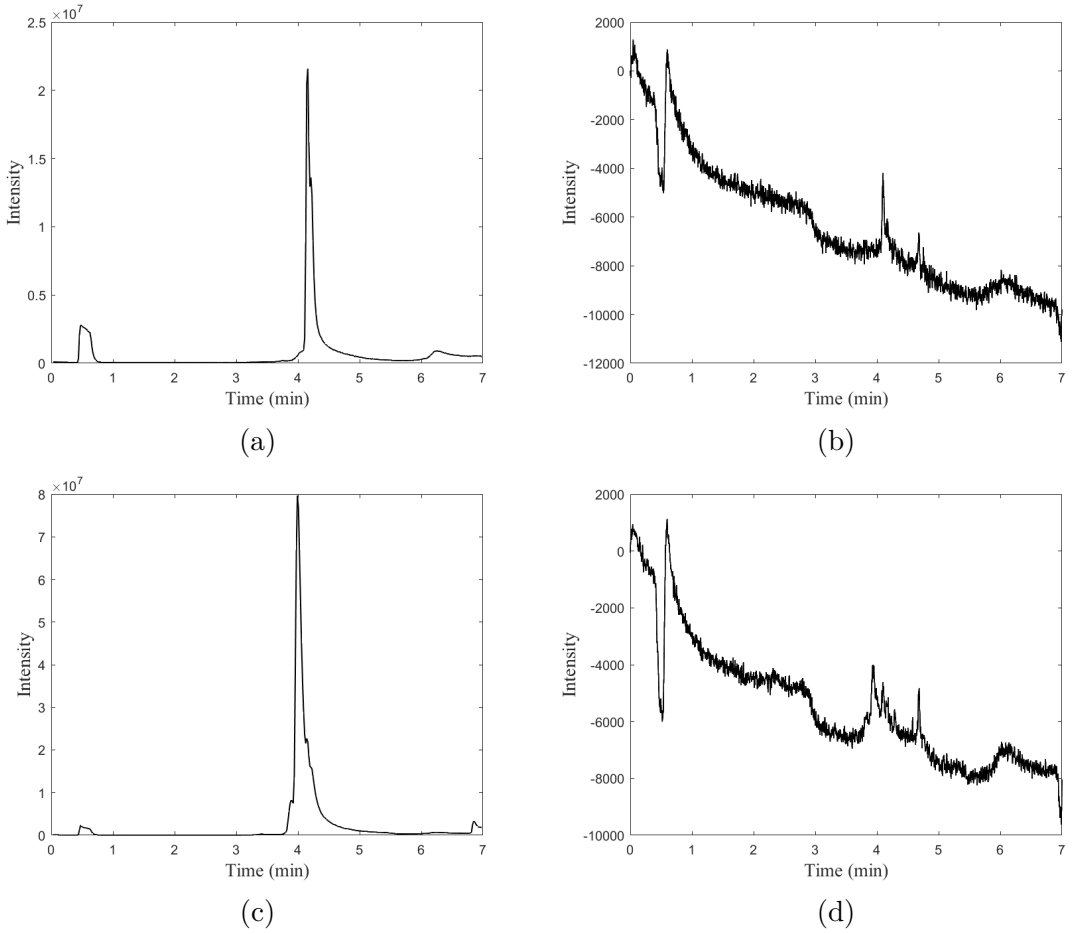

Figure D.2: The total ion chromatogram and UV-absorption at 280 nm for fraction C2 from SEC of the 90 % synovial fluid in (c) and (d), respectively, and for the PBS (blank) measurement run before that in (a) and (b).

D.3 Fraction D1

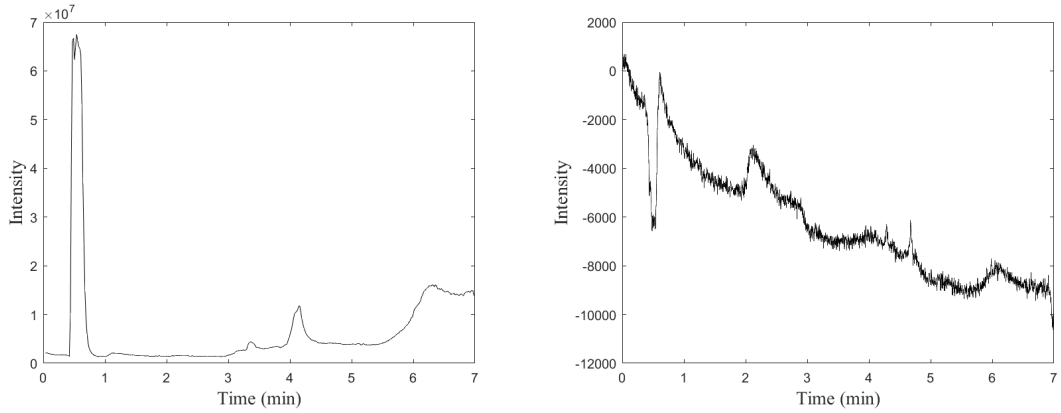

(a) (b)

Figure D.3: The total ion chromatogram and UV-absorption at 280 nm for fraction D1 from SEC of the 90 % synovial fluid in (c) and (d), respectively, and for the PBS (blank) measurement run before that in (a) and (b).

D.4 Fractions D2-D4

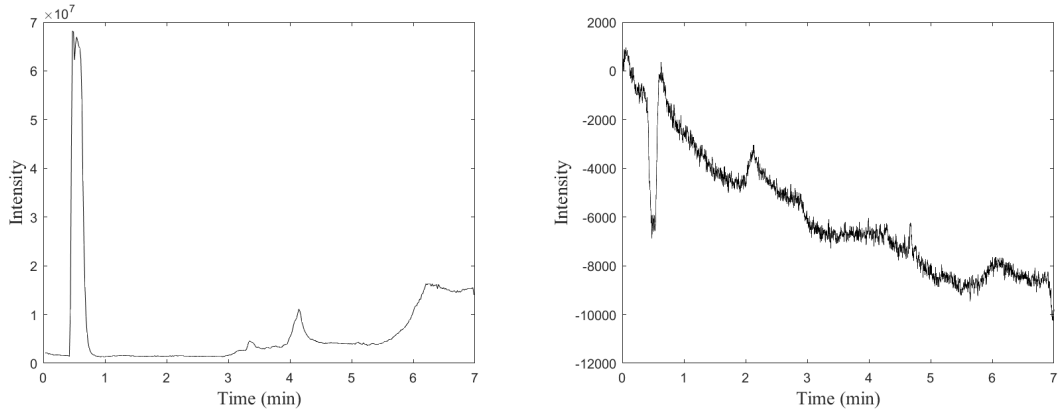

(a) (b)

Figure D.4: The total ion chromatogram and UV-absorption at 280 nm for fractions D2-D4 from SEC of the 90 % synovial fluid in (c) and (d), respectively, and for the PBS (blank) measurement run before that in (a) and (b).

D.5 Fractions D6-D7

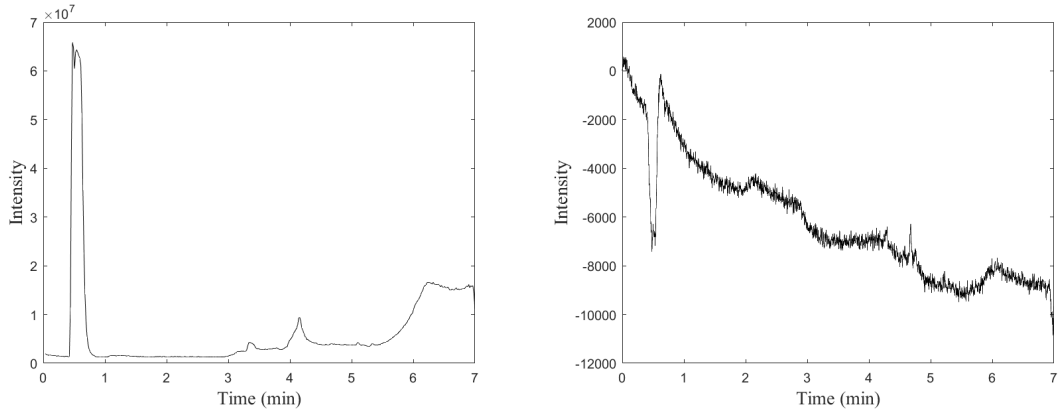

(a) (b)

Figure D.5: The total ion chromatogram and UV-absorption at 280 nm for fractions D6-D7 from SEC of the 90 % synovial fluid in (c) and (d), respectively, and for the PBS (blank) measurement run before that in (a) and (b).

D.6 Fractions D8-D10

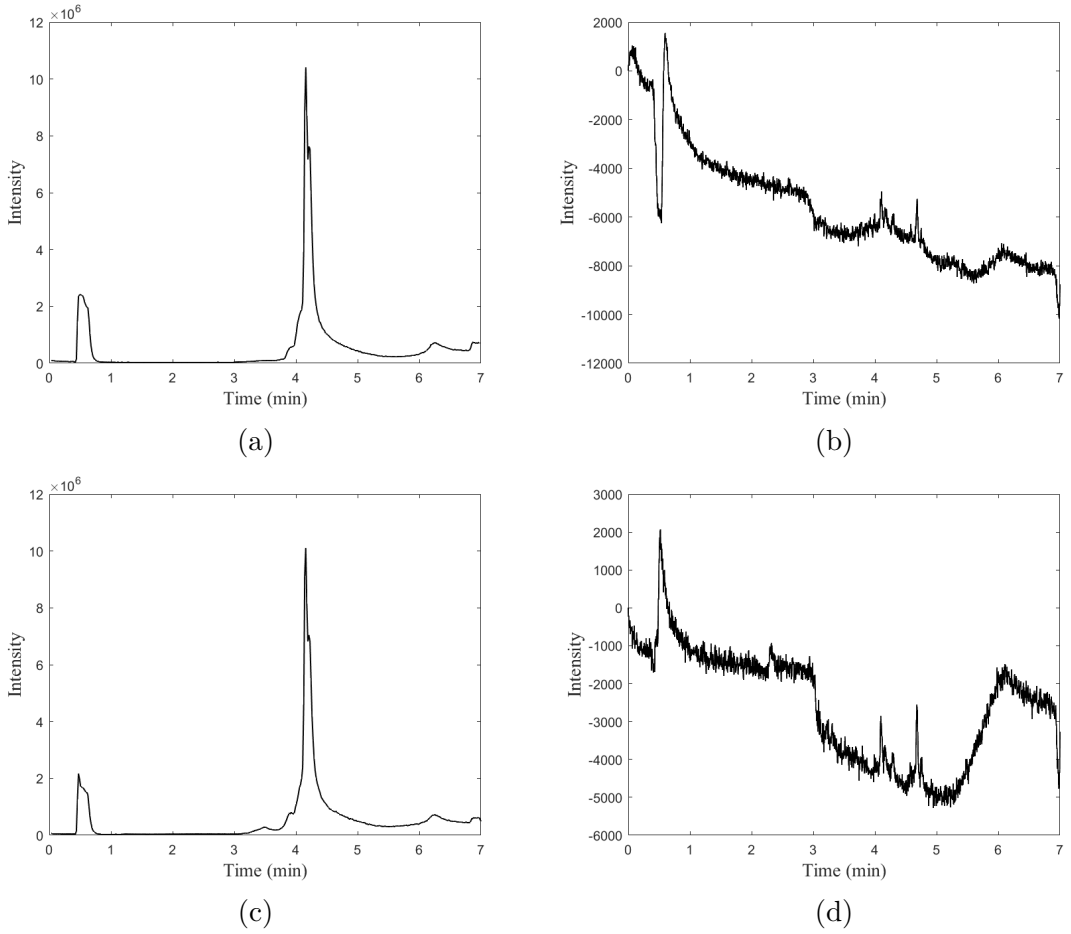

Figure D.6: The total ion chromatogram and UV-absorption at 280 nm for fractions D8-D10 from SEC of the 90 % synovial fluid in (c) and (d), respectively, and for the PBS (blank) measurement run before that in (a) and (b).

D.7 Fraction D11

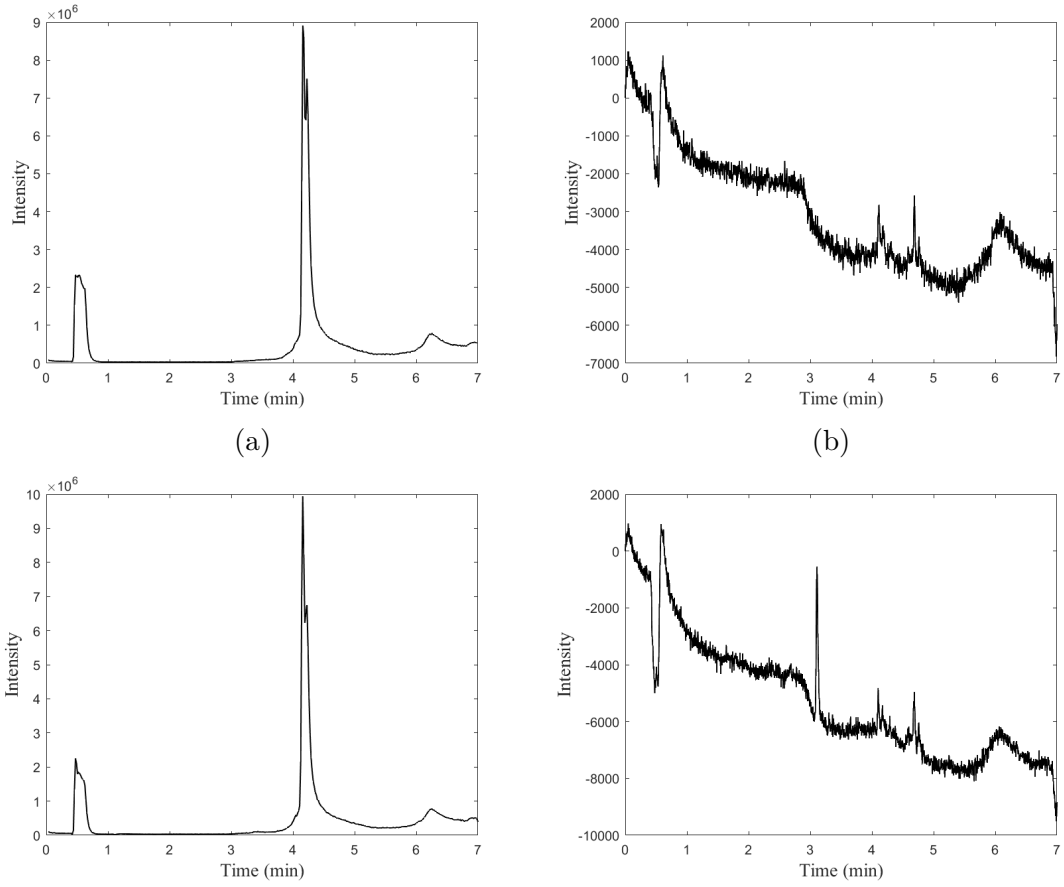

Figure D.7: The total ion chromatogram and UV-absorption at 280 nm for fraction D11 from SEC of the 90 % synovial fluid in (c) and (d), respectively, and for the PBS (blank) measurement run before that in (a) and (b).

E

Liquid chromatography-mass spectrometry of fractions from cation-exchange chromatography

E.1 Fractions A6-A7

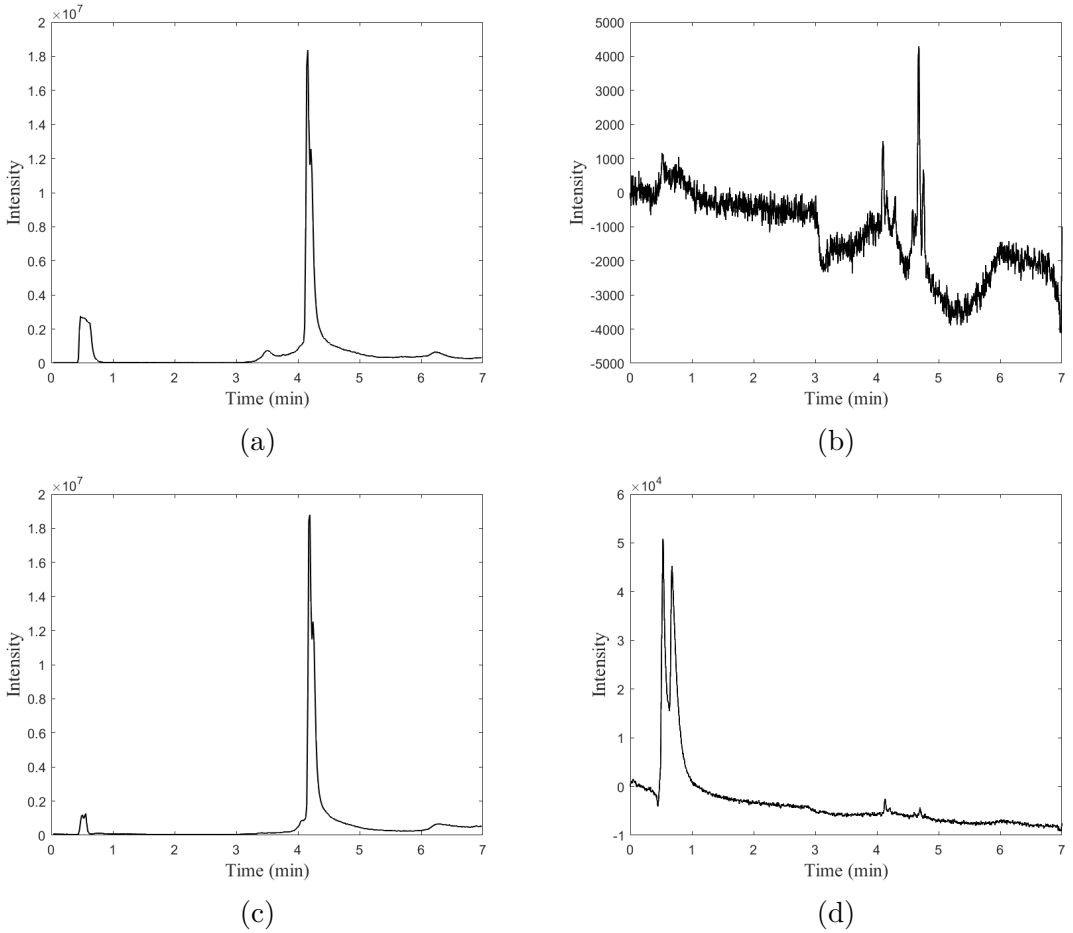

Figure E.1: The total ion chromatogram and UV-absorption at 280 nm for fractions A6-A7 from cation-exchange chromatography of the 90 % synovial fluid in (c) and (d), respectively, and for the PBS (blank) measurement run before that in (a) and (b).

E.2 Fractions A10-A11

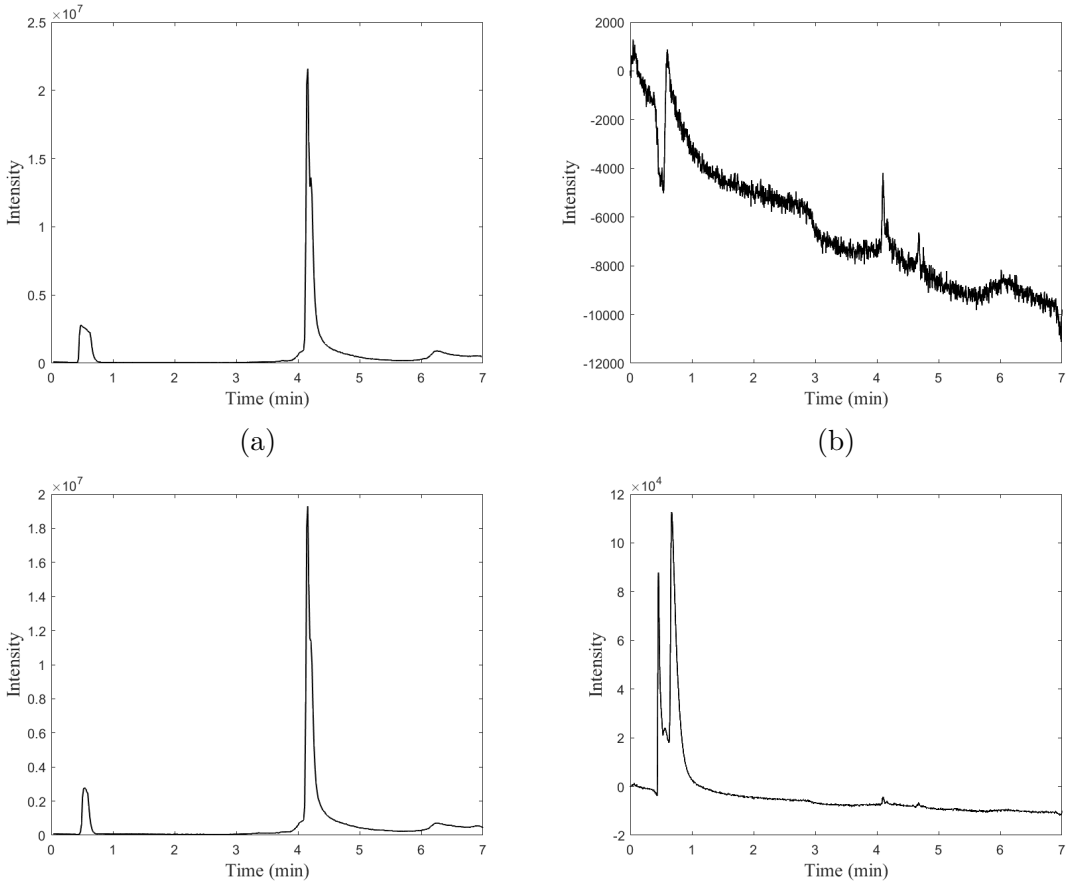

Figure E.2: The total ion chromatogram and UV-absorption at 280 nm for fractions A10-A11 from cation-exchange chromatography of the 90 % synovial fluid in (c) and (d), respectively, and for the PBS (blank) measurement run before that in (a) and (b).

E.3 Fractions B2-B3

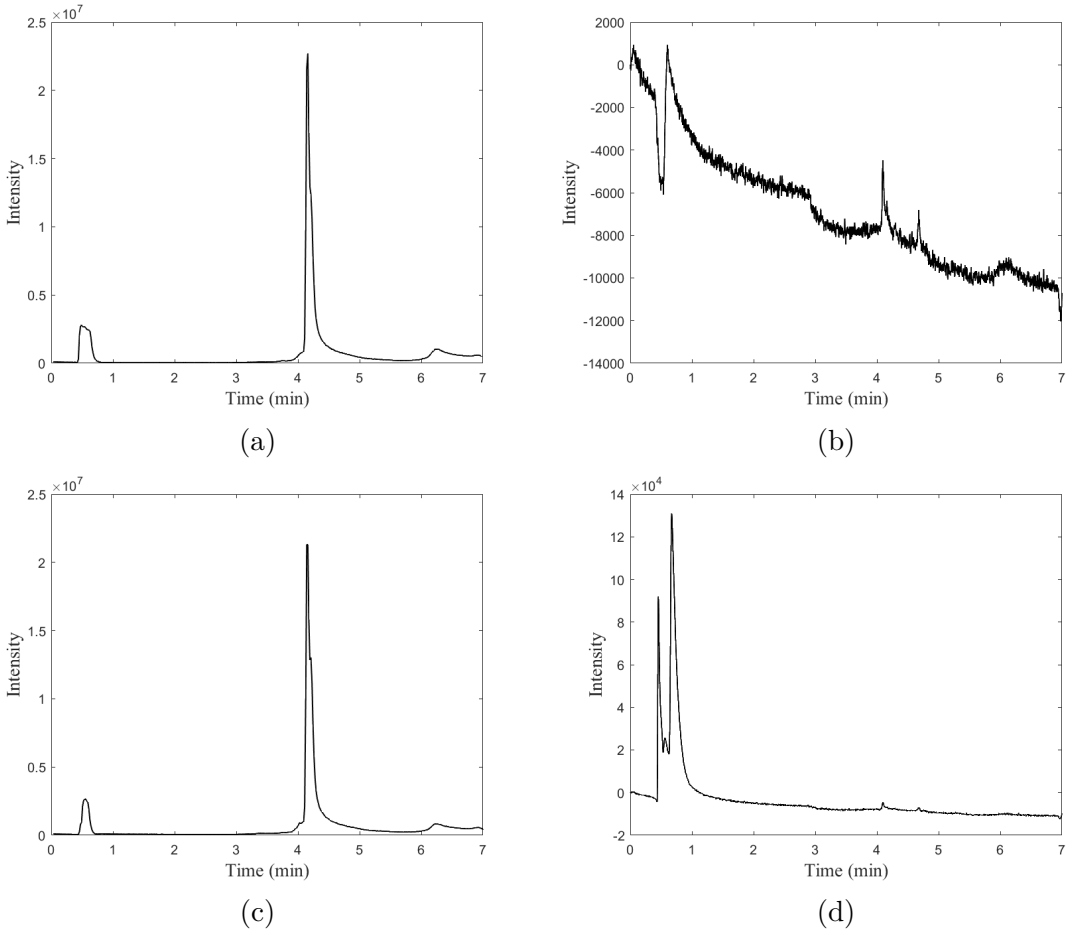

Figure E.3: The total ion chromatogram and UV-absorption at 280 nm for fractions B2-B3 from cation-exchange chromatography of the 90 % synovial fluid in (c) and (d), respectively, and for the PBS (blank) measurement run before that in (a) and (b).

E.4 Fractions B6-B7

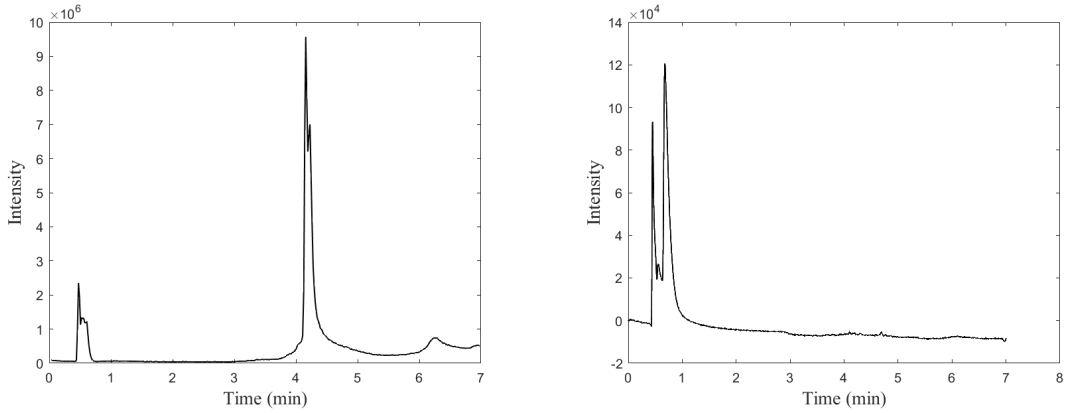

(a) (b)

Figure E.4: The total ion chromatogram and UV-absorption at 280 nm for fractions B6-B7 from cation-exchange chromatography of the 90 % synovial fluid in (a) and (b), respectively.

E.5 Fractions B10-B11

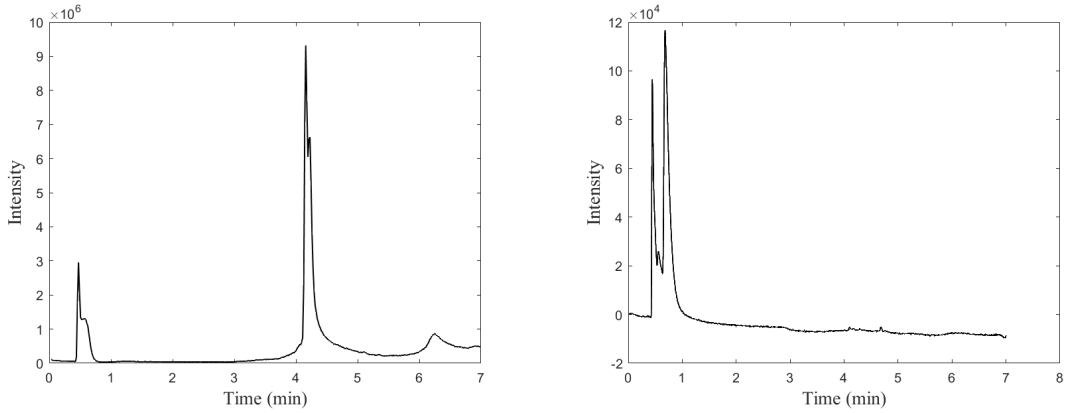

(a) (b)

Figure E.5: The total ion chromatogram and UV-absorption at 280 nm for fractions B10-B11 from cation-exchange chromatography of the 90 % synovial fluid in (a) and (b), respectively.

E.6 Fractions C2-C3

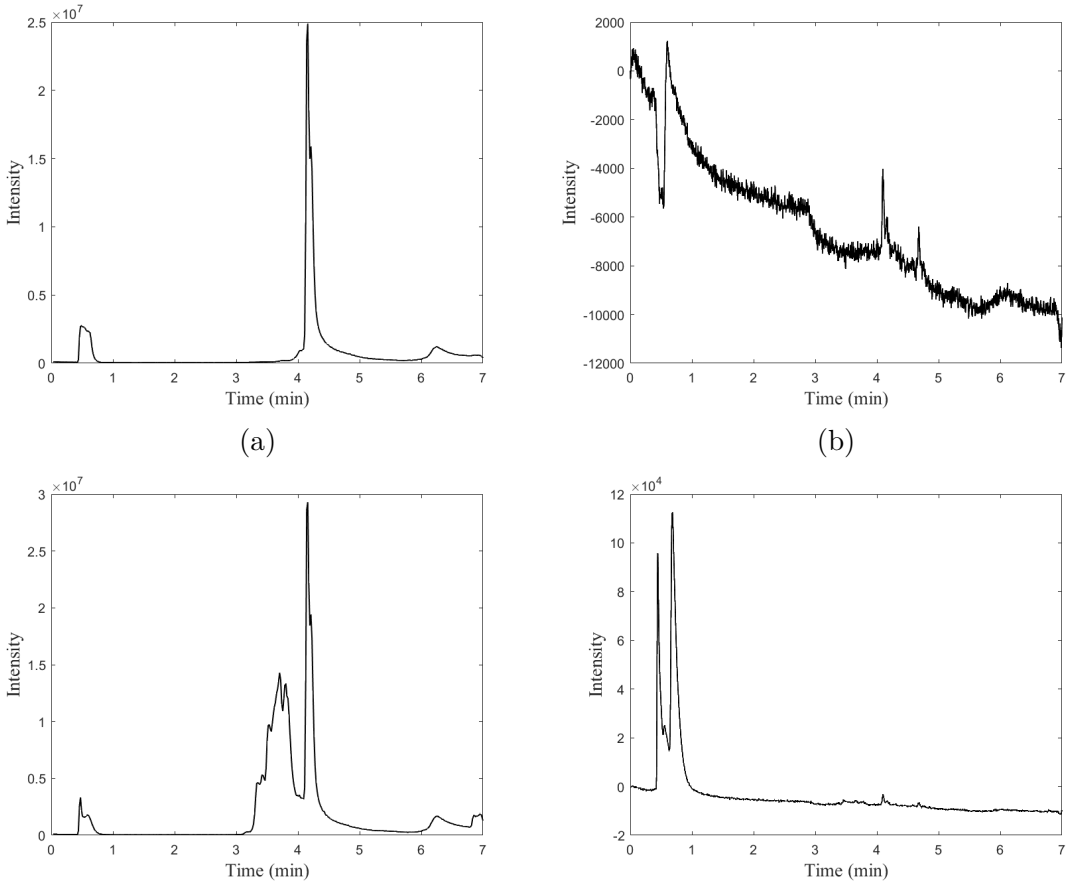

Figure E.6: The total ion chromatogram and UV-absorption at 280 nm for fractions C2-C3 from cation-exchange chromatography of the 90 % synovial fluid in (c) and (d), respectively, and for the PBS (blank) measurement run before that in (a) and (b).

E.7 Fractions C6-C7

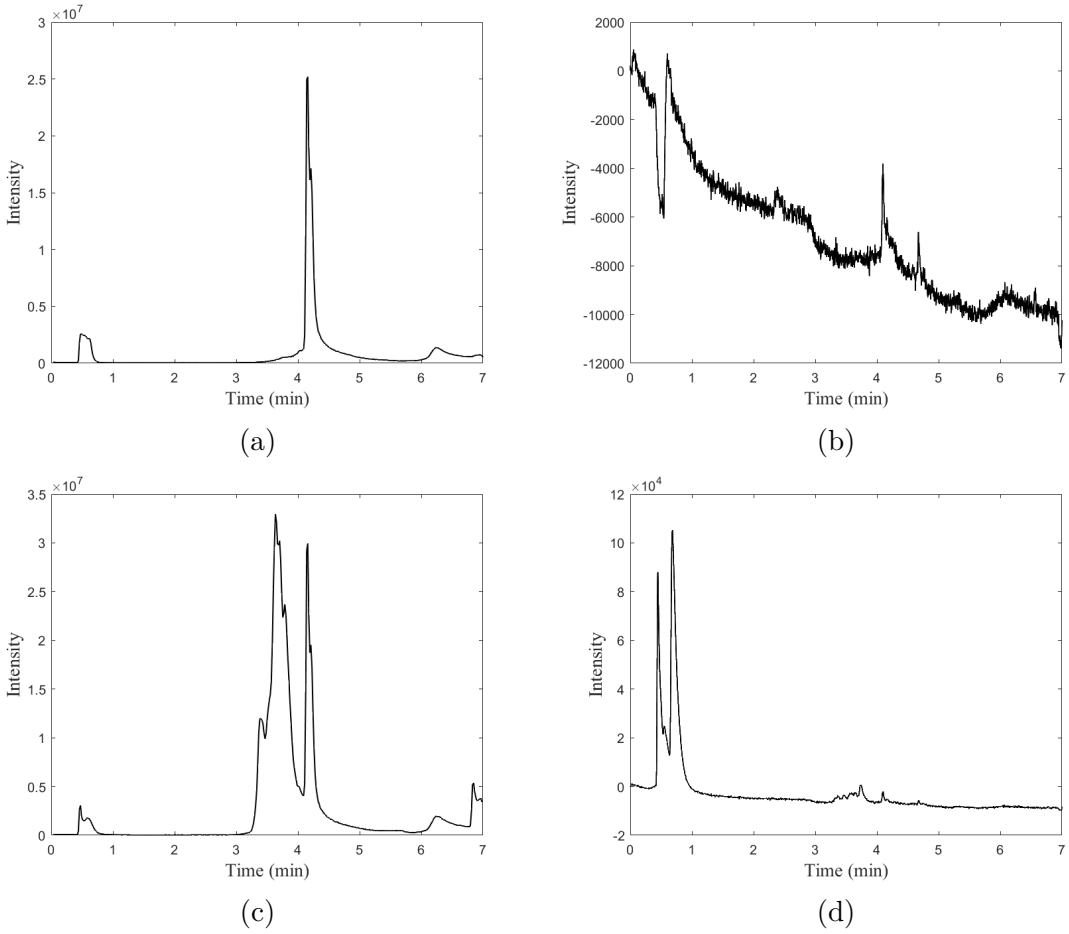

Figure E.7: The total ion chromatogram and UV-absorption at 280 nm for fractions C6-C7 from cation-exchange chromatography of the 90 % synovial fluid in (c) and (d), respectively, and for the PBS (blank) measurement run before that in (a) and (b).

E.8 Fractions C10-C11

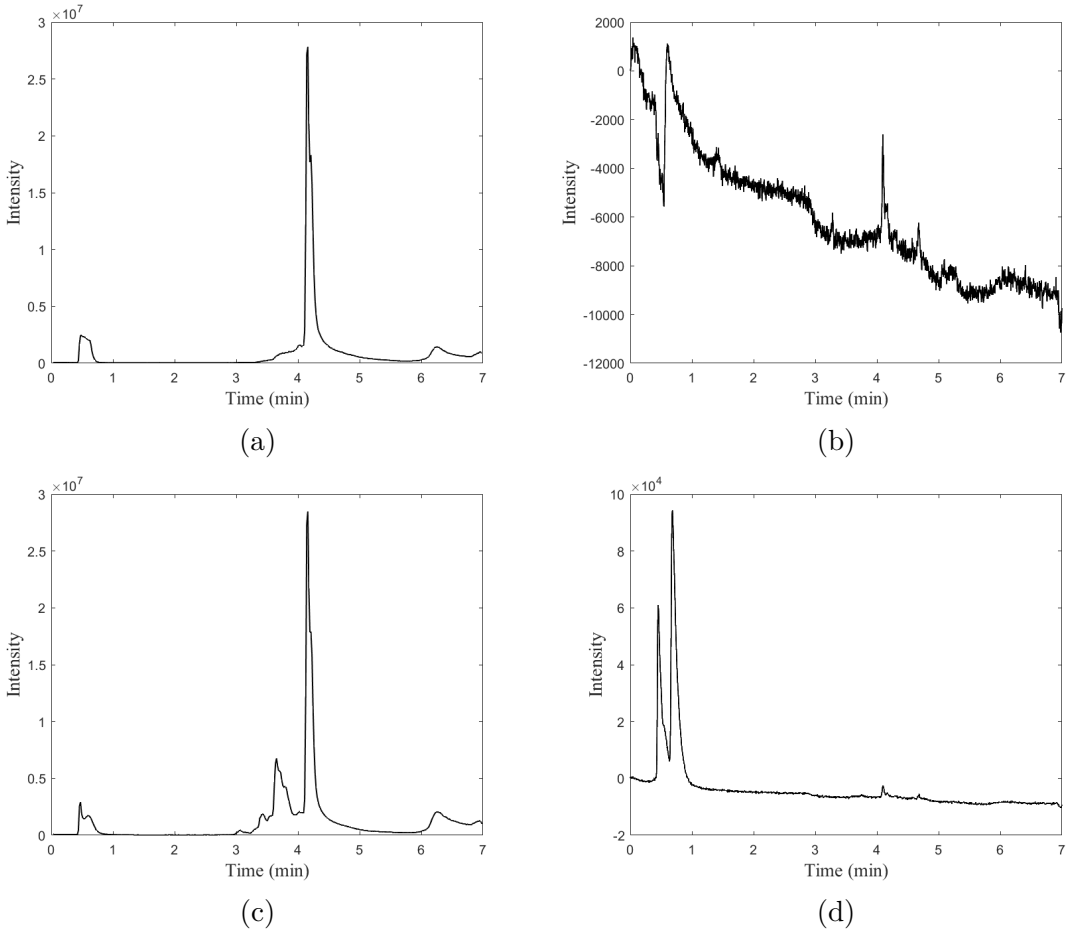

Figure E.8: The total ion chromatogram and UV-absorption at 280 nm for fractions C10-C11 from cation-exchange chromatography of the 90 % synovial fluid in (c) and (d), respectively, and for the PBS (blank) measurement run before that in (a) and (b).

DEPARTMENT OF SOME SUBJECT OR TECHNOLOGY
CHALMERS UNIVERSITY OF TECHNOLOGY
Gothenburg, Sweden
www.chalmers.se

CHALMERS
UNIVERSITY OF TECHNOLOGY